U.S. DEPARTMENT OF COMMERCE / National Bureau of Standards
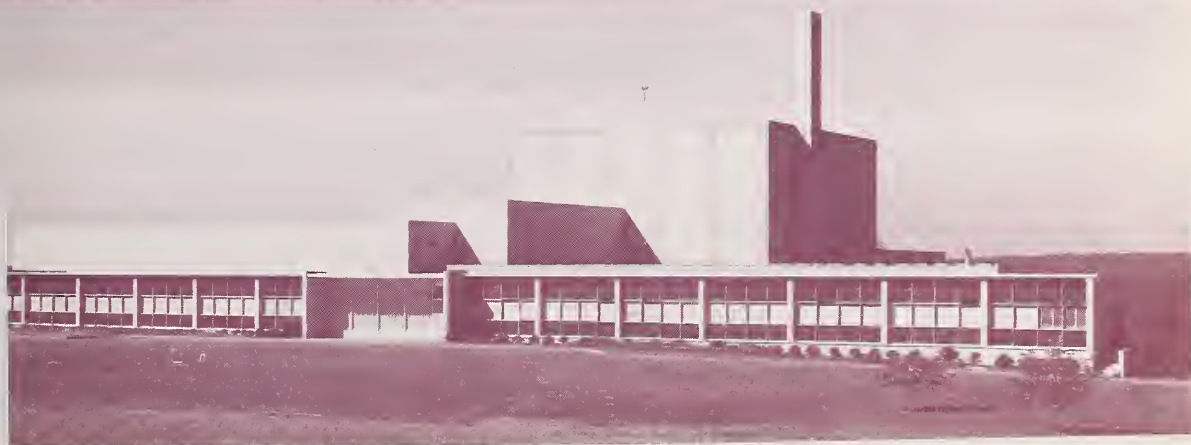
NBS Reactor:
Summary of Activities
July 1975 to June 1976

NATIONAL BUREAU OF STANDARDS

The National Bureau of Standards[1] was established by an act of Congress March 3, 1901. The Bureau's overall goal is to strengthen and advance the Nation's science and technology and facilitate their effective application for public benefit. To this end, the Bureau conducts research and provides: (1) a basis for the Nation's physical measurement system, (2) scientific and technological services for industry and government, (3) a technical basis for equity in trade, and (4) technical services to promote public safety. The Bureau consists of the Institute for Basic Standards, the Institute for Materials Research, the Institute for Applied Technology, the Institute for Computer Sciences and Technology, the Office for Information Programs, and the Office of Experimental Technology Incentives Program.

THE INSTITUTE FOR BASIC STANDARDS provides the central basis within the United States of a complete and consistent system of physical measurement; coordinates that system with measurement systems of other nations; and furnishes essential services leading to accurate and uniform physical measurements throughout the Nation's scientific community, industry, and commerce. The Institute consists of the Office of Measurement Services, and the following center and divisions:

> Applied Mathematics — Electricity — Mechanics — Heat — Optical Physics — Center for Radiation Research — Laboratory Astrophysics[2] — Cryogenics[2] — Electromagnetics[2] — Time and Frequency[2].

THE INSTITUTE FOR MATERIALS RESEARCH conducts materials research leading to improved methods of measurement, standards, and data on the properties of well-characterized materials needed by industry, commerce, educational institutions, and Government; provides advisory and research services to other Government agencies; and develops, produces, and distributes standard reference materials. The Institute consists of the Office of Standard Reference Materials, the Office of Air and Water Measurement, and the following divisions:

> Analytical Chemistry — Polymers — Metallurgy — Inorganic Materials — Reactor Radiation — Physical Chemistry.

THE INSTITUTE FOR APPLIED TECHNOLOGY provides technical services developing and promoting the use of available technology; cooperates with public and private organizations in developing technological standards, codes, and test methods; and provides technical advice services, and information to Government agencies and the public. The Institute consists of the following divisions and centers:

> Standards Application and Analysis — Electronic Technology — Center for Consumer Product Technology: Product Systems Analysis; Product Engineering — Center for Building Technology: Structures, Materials, and Safety; Building Environment; Technical Evaluation and Application — Center for Fire Research: Fire Science; Fire Safety Engineering.

THE INSTITUTE FOR COMPUTER SCIENCES AND TECHNOLOGY conducts research and provides technical services designed to aid Government agencies in improving cost effectiveness in the conduct of their programs through the selection, acquisition, and effective utilization of automatic data processing equipment; and serves as the principal focus wthin the executive branch for the development of Federal standards for automatic data processing equipment, techniques, and computer languages. The Institute consist of the following divisions:

> Computer Services — Systems and Software — Computer Systems Engineering — Information Technology.

THE OFFICE OF EXPERIMENTAL TECHNOLOGY INCENTIVES PROGRAM seeks to affect public policy and process to facilitate technological change in the private sector by examining and experimenting with Government policies and practices in order to identify and remove Government-related barriers and to correct inherent market imperfections that impede the innovation process.

THE OFFICE FOR INFORMATION PROGRAMS promotes optimum dissemination and accessibility of scientific information generated within NBS; promotes the development of the National Standard Reference Data System and a system of information analysis centers dealing with the broader aspects of the National Measurement System; provides appropriate services to ensure that the NBS staff has optimum accessibility to the scientific information of the world. The Office consists of the following organizational units:

> Office of Standard Reference Data — Office of Information Activities — Office of Technical Publications — Library — Office of International Standards — Office of International Relations.

---

[1] Headquarters and Laboratories at Gaithersburg, Maryland, unless otherwise noted; mailing address Washington, D.C. 20234.
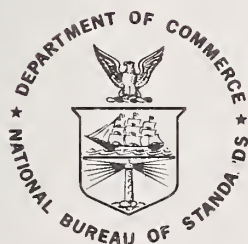
[2] Located at Boulder, Colorado 80302.

NBS Reactor: Summary of Activities July 1975 to June 1976

Technical note, no. 939

Frederick J. Shorten, Editor

Reactor Radiation Division
Institute for Materials Research
National Bureau of Standards
Washington, D. C. 20234

National Bureau of Standards Technical Note 939

Nat. Bur. Stand. (U.S.), Tech. Note 939, 140 pages (May 1977)

CODEN: NBTNAE

FOREWORD

The National Bureau of Standards Reactor was built not only to
serve the needs of the NBS but also those of other government agencies
and the greater Washington Scientific Community. The Reactor Radiation
Division was established to operate the reactor and to foster its scien-
tific and technological use. Toward this end, the Division has a small
nucleus of scientists experienced in the use of reactors for a wide range
of scientific and technical problems. In addition to pursuing their own
research and developing sophisticated experimental facilities, they ac-
tively seek out and encourage collaboration with other scientists, engaged
in challenging programs, whose work can benefit from use of the reactor,
but who as yet do not have the reactor experience necessary to take full
advantage of the facilities available. The Division also provides ir-
radiation services to a wide variety of users as well as engineering and
other technical services.

The reactor operates at 10 MW and is designed to provide more than
20 experimental facilities ranging from intense neutron beams to extensive
irradiation facilities, making it one of the most versatile high flux
research reactors in the country. Thus it is able to serve a large number
of scientists and engineers in a broad range of activities both within
and outside the NBS.

This report attempts to summarize all the work done which is depend-
ent on the reactor including a large number of programs outside the
Division. The first section summarized those programs based primarily
on Reactor Radiation Division (RRD) initiatives whereas the second and
third sections summarize collaborative programs between RRD scientists
and other NBS or non-NBS scientists respectively. The fourth section
summarized NBS work originating entirely outside the RRD which requires
no collaboration with RRD scientists. The section entitled, "Service
Programs" covers those programs originating outside NBS but for which
RRD provides irradiation services. The remaining sections are self-
explanatory.

FOREWORD

Appreciation is extended to F. J. Shorten of the Reactor Radiation Division for his extensive contributions to the editing, organization and preparation of this report, and to L. Sprecher, C. O'Connor and P. Lewis for efforts in typing manuscripts.

J. J. Rush
Chief, Reactor Radiation Division (Acting)
National Bureau of Standards

ABSTRACT

This report summarizes all those programs which depend on the NBS reactor. It covers the period from July 1975 through June 1976. The programs range from the use of neutron beams to study of the structure and dynamics of materials through nuclear physics and neutron standards to sample irradiations for activation analysis, isotope production and radiation effects studies.

Key words: Activation analysis: crystal structure; diffraction; isotopes; molecular dynamics; neutron, nuclear reactor; radiation.

TABLE OF CONTENTS

TABLE OF CONTENTS

TABLE OF CONTENTS

A. Reactor Radiation Division Programs

NEUTRON SCATTERING STUDIES OF HYDROGEN IN METALS

Our long range program to study the binding and diffusion of
hydrogen in metals, and related properties of metal-hydrogen systems has
provided new results particularly in the study of the lattice dynamics
of metal hydride crystals. Our collaborative interactions with the
Argonne and Oak Ridge National Laboratories have continued and a new
collaborative effort has been initiated with scientists at the Allied
Chemical Materials Research Center. New results have been obtained on
the crystal dynamics of VD_x and $CeD_{2.12}$ and on a detailed comparison of
phonon lineshape profiles in a non-stiochiometic deuteride ($PdD_{0.63}$)
with computer simulation calculations of the lattice dynamics of this
disordered high density "defect" structure. We have also continued our
studies of the structure and dynamics of the low concentration (α & β)
phases of TiH_x, as discussed in another part of this report.

1. The Lattice Dynamics of $VD_{0.7}$ - J. J. Rush, C. J. Glinka and J. M. Rowe

The lattice dynamics of a single crystal of α(bcc) $VD_{0.7}$ has been
investigated by coherent inelastic neutron scattering measurements in
collaboration with H. E. Flotow of Argonne National Laboratory. Due to
the very small vanadium coherent cross section, essentially all the
coherent scattering by this compound is associated with the deuterium
(located in tetrahedral interstitial sites). Thus a study of this
system provides a unique opportunity to measure the "in-band" and
optical modes associated with the vibrational displacements of the
deuterium (light atom) interstitials as a function of $\vec{q}$ and ω.

The $VD_{0.697}$ crystal prepared for these experiments had a "mosaic
spread" of <1°. Some example of neutron groups measured under both
constant ΔE and constant $\vec{Q}$ conditions are shown in figure 1. Also
present as a shoulder in figure 1b is the incoherent "density of states"
scattering which is present in all phonon scans at higher energies and
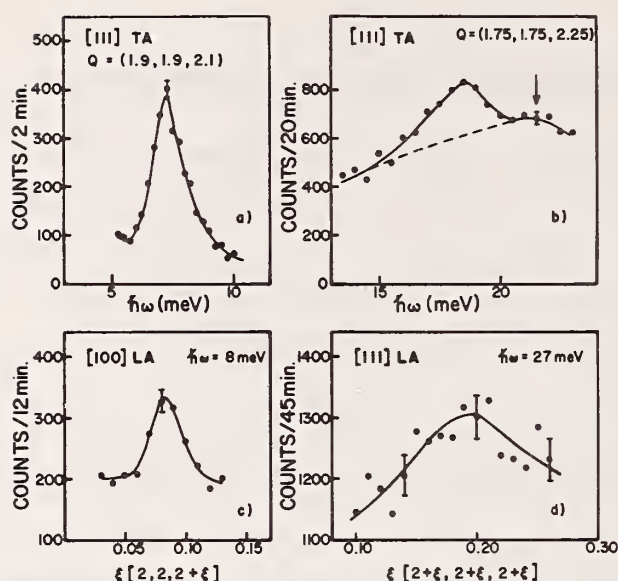
Figure 1. Examples of phonon groups measured for α-VD$_{0.7}$. The arrow and dashed line in group c. ([111]TA at ξ-0.25) indicate the incoherent "density of states" peak.

makes the observation of coherent phonon peaks above ~20 meV quite difficult. The phonons measured thus far at $\xi \leq 0.5$ in the three symmetry directions are shown in figure 2. The results in figures 1, 2 represent a direct measurement of the "in band" vibrations of the interstitial deuterium atoms.

It is interesting to note from these results that: a) the observed neutron groups are well defined, with little apparent broadening (for $\hbar\omega \lesssim 20$ meV) due to the random distribution of interstitials, b) the phonon frequencies measured for VD$_{0.7}$ are in general higher than those for pure vanadium, indicating a general increase in interatomic forces on hydriding in spite of a ~5% expansion of the lattice (a$_o$(V) = 3.03Å, a$_o$(VD$_{0.7}$) = 3.145 Å). In fact the elastic constants obtained from the long wavelength (low Q) slopes of the present measurements (figure 2) are 30-50% larger than the measured values for vanadium.

As a further attempt to elucidate the changes in vibration spectrum which occur on deuteration we have made energy transfer scans at constant

2

$\vec{Q}$ and fixed E_F for both $VD_{0.7}$ and pure vanadium. These results were used to derive phonon "density of states" distributions for V and $VD_{0.7}$, assuming one-phonon incoherent scattering. The results are shown in figure 3. Both of these "distributions" reflect primarily the vibrational displacements of the vanadium atoms (although the contribution of D complicates this analysis). It is clear from the results that the addition of deuterium has considerably altered the frequency distribution. In particular the cutoff of phonon energies is apparently shifted to higher energies for the $VD_{0.7}$ crystal.
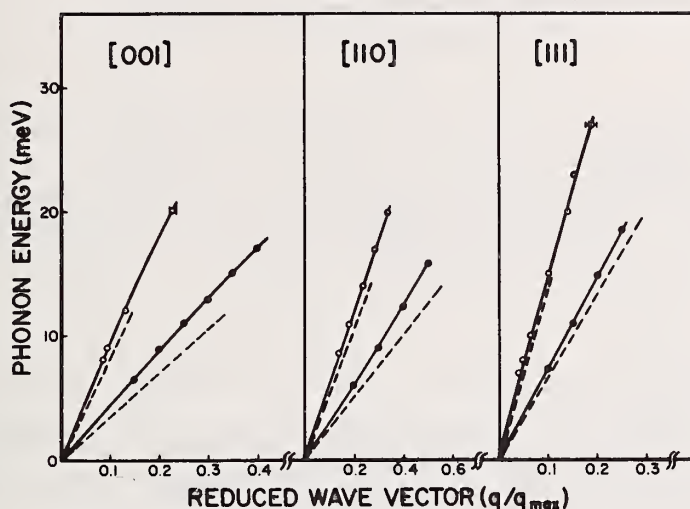
Figure 2. Partial dispersion curves in the three symmetry directions for α-$VD_{0.7}$. Dotted lines indicate the long wavelength slopes of the dispersion curves predicted by the measured elastic constants of vanadium.

As discussed above the coherent inelastic scattering from $VD_{0.7}$ reflects only the D vibrational displacements so that the measurements in figures 1, 2 allow a direct test of the coupling of interstitial deuteriums to the host metal lattice. We have derived integrated intensities from careful measurements of neutron groups in several crystal directions up to phonon energies of 20 meV. The relative intensities of the groups vs. $\vec{q}$ and ΔE show no variation within the

3
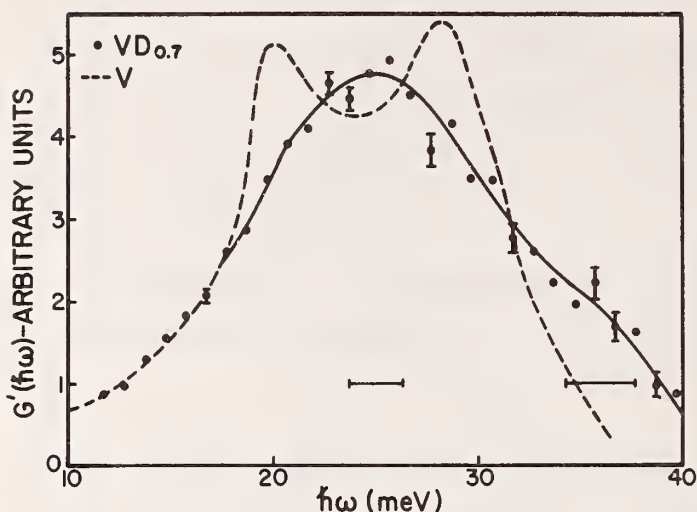
Figure 3.   Phonon "density of states" – G'(hω) derived from energy
spectra measured at constant Q in V and $\alpha VD_{0.7}$. The pure
vanadium results represent a smooth line drawn through many
data points. The phonon densities are only approximately
normalized. Energy resolutions (FWHM) are indicated by the
horizontal bars.

estimated errors, thus providing clear evidence that the D atoms are
strongly coupled to the acoustic vibrations of the vanadium lattice.

No adequate force model fit to the data in figure 2 is possible
without information on phonon frequencies at larger ξ values. Such
measurements are quite difficult due to the superposition of the phonon
"groups" on the density of states scattering at energies ≥20 meV, but
further work is in progress.

2.   Inelastic Neutron Scattering Lineshapes in $PdD_{0.63}$ – C. J. Glinka,
J. M. Rowe, and J. J. Rush

In a previous coherent neutron scattering study[1] of the lattice
dynamics of the non-stiochiometric metal hydride $PdD_{.63}$, severely
broadened lineshapes were observed for the optic phonons even at low
temperature (80K). While the phonon peak positions observed in this

4
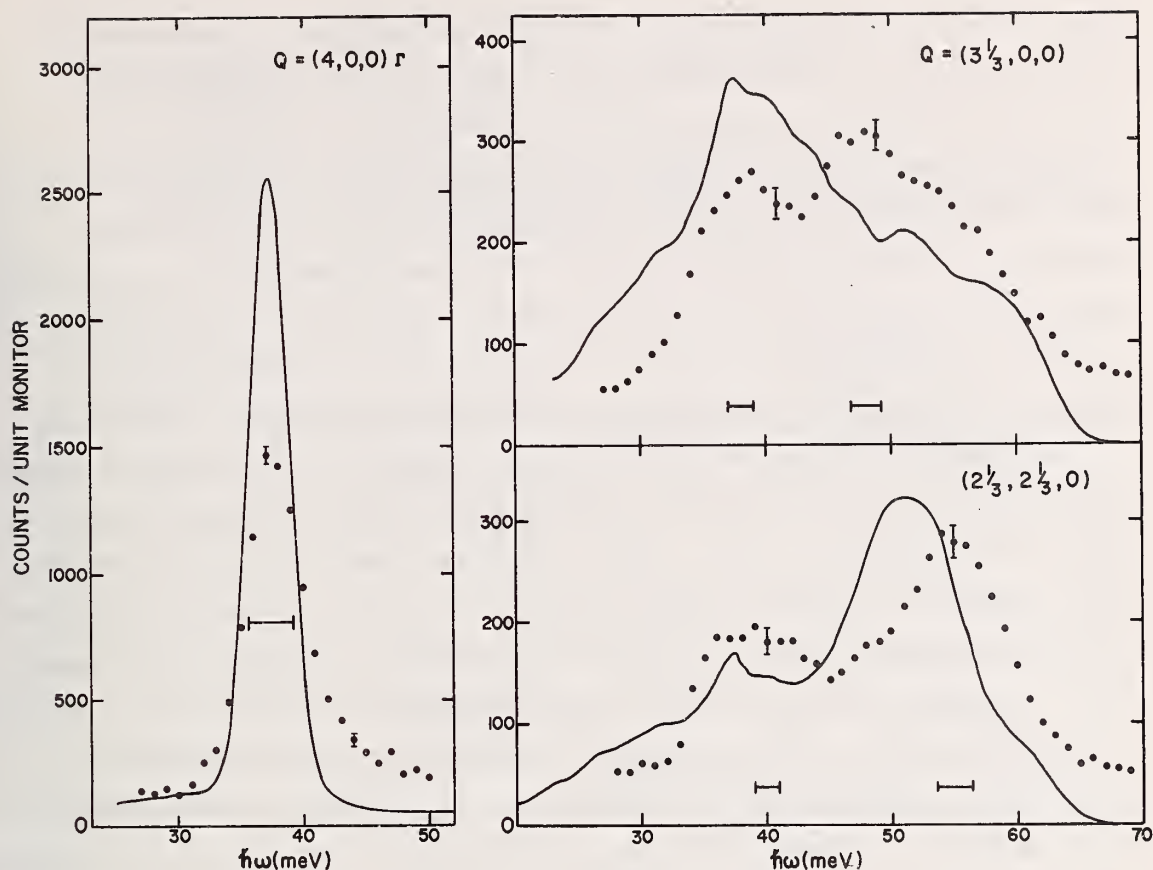
Figure 4. Representative constant-Q scans of the scattering in the optic mode region from PdD$_{.63}$ at 77K. The solid curves are the intensity profiles calculated from the structural model for PdD$_{.63}$.

earlier work could quite adequately be derived from a second near neighbor Born-von Karman model in which the crystal was treated as stoichiometric PdD (NaCl-structure), such a model predicts sharp phonon lineshapes and thus gives no insight into the nature of the observed linebroadening. Recently however, A. Rahman has completed calculations of the coherent "one-phonon" scattering for PdD$_{.63}$ based on a model for the lattice dynamics which incorporates the large number of vacancies in the actual structure. The calculations entail computing the normal modes of vibration of a large unit cell of 108 Pd atoms with 68 deuterium

atoms situated at random on the deuterium sublattice. The frequencies
and polarization vectors obtained by repeating the computations for a
statistical ensemble of such cells are then used to evaluate the one-
phonon cross section. In order to critically test these calculations,
new, more extensive, measurements have been made of the inelastic
scattering in the optic mode region. These measurements and calculations,
(which have been reported in a preliminary publication[2]), have helped to
elucidate not only the dynamics of $PdD_{.63}$, but also the more general
problem of the effects of vacancies on the lattice dynamics of solids.

In figure 4 three typical inelastic scattering lineshapes, measured
with a triple-axis spectrometer at 80K, are shown with corresponding
calculated lineshapes (solid lines). Although the structural detail in
the calculated lineshapes is dependent on the choice of unit cell size
used in the computations, and therefore must be discounted, the overall
widths are not and can be seen to satisfactorily account for the observed
width in each case. This agreement demonstrates that the observed
widths are primarily the result of the defect structure rather than a
manifestation of anharmonic effects, for example. These results strongly
suggest that the character of the excitations in a highly defected
structure is markedly different from the plane-wave behavior found in
stoichiometric crystals.

Efforts are now underway to produce a higher concentration single
crystal sample of PdD_x with $X \sim 0.9$. For $X > 0.8$, PdD_x becomes supercon-
ducting and there is currently much interest in the role of lattice
vibrations in this material in the inducement of superconductivity. To
achieve this higher concentration, a crystal of Pd will be loaded under
a deuterium pressure of 2 kbar in a high pressure sample cell which has
been especially designed for this purpose and may subsequently be
mounted in a cryostat for the low temperature measurements. Further
studies along these lines are planned for the alloy-hydride system
$Pd_yCu_{1-y}D_x$ for which Tc's as high as 18 K have been reported, but these
are awaiting the preparation of appropriate single crystals.

1.   J. M. Rowe, J. J. Rush, H. G. Smith, M. Mostoller, and H. E. Flotow, Phys. Rev. Letters 33, 1297 (1974).

2.   C. J. Glinka, J. M. Rowe, J. J. Rush, A. Rahman, S. K. Sinha, and H. E. Flotow, Proceedings of the Conference on Neutron Scattering, Gatlinburg, TN. 1976 (in press).

3.   Lattice Dynamics of Cerium Deuteride – C. J. Glinka, J. M. Rowe, and J. J. Rush

A comprehensive study of the phonon dispersion curves of CeD_{2+x}, in collaboration with A. Maeland and G. Libowitz of Allied Chemical, has been initiated and thus far preliminary coherent scattering measurements have been made on a single crystal of $CeD_{2.12}$. It should be noted that CeD_2 has the same fcc (CaF_2) structure widely exhibited in transition-metal hydrogen systems (e.g., Ti, Zr, Hf, Y) whose physical, thermodynamic and electronic properties have been extensively studied.[1] The cerium hydrogen system has received considerable attention due in part to the occurrence of composition-dependent metal-to-semiconductor phase
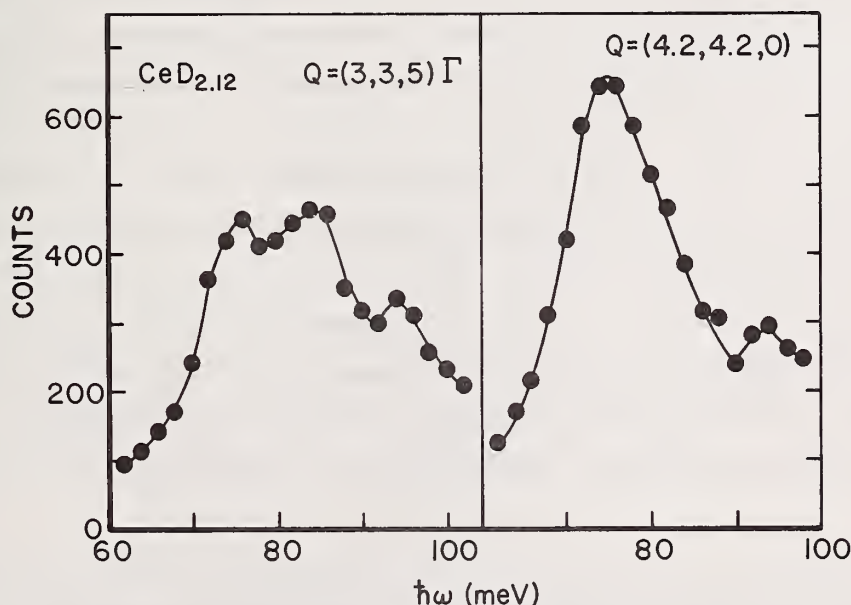
Figure 5. Neutron groups observed in constant-Q scans at room temperature in $CeD_{2.12}$.

transitions at low temperature. Our measurements represent the first coherent inelastic scattering study of a nearly stoichiometric metal hydride and should, therefore, afford the opportunity to investigate the crystal dynamics (including anharmonic deuterium vibrations) and related physical properties, virtually free from any perturbation of the phonons due to nonstoichiometry. This study is also expected to provide a definitive test of the restricted central force model (in which "bond bending" forces are neglected) which has been used[2] in fitting to specific heat data and time-of-flight neutron spectra on this material.

Figure 5 shows two typical optic phonon scans from our preliminary data on $CeD_{2.12}$. The six optic mode branches all lie within 74 to 84 meV and the coherent scattering from these modes is superimposed on a considerable background of incoherent scattering which reflects the high density of states in this region. Although more detailed measurements will be needed to establish the connectivity of the closely spaced optic branches, our present results indicate that a restricted central force model is not adequate to describe their dispersion.

The peak seen in the neutron groups in figure 1 at $\hbar\omega \cong 94$ meV is present in all of our scans and may arise from localized vibrations of hydrogen atoms randomly distributed among the deuterium sites (our sample contains a few atomic percent hydrogen). The observation of such a mode is potentially a very exciting development since the hydrogen represents a light mass substitutional defect with (presumably) no change in the atomic forces. This system may, therefore, provide the first real test case for mass defect theory in the dilute limit.

Measurements at room temperature on the $CeD_{2.12}$ crystal are continuing. We also intend to extend our phonon measurements to low temperature and to a higher concentration of CeD_x.

---

1.   W. M. Mueller, J. P. Blackledge and G. Libowitz, *Metal Hydrides*, Academic Press, New York (1968).

2.   P. Vorderwisch et al., *Phys. Stat. Sol.* (b), <u>65</u>, 171 (1974).

CRYSTAL DYNAMICS, PHASE TRANSITIONS AND ORIENTATIONAL DISORDER IN IONIC CRYSTALS

We have continued and extended our studies of the dynamics and structure of orientationally disordered crystals. It is unfortunately still correct to say that these systems are poorly understood, although some progress has been made.

Our research during the past year has been centered on a study of the structure of KCN and NaCN in all three phases, on extending our measurements of the crystal dynamics of KCN and on measurements of both crystal dynamics and reorientational dynamics of deuterated ammonium halides.

1.   Alkali Cyanides – J. M. Rowe, J. J. Rush, E. Prince, N. J. Chesser, S. Susman and D. G. Hinks

We have completed a study of the crystal structures of KCN and NaCN in all three phases by neutron powder diffraction. A set of characteristic powder patterns of KCN in all three phases is shown in figure 1. The salient feature of the results shown in this figure is the lack of observable peaks in cubic KCN for scattering angles greater than about 62°. This is a reflection of the very large mean square displacements of both metal and cyanide ions in the cubic phase which arise from the soft shear mode (C_{44}) previously observed. The extra peak is a superlattice reflection characteristic of the low temperature fully ordered orthorhombic structure.

The intensity of this superlattice line is proportional to the square of the order parameter for this order–disorder phase transition. The temperature dependence of the intensity is shown in figure 2.

In the ordered low temperature structure the two (CN)- ions in the unit cell are ordered antiparallel to each other along the b axis.

9

In addition, we have completed a more detailed study of the dynamics of KCN. The dispersion relation for acoustic phonons has been observed over a larger fraction of the Brillouin zone as shown in figure 3. This extended information was obtained on the new BT4 three-axis spectrometer, and it was the extra intensity and flexibility of this instrument which allowed us to obtain the new data. However, it must be emphasized that many of the neutron groups (especially at the larger energies) were very poorly defined and that the dispersion curve shown should not be interpreted in terms of harmonic or quasiharmonic models. The characteristic feature of the dynamics of KCN is the strong anharmonicity evidenced in the neutron lineshapes observed.

Finally, we have refined our measurements of the temperature dependence of the soft shear modes characterized by C_{44}. As was shown previously, the elastic constant C_{44} tends to zero as the temperature is lowered towards the first order phase transition at 168K. Our previous measurements of the neutron scattering associated with these soft modes was complicated by the large elastic scattering associated with the Bragg peak about which the measurements were made. By changing the experimental conditions, we have been able to remeasure these modes with very little contamination and have shown that there is no detectable elastic component in the scattering for reduced wave vectors as low as 1/10 the distance to the Brillouin zone. At this wave vector the energy of the phonon is approximately 0.2 meV just above the phase transition. Recent theories have predicted the existence of elastic scattering (central modes) for these phase transitions, so that the present results were not expected. However, the predicted behavior may only occur at smaller wave vectors than could be reached in this experiment, or the first order phase transition may occur at a temperature too far above the point at which C_{44} extrapolates to zero.

We intend to check these and other possibilities by extending our research to mixed alkali halide-akali cyanide crystals, beginning with
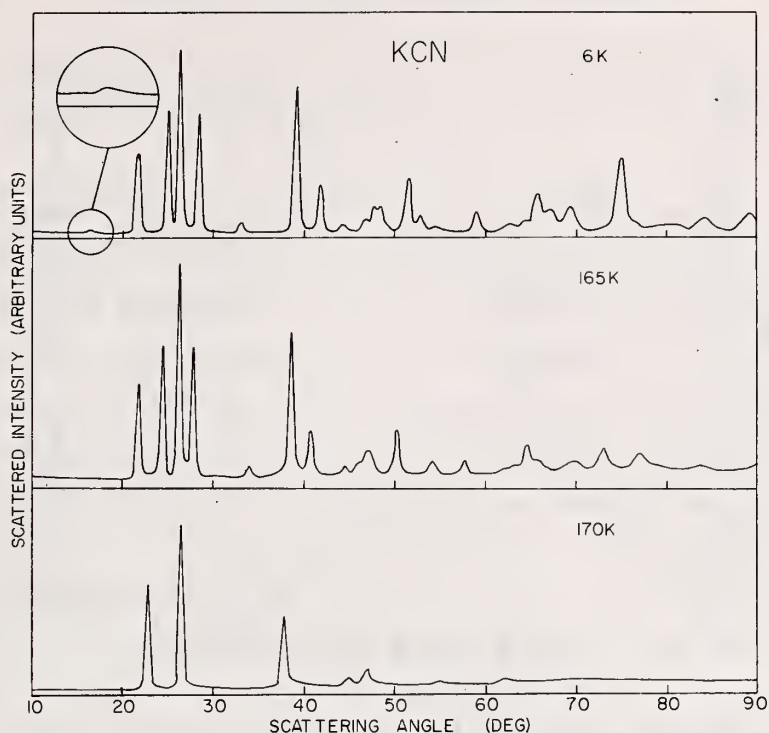
Figure 1. The observed powder diffraction patterns for the three crystal phases of KCN. Note the comparative intensities of high angle reflections in the cubic and intermediate phases and the superlattice peak (blown up in insert in the low temperature phase).
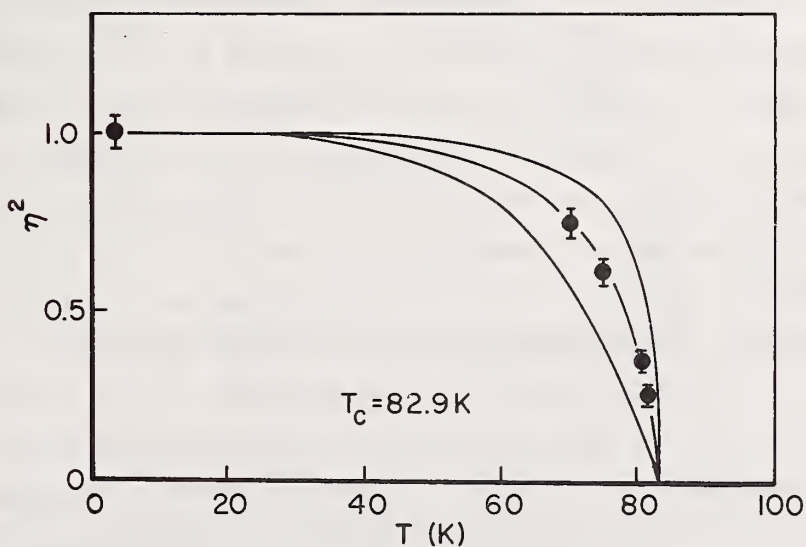
Figure 2. Temperature dependence of superlattice intensity in the low temperature phase of KCN. Solid lines are result of theory described elsewhere (R. Casella).
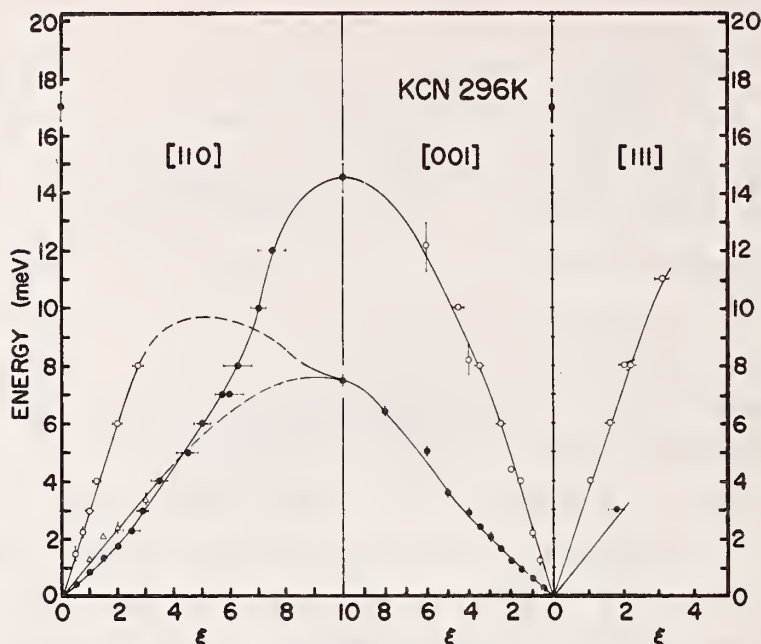
Figure 3.   Dispersion relation for "phonons" in KCN at 295K.   Solid
lines are guide to the eye.   (o) longitudinal acoustic modes
(o,Δ) transverse acoustic modes.

(K Br)$_{0.75}$ (KCN)$_{0.25}$ and proceeding to higher cyanide concentration.

2.   Ammonium Halides - J. M. Rowe, J. J. Rush and N. Vagelatos

We have successfully completed our program to grow large deuterat-
ed single crystals of ammonium iodide and ammonium bromide, and have
made detailed lattice dynamical measurments on the NaCl phase of ND_4I
(see last years report).   In addition we have completed preliminary
measurements on the lattice dynamics of ND_4 Br in the CsCl phase at
room temperature.   We intend to study this system as a function of tem-
perature and hope to make measurements in the low temperature tetragonal
phase.   We have also made preliminary measurements of the quasilastic
scattering from ND_4I in an effort to establish the reorientation mechan-
ism in this high temperature phase.   These preliminary measurements
indicate that the experiments are feasible, but also point up the
difficulty associated with the large amplitude motions of the ND_4 ions
and the broad distribution of equilibrium orientations in this phase.

12

ORDER-DISORDER PHASE TRANSITION IN KCN

R. C. Casella

Experimental work of Rowe, Rush, Prince, and Chesser[1] has indicated that below $T_c \simeq 83$ K the CN^- dipoles undergo antiferroelectric ordering. Earlier attempts to fit the temperature dependence of the order parameter η deduced from their data met with difficulties. I was led to consider the analogue to the Ising model in magnetism. It turns out that their data for the intensity of neutrons from the superlattice reflection ($\propto \eta^2$) lie midway between what one expects for a two-dimensional and a three-dimensional Ising model and is fit (within errors) by the expression

$$\eta^2 = \left[1 - \left(\sinh \frac{T_1}{T} \right)^{-3} \right]^{1/3} \qquad (1)$$

roughly the *square root* of what one expects for the 3-D Ising model
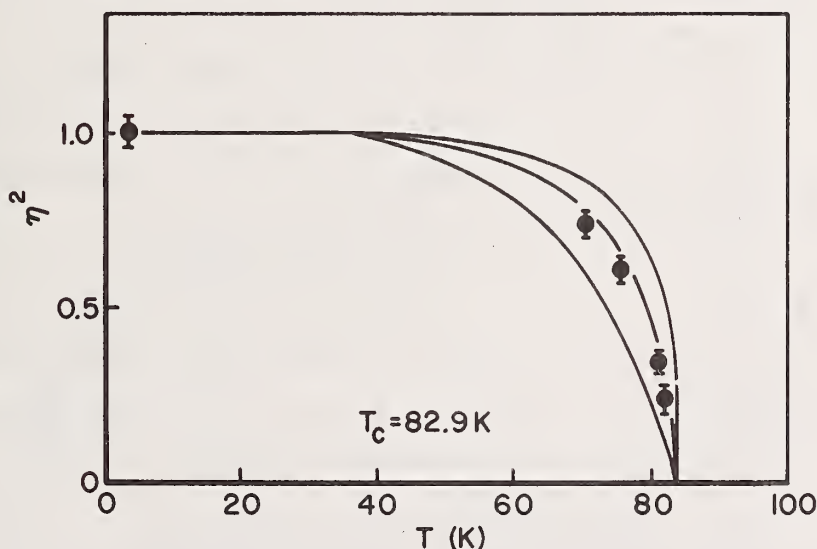
Figure 1. Data of reference 1 compared with various idealizations of the Ising model. Upper curve: $\eta^2 = [1 - (\sinh (T_1/T))^{-4}]^{1/4}$, exact Ising-model square-lattice result in two dimensions. Lower curve: $\eta^2 = [1 - (\sinh (T_1/T))^{-3}]^{2/3}$, an approximate global description of the three-dimensional simple-cubic-lattice Ising-model result (c.f., figure 3). Middle curve: equation (1) of text.

13
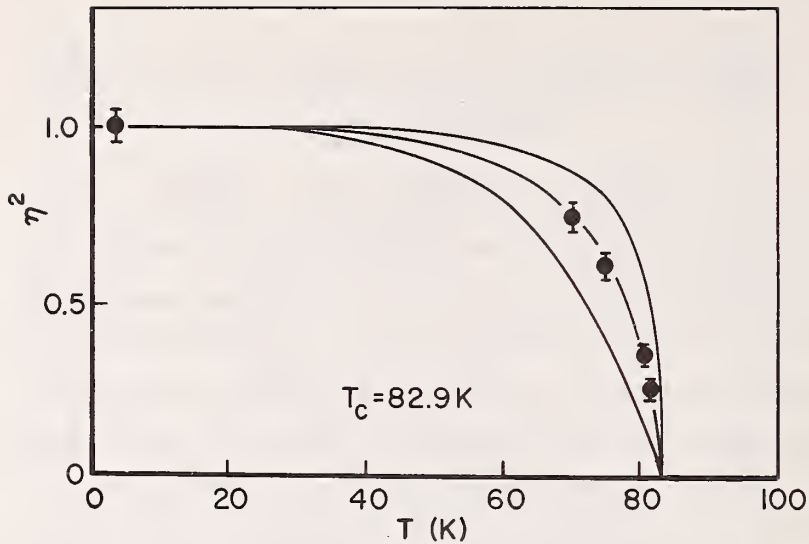
Figure 2. Data from reference 1 compared with Ising model predictions:
lattice symmetry corrections. The CN^- sites lie in a slight
orthrombic distortion of what would otherwise be face-
centered-cubic positions. Here the quasi-f.c.c. structure
of the lattice is taken into account. Upper curve: Two-
dimensional square lattice as in figure 1 (for comparison).
Lower curve: η^2 for f.c.c. Ising lattice, as calculated
numerically.[2] Middle curve: the square root of the lower
curve.
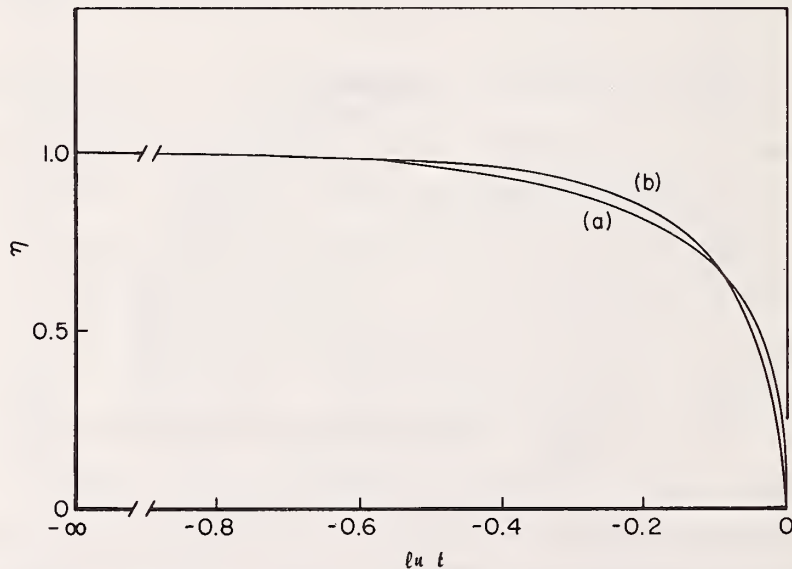
Figure 3. Comparison of the approximate analytical expression (a)
$\eta = [1 - (\sinh (t_1/t))^{-3}]^{1/3}$ for the three-dimensional
simple-cubic Ising lattice with (b) numerically calculated
extrapolations of same.[2]   ($t = T/T_c$, $t_1 = T_1/T_c$)

14

(see figures 1-3). Since T_c (= 82.9 K) is determined from specific heat measurements, there are *no free parameters* in these fits. The physical origin of this "anomalous-dimensional" behavior is not clear, but is possibly associated with long range aspects of the forces, not included in the Ising model.

----

1. J. M. Rowe, J. J. Rush, E. Prince, and N. J. Chesser, elsewhere in this report.

2. D. M. Burley, *Phil. Mag.* **5**, 909 (1960).

NEUTRINO SCATTERING

R. C. Casella

The neutrino, postulated by Pauli in 1930 to save the principles of conservation of energy and momentum in nuclear β decay and experimentally confirmed by Reines, Cowan, and coworkers using a fission-reactor source of electron antineutrinos $\bar{\nu}_e$ in the period 1950-1960, is a unique probe of matter over a range of scales differing by at least 24 orders of magnitude. Because of its weak interaction, the neutrino carries information from the interior of stars ($R_\odot \sim 10^9$ m) as well as entering deep into nucleons ($r < 10^{-15}$ m), where the next layer of building blocks (postulated quarks and partons) can be probed. By modifying the quark-parton model of Feynman and of Bjorken and Paschos in the so-called wee region of the kinematic variable x, I have been able to account quantitatively for the high-y anomaly in antineutrino-nucleon scattering experiments, the rise in the ratio of antineutrino to neutrino charged-current cross sections with energy, and qualitatively to explain the surprising high-strangeness multiplicity associated with neutrino-induced μe production. [μ = muon and y is the fractional energy loss in the laboratory frame of the lepton in the
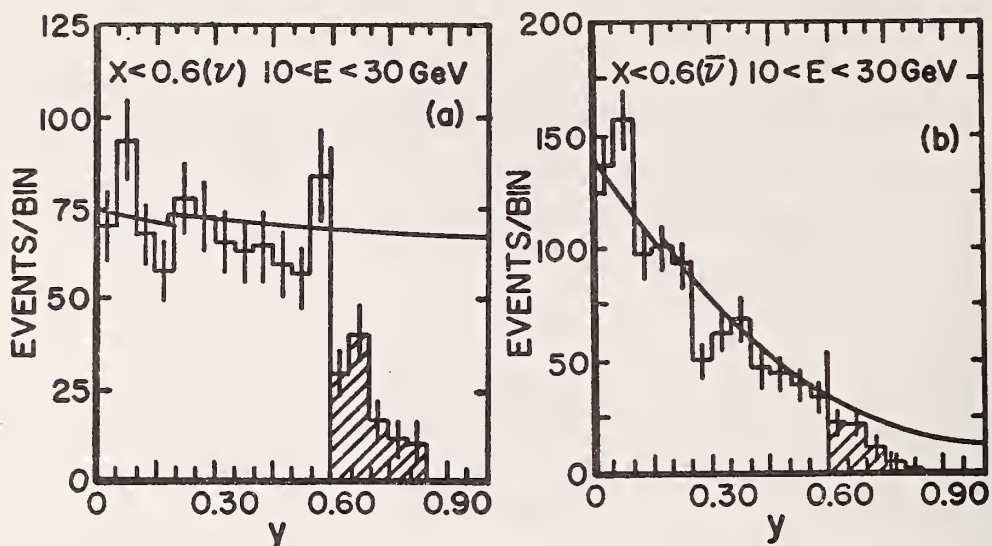
Figure 1.   dσ/dy vs. y for νN and ν̄N scattering. Experiment, as labeled. Theory, E = 20 GeV, normalization relative to data arbitrary. Data from references 1 and 2. Cross-hatched regions indicate detection-efficiency corrections incomplete.
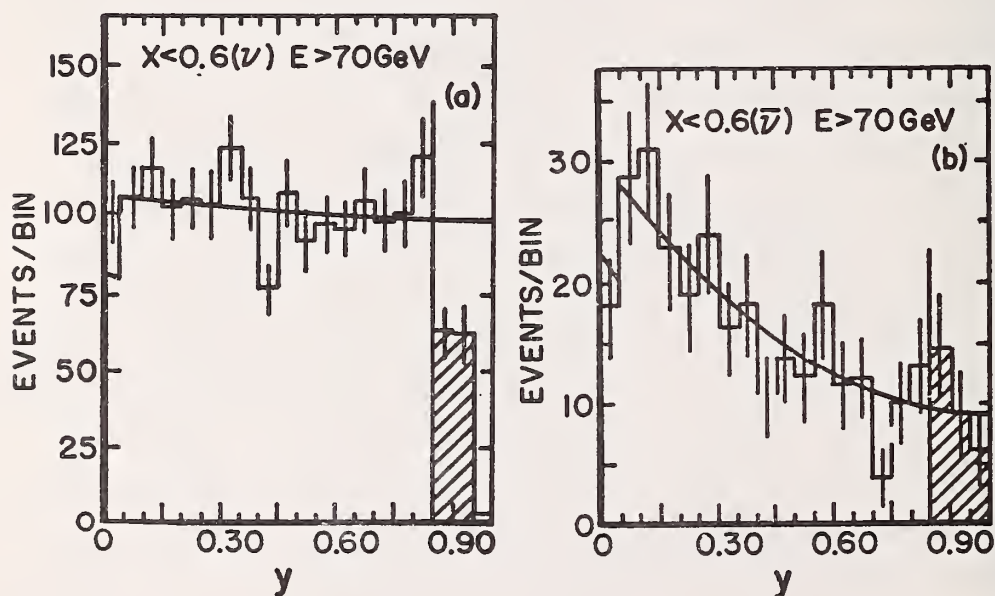
Figure 2.   dσ/dy vs. y for νN and ν̄N scattering. Experiment, as labeled. Theory, E = 100 GeV, normalization relative to data arbitrary. Data from references 1 and 2. Cross-hatched regions require further data reduction.
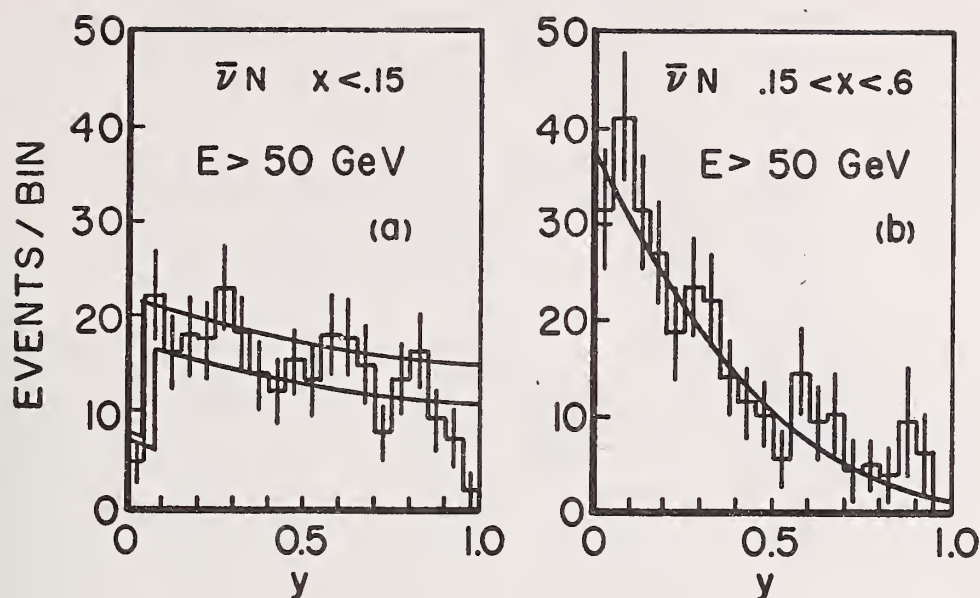
Figure 3.   dσ/dy vs. y for ν̄N scattering (a) in small x region only,
(b) excluding x < 0.15.   Experiment, as labeled.   Theory
(a) upper curve, E = 100 GeV, lower, E = 50 GeV, x < 0.14,
normalization *fixed* relative to that in (b).   Theory (b)
all E > 10 GeV, 0.14 < x < 0.6, normalization relative to
data arbitrary.   Data from reference 2.

process, ν_μ + nucleon → μ^- + anything; i.e., y = $(E_\nu - E_\mu)/E_\nu$].
I have done so without the necessity of introducing right-handed
(V + A) currents not contained in the standard (V − A) version of
Fermi's weak interaction theory as formulated after the discovery of
parity violation in 1956 by Wu, Ambler, Hayward, Hoppes, and Hudson
at NBS.   Theoretical fits to the data[1,2] span an energy range, 10 GeV
to 150 GeV (see figures 1-4).
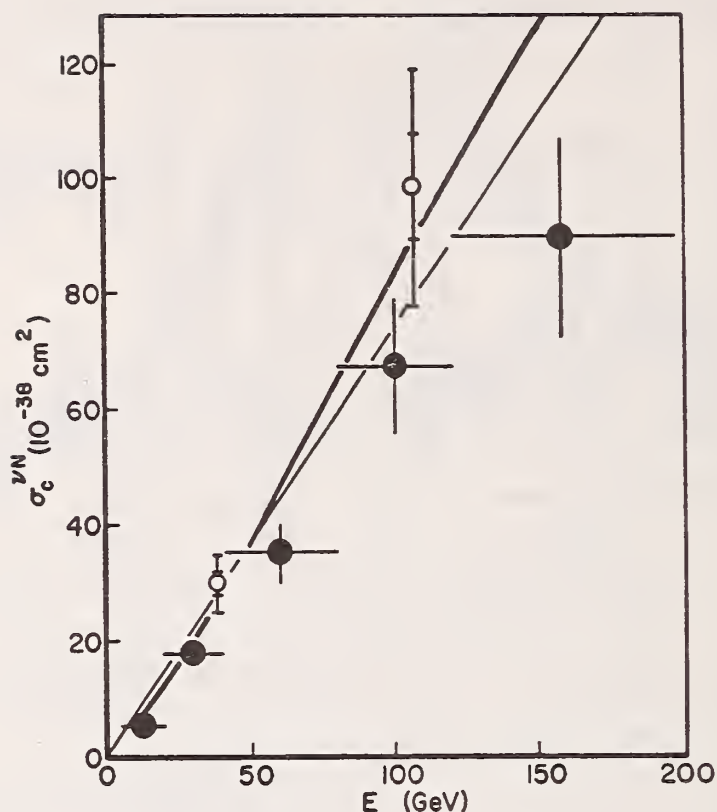
Figure 4. Absolute value of the total charged-current-induced neutrino-
nucleon cross section vs. energy. Theory, E > 10 GeV,
heavy curve. The straight line is an extrapolation from
lower energy Gargamelle data, not shown. Solid circles,
HPWF data, open circles, CF data.

---

1.   A. Benvenuti, *et al., Phys. Rev. Lett.* <u>36</u>, 1478 (1976).

2.   A. K. Mann, paper presented at Orbis Scientiae, Univ. of Miami,
      Coral Gables, Florida (1976).

SPIN WAVES IN FERRIMAGNETIC ERBIUM-IRON

J. J. Rhyne

and

N. C. Koon and J. B. Milstein
(Naval Research Laboratory, Washington, DC)

H. A. Alperin
(Naval Surface Weapons Center, White Oak, MD)

The group of compounds RFe_2, where R is a heavy rare earth, crystal-lize in the close-packed Laves phase or $MgCu_2$ structure. These compounds have high Curie temperatures ($T_c > 550K$) and show extraordinarily large magneto-elastic interactions[1]. The iron moments are ferromagnetically aligned, and are antiparallel to the R moment (ferrimagnetic order). The iron moment as determined from both bulk measurements[1] and neutron scattering[2] on polycrystalline samples shows an anomalous reduction from the expected $2\mu_B$ to approximately $1.6\mu_B$. The rare earth moments have their free ion values.

We have studied the spin wave dispersion in $ErFe_2$ using inelastic neutron scattering and have compared the results to a theoretical model. Inelastic scans along three principal axis directions were made at room temperature (T_c for $ErFe_2$ = 574K)[4] on a single crystal approximately 0.5 cm^3 using a triple axis spectrometer.

$ErFe_2$ has 6 atoms per unit cell with the Er atoms arranged on sites of tetrahedral symmetry and the Fe atoms on octahedral sites. One thus expects six spin wave branches, one acoustic and five optic. As the results in figure 1 show, only three of these branches have energies easily studied by neutron scattering. The data in figure 1 for spin waves propagating in the [q,q,o] and [q,q,q] directions show isotropic spectra consisting of (1) an acoustic mode with no measurable anisotropy energy gap, (2) a very flat optic mode of energy 5.1 meV degenerate with the acoustic mode at the zone boundary and (3) a highly dispersive higher optic mode starting from an energy gap of 8.75 meV. This latter mode has quadratic dispersion ($\hbar\omega = D|q|^2$) in the q range shown with $D = 240$ meV-A^2 only slightly smaller than pure iron metal[5] ($D = 280$ meV-A^2)

and would represent the iron acoustic mode in the absence of rare earth spins and the R-Fe exchange interaction. This mode is shown over only a small portion of the Brillouin zone due to the very high energy transfers involved. The model calculation gives an energy of 172 meV at the zone boundary. The vanishing dispersion in the lower optic mode is a consequence of negligible Er-Er exchange in this compound; rather the Er simply sits in the molecular field from the iron spins. Data were also taken in the [q,o,o] direction which again indicated no evidence of a dependence of the dispersion on propagation direction.

A nearest neighbor interaction spin-wave model has been applied to explain the data of figure 1. The Hamiltonian included exchange and crystal field terms (the latter are negligible at room temperature) and had the form

$$H = \sum_{n,m} \sum_{i,j} 2J_{ij}^{nm} \vec{S}_i^n \cdot \vec{S}_j^m + H_{c.f}$$

where J_{ij}^{nm} describes the interaction between the i'th ion of spin S_i in cell n with the j'th ion of spin S_j in cell m (i and j thus range from 1 to 6 and n, m were restricted to only nearest neighbors). The spin wave energies were calculated from Fourier transforms of the equations of motion for the spin raising and lowering operators $S^{\pm} = S_x \pm iS_y$ as follows:

$$\hbar\omega(q) \ S^+_i(q) = -2\sum_{j=1}^{6} \langle S_i^z \rangle \ J_{ij}(q)S_j^+ - \langle S_j^z \rangle \ J_{ij}(o)S_i^+$$

where $J_{ij}(q) = \sum_{mj} J_{ij}^{nm} \exp[i\vec{q} \ (\vec{r}_{mj} - \vec{r}_{ni})]$

and the six equivalent relations for S^-. In fitting the spectra the spins on the Er and Fe atoms were fixed at 3.6 μ_B and 0.66 μ_B respectively as obtained from a combination of neutron diffraction and bulk magnetization data[1-2]. At the zone center the energies of the two optic modes are given simply by $\omega_1^{op} = 24J_{Er-Fe} \langle S_{Fe}^z \rangle$ and $\omega_2^{op} = 12J_{Er-Fe}(\langle S_{Er}^z \rangle - 2\langle S_{Fe}^z \rangle)$ respectively. These relations and the known values of $\langle S^z \rangle$ thus allowed the rare earth-iron exchange constant $J_{Er-Fe} = -0.32$ meV to be determined.
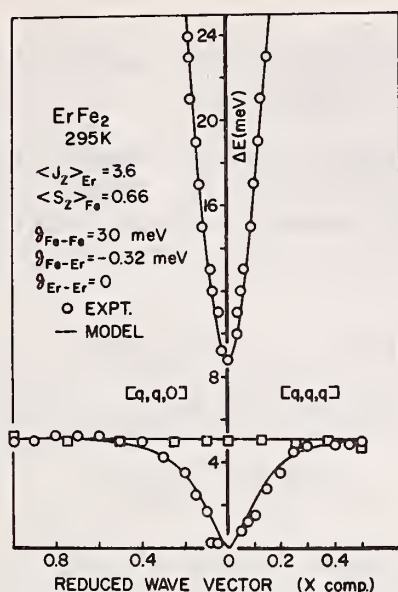
Figure 1. Magnon dispersion of $ErFe_2$ along [q,q,o] and [q,q,q] symmetry directions. The solid line is the result of a nearest neighbor spin wave calculation.

The remaining exchange constant J_{Fe-Fe} = 30 meV was adjusted to obtain the correct dispersion in the higher optic mode. These values were similar to those for the analogous compound $Ho_{.88}Tb_{.12}Fe_2^3$. J_{R-R} is equal to zero in both cases to an accuracy of approximately $\pm.01$ meV as determined from the maximum dispersion in the lower optic mode. Within the restricted q-range of the higher energy data, this model fits the experimental results extremely well. Its success in predicting accurately the E and q dependence of the remaining magnon branches is not known.

The measurements are currently being extended to lower temperatures to examine the effects of the strongly enhanced anisotropy and magneto-elastic interaction on the spin wave spectrum.

1. A. E. Clark, A.I. P. Conf. Proc. Series 18, 1015 (1974).

2. J. J. Rhyne, to be published; M. O. Bargouth and G. Will, *Journal de Physique* C1 32, 675 (1971).

3. R. M. Nicklow, N. C. Koon, C. M. Williams, and J. B. Milstein, *Phys. Rev. Letters* 36, 532 (1976). (Note: Due to a difference in definition of the Hamiltonian, exchange constants quoted in this reference are larger by a factor of two than those in the present paper.)

4. E. Burzo, Z. Angew, *Phys.* 32. 127 (1971).

5. H. A. Mook and R. M. Nicklow, *Phys. Rev.* B 7. 336, (1973).

ORDER-DISORDER IN V_3 Ga

J. J. Rhyne
and
B. N. Das and R. A. Meussner
(Naval Research Laboratory, Washington, DC)

It is known that the superconducting transition temperature of compounds of stoichometry near V_3Ga can be varied by appropriate heat treating. In an effort to discover if a correlation exists between the T_c and the degree of atomic order of the V and Ga atoms a neutron diffraction study was undertaken of several samples of different heat treating and also of slight composition variation from stoichometric V_3Ga. Neutrons are significantly superior to x rays for this type of investigation due to the very similar x-ray scattering factors of V and Ga which makes separate site occupancy factors difficult to determine. In the neutron case V and Ga scattering amplitudes have opposite signs and differ by more than a factor of 10.

Initial results have indicated that compounds even in the "as cast" state are highly ordered with long range order parameters as high as 0.95 and that heat treatment annealing at 1400° C produces only a slight increase in the long range order parameter while it lowers the super-conductivity transition temperature by about 0.5 K.

As a result, first indications suggest that the variations in T_c are not strongly correlated with long-range crystallographic order in V_3Ga and certainly that T_c does not increase with crystallographic order as previously predicted.

APPLICATION OF ROBUST/RESISTANT TECHNIQUES TO CRYSTAL STRUCTURE REFINEMENT

W. L. Nicholson
(Battelle Pacific Northwest Laboratories, Richland, WA)

and

E. Prince

A technique for fitting a theoretical model to a set of experimental data points and estimating the best values of adjustable parameters in the model is said to be "robust," or, more precisely, "robust of efficiency," if the parameter estimates have near minimum variance for a broad class of distributions for the errors in experimental data. A technique is "resistant" if the estimates are not highly dependent on any small subset of the experimental data. To date, all techniques that are robust of efficiency are also resistant. Many data analysts feel that this is inevitable, hence, the splice word, robust/resistant.

The technique of least squares, the one most commonly used for refining crystal structures, is neither robust nor resistant. Least squares was designed specifically by Gauss for normally distributed errors. With broad-tailed error distributions and/or the presence of a few bad data points in a large data set, least squares can give anomalous results. In recent years, statisticians have been developing methods of fitting and parameter estimation which work nearly as well as least squares for ideal data sets, but which are robust/resistant. The purpose of this research is to apply these methods to crystal

structure refinement, both as a non-trivial test of the robust/resistant approach and as a development in calculational crystallography.

The technique of least squares is based on finding the minimum value of the quantity $\sum_i w_i (y_{io} - y_{ic})^2$, where y_{io} is the value of the observed data, y_{ic} is a calculated value of that point based on some theoretical function containing adjustable parameters, and w_i is a weight. For the method to work well, the weight, w_i, must be proportional to $1/\sigma_i^2$, where σ_i^2 is the variance of the observation y_{io}. This variance is, however, usually not known *a priori*, but is approximated by a formula containing a term arising from an assumed Poisson distribution of random counts and one or more other terms which estimate additional experimental error associated with the observed value, y_{io}.

Tukey[1] describes a robust/resistant alternative to least squares estimation which is particularly attractive for crystal structure refinement. In the least squares program, the response of a refinement is modified by adjusting the weight according to the formula $w'_i = w_i W(x)$, where $x = (y_{io} - y_{ic})/K\hat{\sigma}_i$. $\hat{\sigma}_i$ is the standard deviation approximation described above and K is a robust/resistant estimate of scale. The function $W(x)$ is called a "W-function." Characteristics that a W-function should have in order to create a robust/resistant refinement are discussed elsewhere by the authors.[2] To perform the refinement, an initial set of parameters is used to form normalized residuals $r = (y_{io} - y_{ic})/\hat{\sigma}_i$. These are used to construct K. Independent work of Andrews[3] and Beaton and Tukey[4] suggest a K of 6 times the median absolute residual. With K specified, $W(x)$ is calculated and the weighted least squares iteration performed. After each iteration, K is recalculated as above.

The crystallographic least squares program RFINE4[5] was modified to include, as options, several different W-functions. One of these W-functions was used to investigate the operational characteristics of the robust/resistant approach using a lead deuterium orthophosphate

data set. The details of the investigation are described elsewhere.[2,6]
A second option is the biweight W-function $W(x) = (1-x^2)^2$ $(|x| \leq 1)$;
$= 0$ (otherwise).

RFINE4 with the Tukey biweight W-function is being used to
repeat the refinements of the structure of D(+) tartaric acid originally
carried out by Hamilton and Abrahams[7] as part of the single-crystal
intensity project of the International Union of Crystallography.
Three of the 17 experiments considered by Hamilton and Abrahams,
selected on the basis of reasonably large numbers of reflections,
have been analyzed so far. The refinement for each data set has
three stages: 1) attempt to "recreate" the results of Hamilton and
Abrahams by repeating as closely as possible the condition of their
refinements; 2) add secondary extinction to the classical weighted
least squares refinement; and 3) incorporate the biweight W-function
and do a robust/resistant refinement. The results of Hamilton and
Abrahams are not reproduced exactly, possibly because of small
differences in the handling of atomic scattering factors in the
original refinement. Inclusion of the Zachariasen model for secondary
extinction significantly improves the refinements of all three experi-
ments. Inclusion of the biweight function again significantly improves
the refinement with weighted r indices decreasing by up to 40%.

Based on the refinement of these three experiments, the robust/
resistant approach looks very promising. Individual atom positions
and thermal vibration parameters agree more closely than in the
original analysis. For each experiment, a small fraction of the data
fail to fit the robust/resistant estimated model and, hence, are
identified as extreme outliers. These outliers can be identified on
theoretical grounds as very imprecise reflections. For example, for
one experiment the extreme outliers were mostly weak reflections.
Such residual patterns suggest that the biweight approach succeeds in
minimizing the influence of poor data on the refinement. The above
work was reported at the 1976 winter meeting of the American Crystallo-

graphic Association, Clemson, SC. A written version is being submitted for open literature publication.

Work is now in progress on refinement of the remaining experimental data sets reported by Hamilton and Abrahams. Several of their refinements give very discrepant individual atom parameter estimates. Elimination or a least reduction of these discrepancies would establish robust/resistant techniques as a viable approach to crystal structure refinement.

1. J. W. Tukey in Critical Evaluation of Chemical and Physical Structural Information, National Academy of Sciences, Washington, DC, 1974.

2. E. Prince and W. L. Nicholson, NBS Tech. Note 896 (1976).

3. D. F. Andrews, *Technometrics*, 16, 523 (1974).

4. A. E. Beaton and J. W. Tukey, *Technometrics*, 16, 147 (1974).

5. L. W. Finger and E. Prince, NBS Tech. Note 854 (1975).

6. C. S. Brickenkamp and E. Prince, NBS Tech. Note 860, 55 (1975).

7. W. C. Hamilton and S. C. Abrahams, *Acta Cryst.*, A26, 18 (1970).

A FLAT-CONE DIFFRACTOMETER UTILIZING A POSITION-SENSITIVE DETECTOR

E. Prince, J. C. Norvell, and A. Santoro

The use of flat-cone geometry to take advantage of linear position-sensitive detectors for single crystal neutron diffractometry was described in last year's progress report.[1] An instrument employing these principles is under construction. The detector itself has been received and tested, and most of the electronic components are in hand. Work on hardware and software is proceeding.

1. E. Prince and A. Santoro, NBS Tech Note 896, 17 (1976).

CONVERSION OF THE SPECTROMETER CONTROL SYSTEM TO THE DECLAB 11/40

E. Prince, J. J. Rhyne, J. M. Rowe

and

S. F. Trevino
(Picatinny Arsenal, Dover, NJ)

It was apparent several years ago that the existing data acquisition system for controlling beam tube experiments would be inadequate for controlling the new 4-axis spectrometer being installed at BT-4. More recently, various developments made it desirable to phase out the existing system, which was installed in 1967, and which was based on obsolete equipment that was becoming more and more difficult to maintain adequately. After extensive consideration of the alternatives, the new system chosen was a Digital Equipment Corporation DECLAB 11/40, supplemented by an industrial control subsystem (ICS-11) provided by the same manufacturer. A major effort to adapt a DEC supplied operating system (RSX11M) so that it could handle spectrometer and diffractometer operations was nearly complete at the end of the year. Most of the task of adapting user programs to the new system was also complete, and the work of rewiring the instruments was proceeding. It is anticipated that the conversion will be complete well before the end of calendar year 1976.

The new operating system possesses much greater flexibility than the existing system. It can accommodate an arbitrary number of motors for each instrument, and also an arbitrary number of detector scalers. Furthermore, it is now possible to do program development, including compiling and linking of programs and editing of source text, without interrupting the data collection process.

THE NEUTRON RADIOGRAPHY PROGRAM

D. Garret, H. Berger, M. Ganoczy, M. Dorsey

and

W. Parker
(Reed College, Portland, OR)

The goals of the Neutron Radiography Group of the Reactor Radiation Division are to develop neutron radiographic standards, techniques and hardware and to participate in the National Bureau of Standards Nondestructive Evaluation Program. In these capacities, the group provides assistance to both the public and private sectors in the development of neutron applications.

Accomplishments of the Neutron Radiography Group during the past year consist of a number of collaborative efforts with outside agencies in the public sectors. Internal efforts have been devoted to the development of three dimensional laminagraphy, three dimensional image enhanced laminagraphy, extensive beam diagnostics on the thermal column, modifications to the thermal column beam facility and fabrication of the new vertical beam facility. Preliminary conceptual design work has been completed on the external hardware for both the thermal and fast vertical facilities.

1. Three-Dimensional Inspection by Thermal-Neutron Laminagraphy

Radiographic inspection of thick, complex objects presents problems because overlaying radiographic shadows from different object depths complicate interpretation and because it is often difficult to assign an object depth to an observed shadow. Three-dimensional (3-D) radiographic methods including computerized image reconstruction optical and holographic methods, and multiple-film laminagraphy mimimize these inspection problems. In this work, multiple-film laminagraphy has been demonstrated with thermal neutrons, thereby expanding the capability of neutron radiography to inspect complex objects.

In this technique, radiographic views from several angular orientations are obtained and superimposed to bring a desired object image plane into registration (focus) while information from other planes is blurred. New developments reported here include the use of thermal neutrons as the imaging radiation and the rotational movement of the object-detector assembly as opposed to the usual translational source movement to obtain the angular views.

One object used to demonstrate the method was a simulated EBR-II fast reactor fuel subassembly. A hexcan, 5.7 cm across the flats, normally holds 91 rod-shaped fuel elements in 11 rows. For our tests the can was filled with solid aluminum rods and occasional Bakelite rods. These neutron attenuating rods were used to demonstrate spatial resolution at various locations in the assembly. To aid in that determination several through holes varying in size from 0.5- to 2.5- mm diam were drilled in each Bakelite rod.

Thermal-neutron radiograph of the fuel subassembly were obtained over a 40-deg angular coverage, with a 5-deg rotation between exposures. These nine individual neutron radiographs were viewed superimposed to focus on any desired plane. Since it is necessary to view through all the films, a light exposure on each film (typical density 0.4) and a clear base are desirable. This was accomplished by one of two methods. In one approach the neutron radiographs were obtained on a clear base x-ray film.   In the other, neutron radiographs were obtained with conventional x-ray film; the films were then copied on clear-base graphic arts film (Kodak types 6127 and 4135 were used). In both cases, neutron radiographs were prepared with gadolinium vapor-deposited screens in vacuum cassettes.

Figure 1 pictures example of two laminagraphic views from these tests. The results show that one can focus on individual fuel rows and that detail as small as 0.5 mm can be resolved in the hexcan assembly. In tests with a high-contrast cadmium test object, a spatial resolution of 0.25 mm was obtained for a similar thickness object.
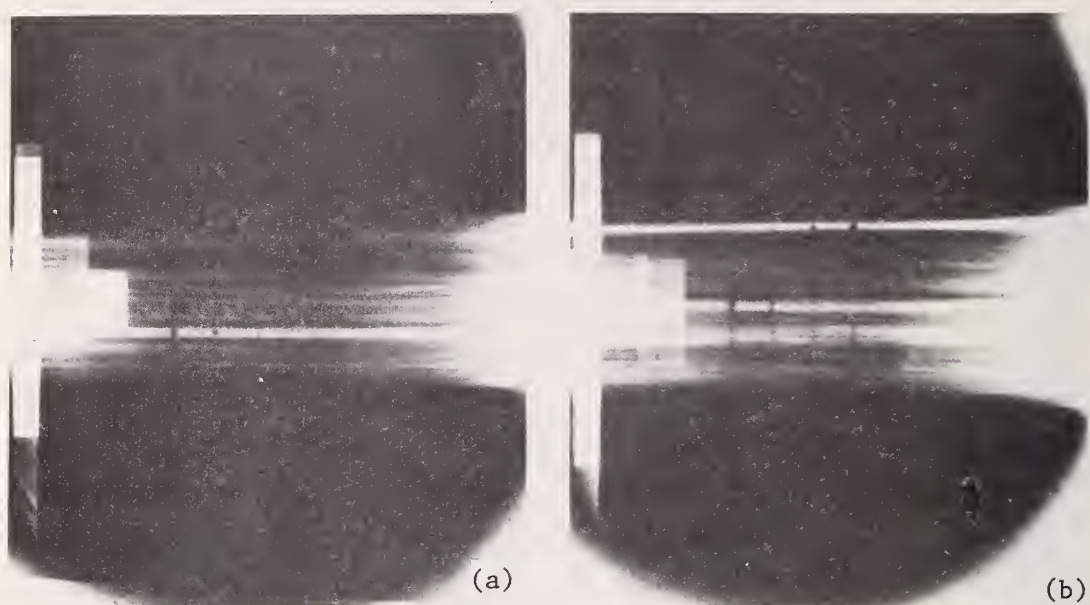
Figure 1. Photographs of 9-film thermal neutron laminagrams of an EBR-II fuel subassembly hex-can containing aluminum and Bakelite rods instead of fuel. View a focuses on a plane adjacent to one hex-can face and shows a single Bakelite rod in focus; four holes 2.5 mm, 1.5 mm, 1.0 mm and 0.5 mm (left to right) are detectable. View b focuses on the middle row of simulated fuel rods; one Bakelite rod is in focus. Three holes (1, 1.5 and 2.5 mm in diameter) are visible on the print. Note the different images of the radiographic markers at the left of each view. These two laminagrams were obtained with one set of neutron radiographs.

Three-dimensional thermal-neutron radiography with a spatial resolution better than 1 mm can now be accomplished with a technique requiring minimum equipment investment. This broadens the application of thermal-neutron radiography. The 3-D method will prove useful for assembly inspection. Additional capabilities of isotopic differentiation and radioactive material inspection make this neutron laminagraphic method particularly attractive for nuclear problems.

2. Film Investigations

Work has continued on the investigation of the suitability for
neutron radiography of other emulsions than the standard x-ray emulsions.
Most of this work has been done with an electron-sensitive emulsion de-
veloped for transmission electron microscopy. This film is now produced
on a regular basis by Eastman Kodak as Type SO 163. It has from two and
a half to three times the speed of Type SR, depending on the development.
Qualitatively the resolution approaches that of SR, but a radiograph on
SO 163 does not have the "snap" of one of the same density done on SR.
The ratio of neutron sensitivity to gamma ray sensitivity is definitely
better than that for the double emulsion x-ray films.

We have also looked at the possibility of using graphic arts films
for neutron radiography. Generally these are high contrast emulsions
with extremely fine grain with resulting high resolution. They are also
single emulsion on a clear base. With proper development they will pro-
duce a gray scale satisfactorily. Preliminary work indicates that the
ones tried so far are much too slow when used with a gadolinium foil con-
verter to be useful. There does appear to be a possibility that they
can be used for certain applications with a scintillating screen such as
^{6}LiFZnS:Ag or Gd_2O_2S:Tb. They may also be useful for neutron lami-
nagraphy where low density and a clear base are required.

3. Image Enhancement

A Spatial Data Image Enhancement system has been installed and
placed in operation in the image analysis laboratory of the Neutron
Radiography Group. The purpose of this unit is to perform various op-
erations on the radiographic image which causes subtle details to become
more easily visible to the eye. This image enhancement system operates
strictly in the analog mode, utilizing a standard video camera and moni-
tor. The signal from the video camera is routed to the enchancement
circuitry which manipulates the image in such a way that it can be dis-

played in one of three ways, i.e. (a) edge enchancement in which the first derivative of the black and white image is displayed, (b) a normal enlargement of the original image is displayed and (c) color enhancement in which the shades of gray of the radiograph are divided into the hues of twelve colors. A standard radiographic image is illustrated in figure 2. Color enhanced and edge enhanced images of this radiograph are illustrated in figure 3 and figure 4 respectively.
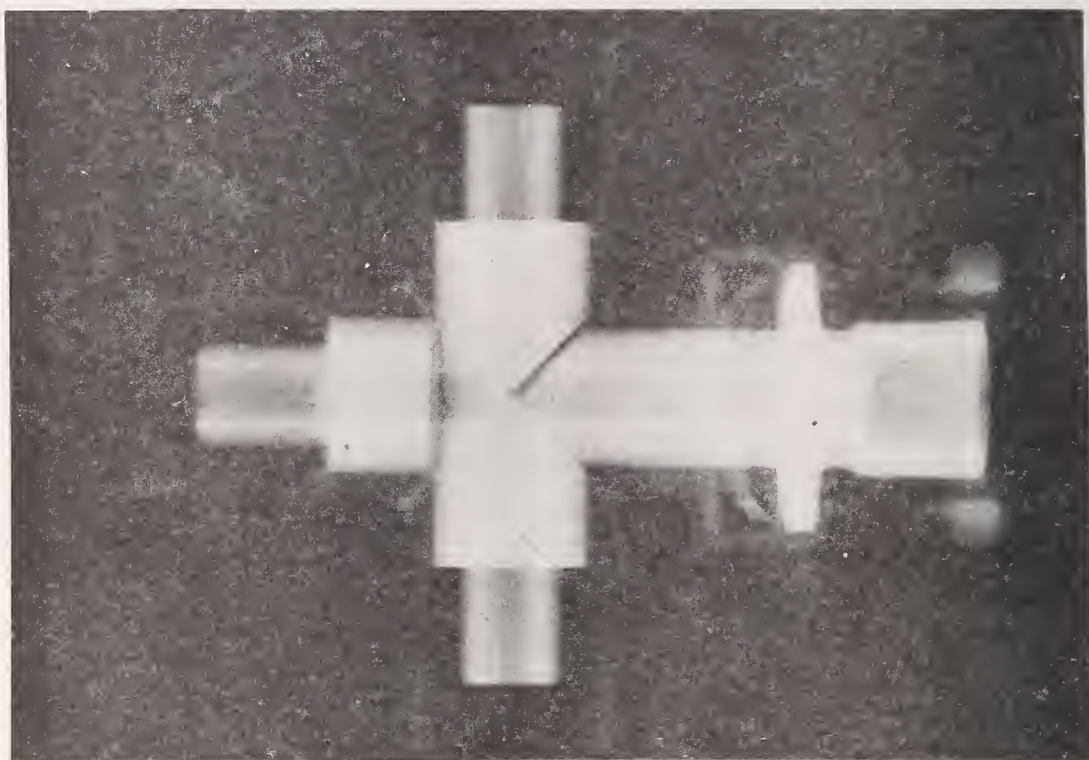
Figure 2. Normal neutron radiograph, no image enhancement.
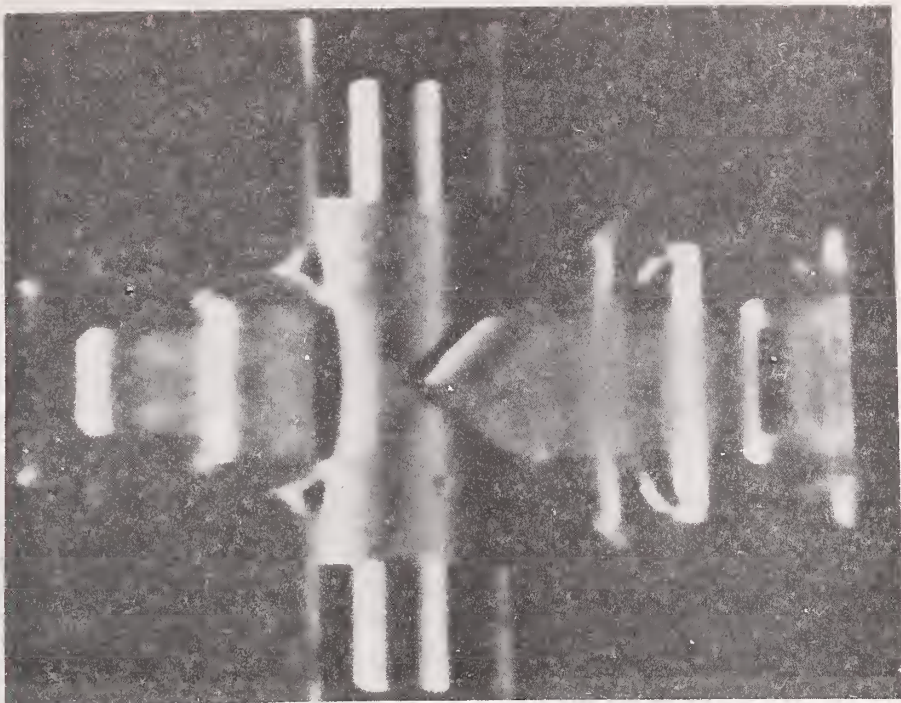
Figure 3.   Neutron radiograph, edge enhancement mode.
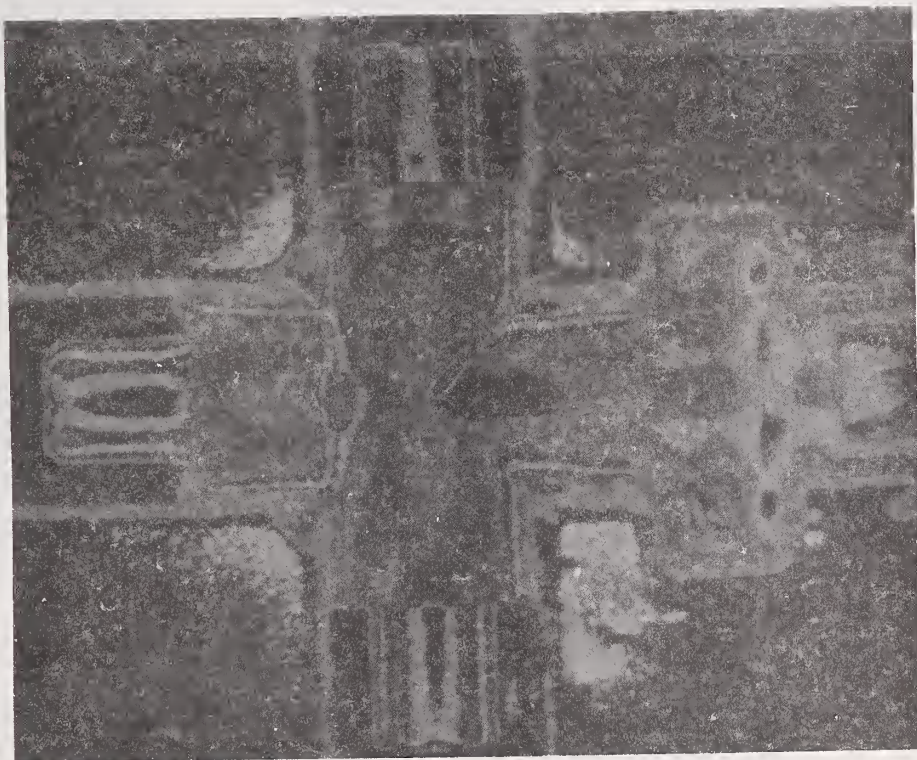
Figure 4.   Neutron radiograph, color enhancement mode.

4. Image Enhanced Laminagraphy

A successful demonstration has been made to adapt the color image enhancement system to three dimensional laminagraphy viewing. The video camera of the image enhancement system views the laminagraph image as the depth below the surface of a test object is viewed. As the layer image comes into view, the enhanced image of the structure under observation is displayed on the video output of the enhancement system.

The method can be employed to view complicated structures or it can be employed to view in three dimension microstructure below the surface of components. Figure 5 illustrates microshrinkage below the surface of a stainless steel casting covering a depth of approximately 1/4 in. in equal depth steps.
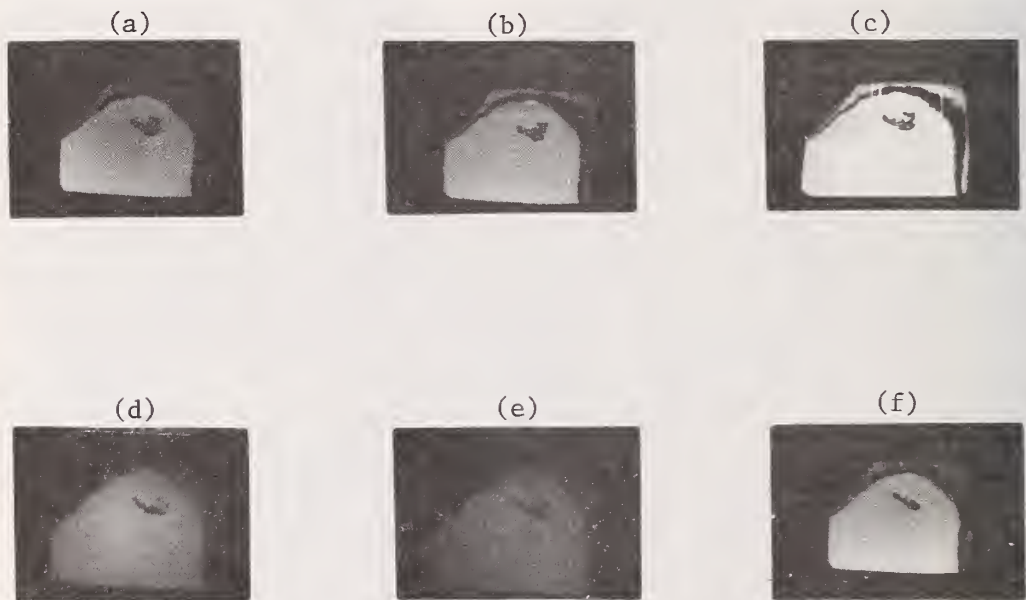
Figure 5. Color enhanced laminagraph microshrinkage in stainless steel casting showing the shape of the cavity at various depths below the surface.

34

5.   Pacemaker Studies

The Food and Drug Administration requested the group to investigate the feasibility of using neutron radiographic techniques to inspect pacemakers and the individual components used in their manufacture. Specifically, the FDA hoped to have developed a method for detecting leaks between the insulation surrounding the electrodes and the seal entering the pacemaker module. A second series of studies was to be conducted on neutron radiography of mercury and lithium iodide batteries used to power the pacemaker.

a. Seal Leakage Studies

The pacemaker was inspected by neutron and x-radiography in an attempt to visualize water that had been injected between the module seal and the electrode insulation. Neither technique could be used to visualize details of the water. In the case of neutrons, the hydrogen content of the insulation was probably very close to that of the water. In the case of x rays, the density of the insulation was possibly very close to that of water.

b. Mercury Cell Studies

A set of two new and four depleted mercury cells were radiographed with neutrons and x rays. Two views of the cells were taken for each specimen - one view along the cell axis and the other at right angles to the cell axis. A schematic diagram of a typical cell is illustrated in figure 6.

In the case of neutron radiography good detail could be visualized in the views taken down the cell axis; some detail could be visualized but not as satisfactorily at right angles to the axis. In both cases, migration of the mercury toward the cell axis could be observed in the depleted cells, but not in the unused cells. The new cells could unambiguously be identified by the absence of the mercury migration.

CERTIFIED CELL
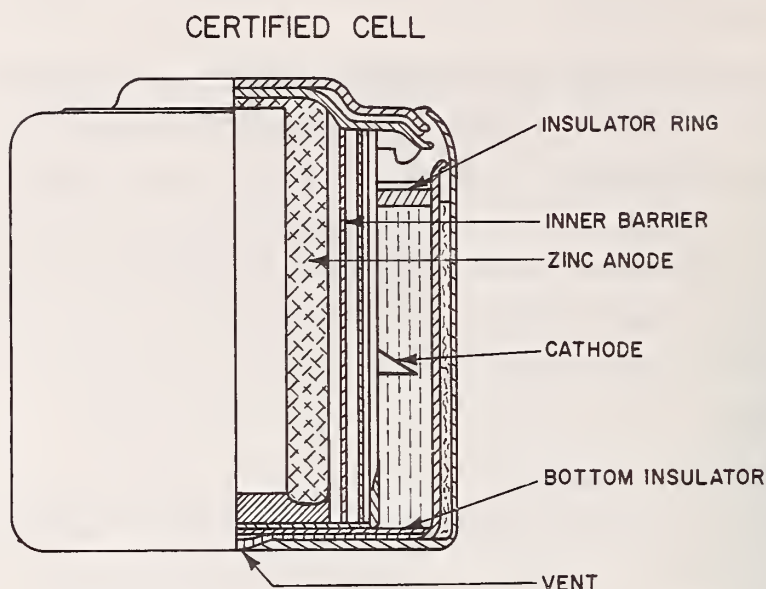
Figure 6.   Schematic diagram of mercury cell for pacemaker application.

The mercury cells were x-rayed at an optimum energy. Although no detail could be observed in the right angle shots, mercury migration could be observed in the axial x-rays of the depleted cells.

The possibility of a microbeam neutron or x-ray transmission measurement along the cell axis to determine remaining battery life remaining in the cell appears to be a real one. No method exists to produce this specification at this time. A microbeam gamma ray backscatter gauge could possible be considered for insitu measurements.

c. Lithium Battery Studies

Lithium batteries are being seriously considered as power sources for pacemakers because of their long life - 13 years as compared to 5 years for a mercury cell. X-radiography is unsatisfactory for lithium battery evaluation because of the double stainless steel case and the relativley low atomic number of the materials used in the electrolyte.

With neutrons it was possible to observe a phenomenon which appeared to be a function of cell life. This apparent electrolyte migration or
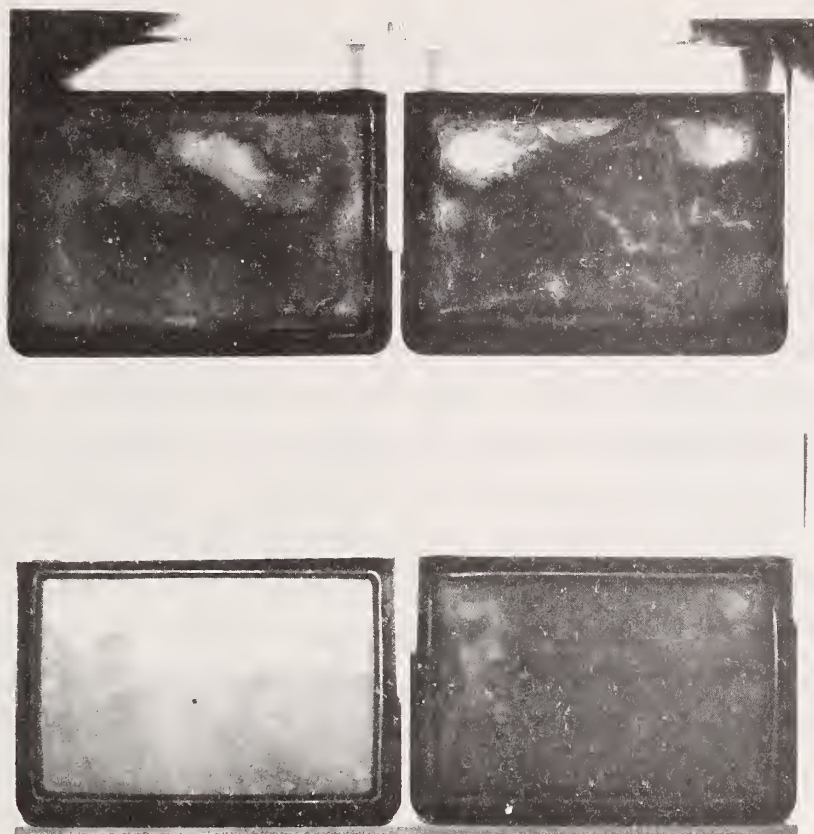
Figure 7. Neutron radiographs of lithium iodide pacemaker batteries
showing gas pocket formation as a function of depletion.

gas pocket production is not understood at this time. The cell is fab-
ricated in a slab geometry consisting of a rectangular lithium slab sand-
wiched between two slabs of iodine. As the battery becomes depleted,
lithium iodide is formed causing no change in the total attenuation to
the neutron beam.

A series of four lithium batteries was subjected to use tests
ranging from 10% to 105% of the expected life. Neutron radiographs of
the four units are shown in figure 7. It can be seen that as the use
factor increases, the formation of gas pockets appears to take place.
Further study on this project will continue once a set of new batteries
from the same manufacturing batch are received from the FDA.

6.   Pair Production Generated In Objects Under Inspection

A lack of contrast sensitivity has been observed from film fogging when thin Al (a few mils) window cassettes are used. We believe it is due to pair production products generated in the object under inspection. Presumably the radiation products generated do not possess great pene- trating power in Al since the effect caused by an object in front of the cassette appears to disappear when aluminum of 0.125 in thickness is employed as an entrance window. We attribute the effect to the high energy prompt gamma rays resulting from radiative capture of thermal neutrons in D_2 (6.2 MeV) and graphite (4.4 MeV). Experiments are in progress to determine the cause of the phenomenon and the effect it may have on cassette design.

The magnitude of the film fogging is illustrated in figure 8 which is a copy of a radiograph made in a neutron-free beam, i.e., when the thermal column curtain was in the closed position.

Figure 8.   Film fogging due pair production in specimen under inspection.

7.   Standard Measurements

Preliminary design work has been started on two standard measurements which will make it possible to compare individual neutron radiographic facilities. These standard measurements are:

1. Thermal Neutron to Gamma Ray Ratio

A means to measure the thermal neutron to gamma ray ratio of a neutron beam for radiographic purposes. At the present time, these measurements are made using a gold foil to measure the thermal neutron flux and TLDS to measure the gamma content. The gamma measurement is the most inaccurate since the presence of the neutrons has an effect on the readings.

The effect of the gamma ray content on the image recorder is the important factor to be considered, and not necessarily the mr content. Both the mr and the energy spectrum of the gamma beam will have an effect on the gamma film fogging.

We propose to accomplish this measurement using a standard package which will consist of a film in contact with a Gd converter screen sufficiently thick to stop the neutron beam. This will be backed by an aluminum filter sufficiently thick to stop the electrons generated by the Gd. A second film will be employed to determine the effect of the gamma ray content of the beam plus the effect of knock on protons created in the film base by fast neutrons. The ratio of these two numbers at the same front film density would be the meaningful number for comparison of facilities.

2. Beam Divergence Meter

One requirement that has been presented to the NBS Neutron Radiography group has been that of measuring the new beam divergence of a radiographic facility. Preliminary design work has been started on such a device which essentially measures the L/D ratio of the beam. The concept is illustrated in figure 9.
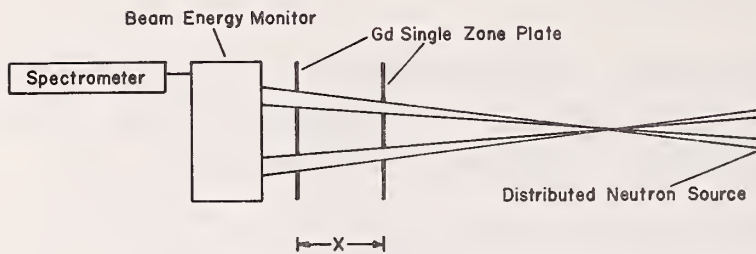
Figure 9.   Schematic diagram of the beam divergence meter.

8.   Facilities

Extensive modifications to the thermal column neutron radiography facility. Swellage of the magnetite concrete outer shield caused the collimator to shift, directing the neutron beam into neighboring experiments. A new outer shield box fabricated from 0.5 in. thick welded steel plate and filled with lead has been installed. Larger beam pipes have been designed into the new system to produce a larger beam and to run cryogenic cooling to crystal beam filters.
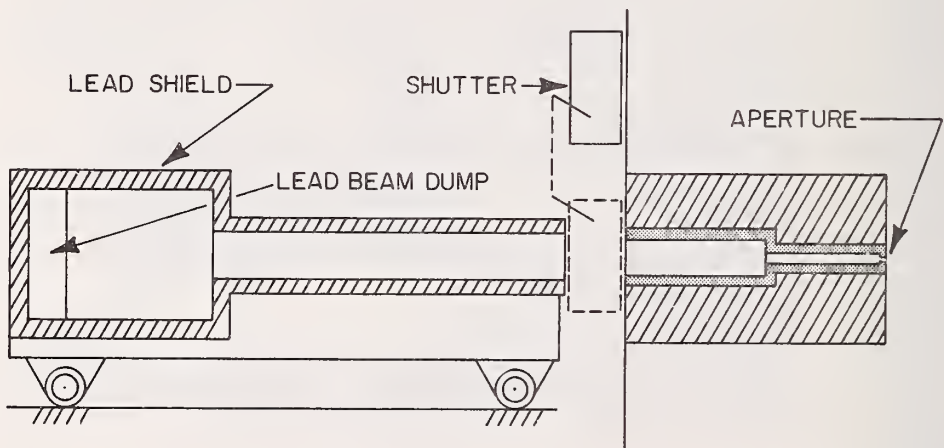
Figure 10. The components comprising the meter consist of a pancake fission beam monitor, two single zone plates of Gd, and the distributed neutron source. As C is moved in the direction of the source, the counts above background in the stop when the neutron beam can no longer be seen by the fission chamber. The distance x can then be used as a measure of the beam divergence.

40

Pinhole radiographs of the thermal column aperture have exhibited extensive haloing at the image plane. Further diagnostic work will be necessary to determine the cause of this effect.

A problem has arisen in that gamma scatter from the object being radiographed raise the background to an unacceptable level. A new lead lined cave is being designed to eliminate this problem. In addition, the design of a gravity-operated shutter mechanism for the thermal column facility A schematic diagram of the proposed shield and shutter is illustrated in figure 10.

THERMAL NEUTRON FLUX MEASUREMENTS

V. W. Myers and M. Ganoczy

Analysis of the data for calibrating boron loaded cobalt glass beads in a known thermal neutron beam is being completed. An unknown thermal flux can then be determined by comparing the Co-60 counting rate from a bead activated in the unknown flux to a calibrated bead.

SOLUTIONS OF THE KLEIN-GORDON EQUATION

V. W. Myers

The time-independent Klein-Gordon equation for a particle of rest mass m is $(E-V)^2\psi = (m^2-\nabla^2)\psi$. This equation is valid in the classical field limit for a spin zero particle, for example a Π meson in an external field. Solutions for ψ such as e^{-r}, e^{-r^2} have been investigated to determine if they conform to a real potential V over all space $0 \leqslant r \leqslant \infty$. There are rather stringent limitations on solutions because of the presence of $(E-V)^2$ rather than E-V of the non-relativistic Schrödinger equation. For example, e^{-r} corresponds to a real potential over all space, but e^{-r^2} does not. There are similar restrictions on solutions of the Dirac equation.

SEPARATION OF OVERLAPPING PEAKS IN NEUTRON
DIFFRACTION POWDER PATTERNS

A. Santoro

and

P. Brown
(Center for Building and Technology)

1. Method

Important applications of powder diffraction data, such as quanti-
tative analysis and determination of lattice parameters, lattice distor-
tions, crystallite sizes etc., are possible only if the patterns contain
a large number of single, non-overlapped peaks. This requirement consti-
tutes a serious limitation in most cases and, not surprisingly, attempts
have been made to circumvent the problem. In the case of x-ray diffrac-
tion the possibility of separating overlapping peaks has been analyzed
in detail, especially by Parrish and co-workers. A major difficulty in
the use of x-ray patterns is due to the fact that the x-ray peak shapes
are not well known and therefore cannot be accurately described by means
of a simple mathematical function. However because the neutron diffrac-
tion peak shapes are nearly gaussian, the treatment of overlapping re-
flections relatively simple in this case. The use of neutron powder
patterns for the characterization and the analysis of the crystalline
components of Portland cements has been considered in this laboratory
for this reason. With this approximation the total intensity y_i observed
at the angular position $2\theta_i$ is given by the expression

$$y_i = \sum_{1}^{m}{}_n \; y_{i,n} = \sum_{1}^{m}{}_n \left\{ a_n \left[1-p \frac{(2\theta_i-2\Theta_n)^2}{\tan\Theta_n} s \right] \exp \left[-b_n(2\theta_i-2\Theta_n)^2 \right] \right\}$$

where $y_{i,n}$ is the contribution of reflection n to the intensity measured
at $2\theta_i$, Θ_n is the Bragg angle of reflection n, a_n the peak height and
$b_n = (4\ln2)/H_n^2$ where H_n is the full width at half maximum (fwhm). P is
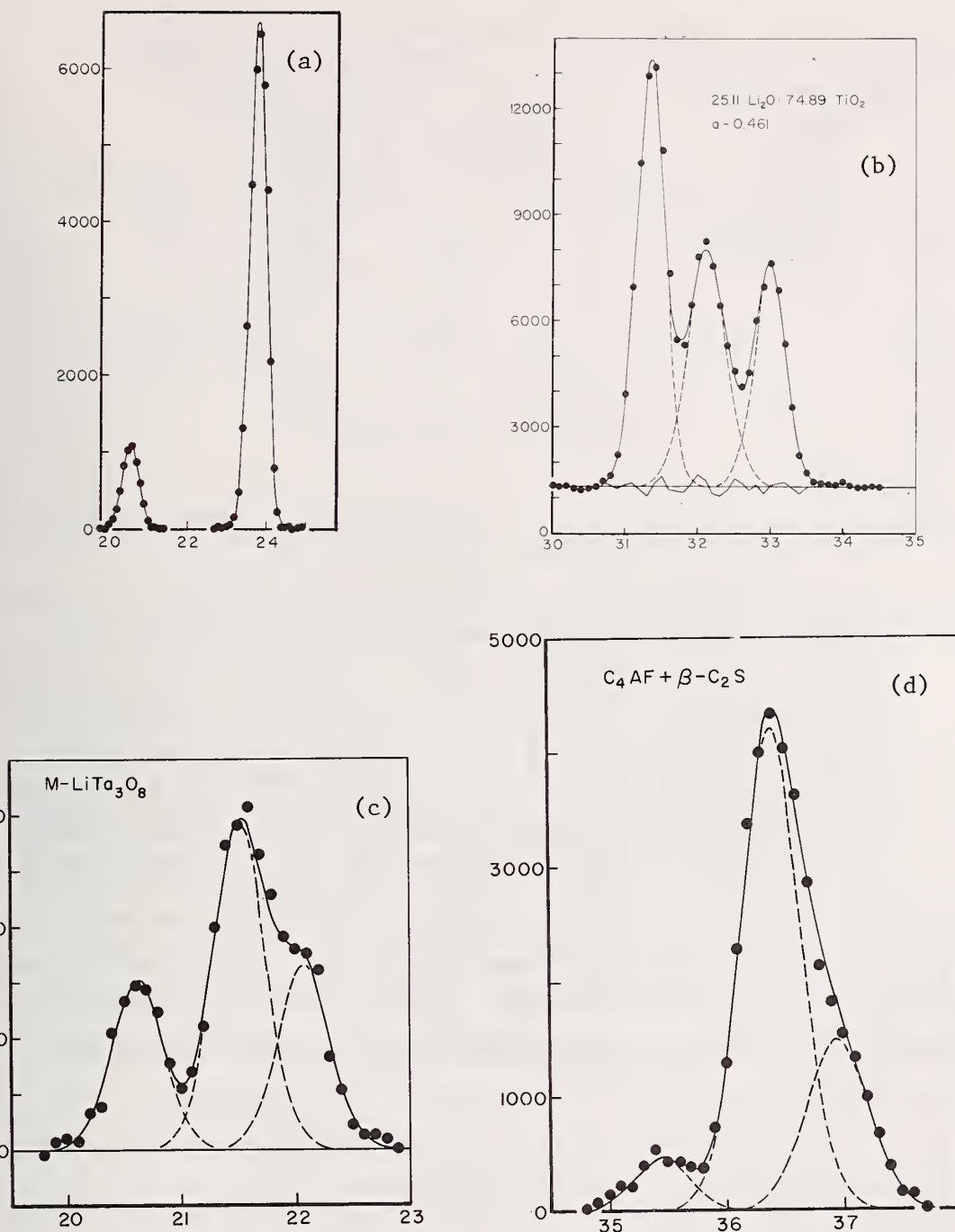
Figure 1.   Observed values (dots) and least-squares profiles (continuous lines) for the compounds indicated on each figure. The broken lines represent the separated gaussians. The experimental conditions are indicated on figure 1a. In all the figures the abscissas are the 2θ angles and the ordinates the number of counts.
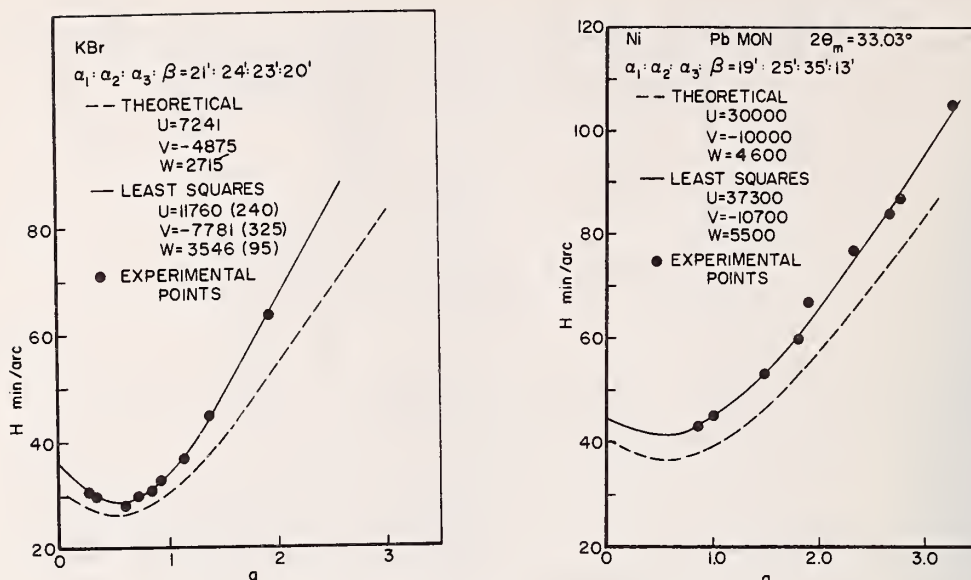
Figure 2.   Comparison between the theoretical and the experimental values
of the full widths at half maximum of neutron diffraction
peaks. The "experimental" points of figure 1a. have been ob-
tained by least-squared fitting of the peaks of KBr by assuming
gaussian shapes. The points of figure 1b. are those given by
Caglioti et al. (loc. cit.). The broken lines represent the
theoretical preditions according to the equation
$H^2 = U\tan^2\theta + V\tan\theta + W$. The continuous lines are the least-
squares lines through the experimental points. The parameter
a is given by $a = \tan\theta/\tan\theta_M$ where $2\theta_M$ is the take-off angle

the so called "asymmetry parameter", introduced to correct for the dis-

tortions caused by the vertical divergence and s = -1,0,+1, depending on

the sign of $2\theta_i - 2\Theta_n$. m is the number of reflections contributing to

the intensity y_i. A least-squares program has been written which mini-

mizes the function

$$F = \sum_{i=1}^{k} W_i \left[y_i(\text{observed}) - y_i(\text{calculated}) \right]^2$$

with respect to the parameters H, a, 2R and P of each reflection.   In

the above expression W_i are weights, assigned according to the expression

$W_i = 1/(y_i + \text{background})$. The main difference between Rietveld method

(*J. Appl. Cryst.*, 2, 65, 1969) and the one described here is that the

latter does not require any structural information.

44
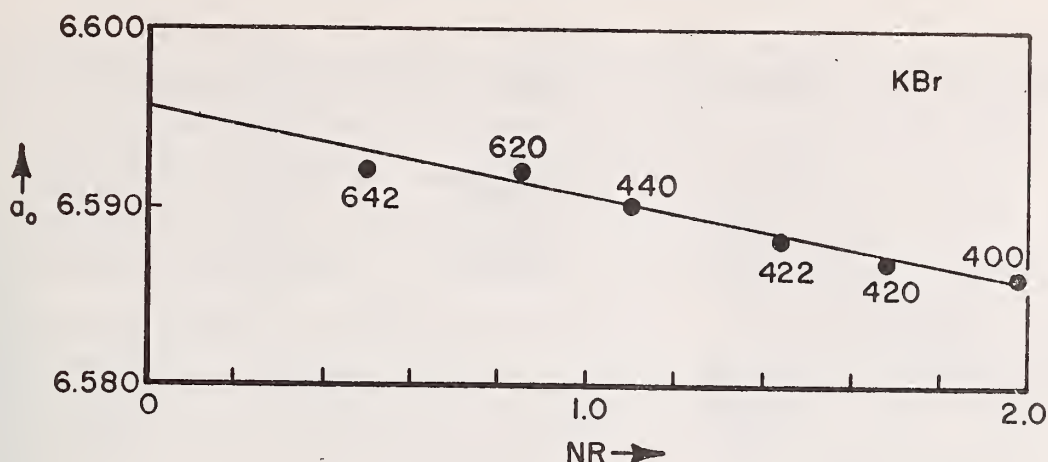
Figure 3. Lattice constant of KBr calculated from the indicated re-
flections and plotted against the function
$(\cos^2\theta)/\sin\theta + (\cos^2\theta)/\theta$. The extrapolated value of the
lattice parameter – a = 6.596 – is in good agreement with
the literature values which range between 6.596 and 6.599.

2. Results

Examples of the application of the least-squares program are illus-
trated in figures 1a, b, c, and d for cases of increasing degree of over-
lapping. The data obtained after refinement are given in table 1 and
compared, whenever possible, with the theoretical predictions.

The powder pattern of KBr contains good quality, non overlapped
peaks. Therefore, a detailed analysis of these peaks has been carried
out in order to clarify a number of questions related to the profile
fitting procedure proposed by Rietveld and now widely used. Preliminary
results of this study seem to suggest the following conclusions:

a. The neutron diffraction peaks are very nearly gaussian. The analy-
sis of all the peaks, however, shows that with our experimental arrange-
ment the least-squares fit results in a value of the R_W factor around
4–5%. This means that the so called "expected" R factor cannot be eval-
uated on counting statistics alone and that it is unrealistic to expect
structural refinements with R_W factors lower than 4–5%.

b. There is a discrepancy between the theoretical values of the full
widths at half maximum (fwhm) calculated with the procedure of Caglioti

Table 1. Results from the least-squares separation of overlapping peaks

	$2\theta_{LS}$	$2\theta_{THEORY}$	H_{LS}	H_{THEORY}
KBr	20.56°	20.53	30'	27'
	23.78	23.76	29	26
$R_W = 4.4\%$				
$25Li_2O:75TiO_2$	31.34		28	26
	32.12		38	26
	32.99		31	26
$R_W = 3.6\%$				
$M-LiTa_3O_8$	20.62	20.63	32	27
	21.51	21.51	32	27
	22.08	22.05	32	27
$R_W = 8.2\%$				
$C_4AF+\beta-C_2S$	35.45		33	26
	36.39		35	26
	36.94		37	26
$R_W = 5.2\%$				

et al. (*Nucl. Instr.*, 3, 223, 1958) and the experimental data. The nature
of the discrepancy is illustrated in figures 2a, b. These figures show
that the functional relationship between fwhm and dispersion parameter
seems to hold. It is clear, however, that more careful analysis of the
equation relating the fwhm and θ is required before we can apply with any
confidence the equation to a profile fitting procedure such as that of
Rietveld.

c. In figure 3 the lattice parameter of KBr obtained from each dif-
fraction line is plotted against the Nelson and Riley extrapolation func-
tion (Klug & Alexander, "X-Ray Diffraction Procedures," 2nd Edition,
Wiley, 1974, p. 594). While the choice of this function may not be quite
appropriate for our particular case, the figure shows clearly that the
peak positions are affected by systematic errors as in the x-ray case.
The nature of the systematic errors does not have to be necessarily the
same in x-ray and neutron diffraction, however. For example, the vertical

component of the eccentricity error cannot be eliminated experimentally in the neutron patterns (as it is done in the x-ray patterns) because this would require measurements of peak positions in the unfavorable anti-parallel geometry. According to our preliminary results, this error unfortunately varies with θ according to $\cos 2\theta \cot an\theta$, making it difficult to apply the ordinary extrapolation procedures. Another significant difference between x rays and neutrons is that in the latter case the problem of absorption is only rarely important, while in the former case is the major source of errors. The refinement procedure of Rietveld does not take into account systematic errors in the lattice parameters. The above results strongly indicate that this is another area where further study is required.

POWDER NEUTRON DIFFRACTION ANALYSIS OF THE CRYSTAL STRUCTURES OF $LiNb_3O_8$, $M-LiTa_3O_8$ AND $H-LiTa_3O_8$

A. Santoro

and

R. S. Roth and D. B. Minor
(Inorganic Materials Division)

The principles of the crystal chemistry of Li^+ in oxide structures is largely unknown, as this ion generally cannot be located with any accuracy by x-ray diffraction methods. However, neutron diffraction offers unique advantages over x rays in scattering of both Li^+ and oxygen and opens up the promise of learning some of the details of the Li-oxygen coordination scheme. The compound $LiTa_3O_8$ was found to be trimorphic (Roth et al. in Fast Ion Transport in Solids, p. 218, Ed. W. vanGool, North Holland Publish Co., Amsterdam, 1973). As the crystal structures of all the polymorphs are known in principle, it appeared that these three phases might be appropriate to use as a starting point in this study. However, the lowest temperature polymorph has never been synthesized as

a pure single phase, so the apparently isostructural compound $LiNb_3O_8$ was substituted. Stoichiometric $LiTa_3O_8$ was prepared from $LiTaO_3$ and Ta_2O_5, and converted to the M- and H-polymorphs by heating at 1025°C and 1200°C respectively. The $LiNb_3O_8$ was prepared from $LiNbO_3$ and Nb_2O_5 by reaction at 1100°C. All heat treatments were performed in open containers of pure platinum.

Neutron diffraction measurements were made at room temperature on a powder diffractometer of moderate resolution at the National Bureau of Standards reactor. The details of the experimental conditions are summarized in table 1.

Table 1. Experimental conditions used to collect powder diffraction data

Monochromatic beam: reflection 220 of a Cu monochromator

Mean neutron wavelength = 1.358(1)Å

Take-off angle = 63.8°

Horizontal divergences: (a) In-pile collimator α_1 =21 min. arc

(b) Monochromatic beam collimator α_2=24 min. arc

(c) Diffracted beam collimator α_3=23 min. arc

Monochromator mosaic spread ∿10 min. arc

Theoretical values of full width at half maximum (fwhm) parameters:[*]

$$U = 7200, V = -4650, W = 2420 \times 10^4 \text{ deg}^2$$

Sample container: Vanadium can of ∿1 cm. diameter

[*] The parameters U,V,W appear in the expression

$$H_n^2 = Utan^2\theta_n + Vtan\theta_n + W$$

where H_n is the fwhm of reflection n with Bragg angle θ_n. Their theoretical values are calculated with the expressions given by Caglioti et al. (Nucl. Instr., 3, 223, 1958).

The structural models of the title compounds were refined by using the profile fitting procedure proposed by Rietveld (J. Appl. Cryst., $\underline{2}$, 65, 1969).

Starting Models

a. $LiNb_3O_8$ - The structure of lithium triniobate has been determined by single-crystal x-ray techniques by Lundberg (Acta Chem. Scan., $\underline{25}$, 3337, 1971) and by Gatehouse & Leverett (Cryst. Struct. Comm., $\underline{1}$, 83, 1972). It has been re-considered in this work not only to provide a useful comparison between x-ray and neutron diffraction results, but also to test if the total profile analysis proposed by Rietveld can be extended to the refinement of crystal structures of the complexity encountered in the study of this class of compounds. The results of the refinement, reported in table 2, show that the method can be safely applied to the study of oxide structures. Figure 1 shows the calculated and observed profiles for this compound.

b. $M-LiTa_3O_8$ - The x-ray analysis of the intermediate temperature phase of lithium tantalate (Gatehouse, Negas & Roth, J. Solid State Chem. $\underline{18}$, 1, 1976) failed to reveal the exact location of the Li atoms. An attempt made by powder neutron diffraction techniques showed immediately that the lithium ions are located in the octahedral sites indicated by the idealized structure represented in figure 2. The results of the profile refinement are summarized in table 3.

In figure 3 are shown the calculated and observed profiles for $M-LiTa_3O_8$. A comparison between the atomic coordinated obtained by single-crystal x ray analysis and by powder neutron diffraction is shown in table 4.

Table 2. Results of the refinement of the structure of $LiNb_3O_8$

$LiNb_3O_8$ –$P2_1/c$, a = 7.457(2), b = 5.033(1), c = 15.270(2) $\overset{\circ}{A}$, β = 107.34(1)°

$2\theta_{initial}$ = 6.00°, $2\theta_{final}$ = 64.50°, step = 0.1°

No. of reflections = 269, no. of observations above background = 519

Scattering amplitudes: b_{Nb}=0.711, b_O=0.575, b_{Li}=-0.194x10^{-12}cm

U = 15700(1400), V = -11600(1100), W = 4300(200)

R_p = 6.3%, R_{pw} = 7.6%, $R_{expected}$ = 4.2% (**)

Atom	x	y	z	B(*)
Nb1	0.493(2)	0.228(3)	0.331(1)	0.56
Nb2	0.751(2)	0.232(4)	0.073(1)	0.60
Nb3	0.987(1)	0.247(4)	0.333(1)	0.56
01	0.998(2)	0.055(4)	0.098(1)	0.74
02	0.413(3)	0.079(4)	0.216(1)	0.74
03	0.767(3)	0.096(3)	0.345(1)	0.74
04	0.539(2)	0.419(4)	0.105(1)	0.74
05	0.911(3)	0.418(5)	0.216(1)	0.74
06	0.641(2)	0.384(3)	0.461(1)	0.74
07	0.149(2)	0.071(3)	0.453(1)	0.74
08	0.275(3)	0.417(4)	0.345(1)	0.74
Li	0.245(9)	0.245(20)	0.082(4)	2.3

(*) The isotropic temp. factors were kept fixed at the values found by x rays.

(**) For the definitions of R_p, R_{pw} and $R_{expected}$ see Hewat, ILL report #74H62S, April 1974.

Table 3.   Results of the refinement of the structure of $M-LiTa_3O_8$

$M-LiTa_3O_8$ - C2/c, a = 9.409(1), b = 11.519(1), c = 5.050(1) Å
β = 91.11(1)° $2\theta_{initial}$ = 9.00°, $2\theta_{final}$ = 78.00°, step = 0.1°
No. of reflections = 247, no. of observations avove background = 641
b_{Ta} = 0.691×10^{-12} cm

$\qquad$ U = 15000(1100), V = -10900(900), W = 4300(200)

$\qquad$ R_p = 6.1%, R_{pw} = 7.3%, $R_{expected}$ = 5.3%

Atom	x	y	z	$B^{(*)}$
$Ta1^{(*)}$	0.2415	0.0864	0.2466	0.27
$Ta2^{(*)}$	0	0.3299	1/4	0.27
01	0.3533(5)	0.4502(5)	0.4386(11)	0.62
02	0.3839(5)	0.1794(5)	0.4226(10)	0.61
03	0.1322(5)	0.4366(5)	0.0834(12)	0.48
04	0.1187(5)	0.1961(4)	0.1050(10)	0.64
Li	0	0.8357(20)	1/4	0.70

$^{(*)}$All thermal parameters and the positional parameters of the Ta
atoms were kept fixed during refinement.

c. $H-LiTa_3O_8$ - The structure of the high temperature phase of $LiTa_3O_8$
has not been determined previously, but lattice parameters measurements
indicated that the structures of $H-LiTa_3O_8$ and $LiNb_6O_{15}F$ (Lundberg, Acta
Chem. Scan., 19, 2274, 1965) must be closely related.   A refinement based
on this assumption gave a final R factor of 15%, i.e. significantly higher
than the expected value.   These preliminary results indicate that the
gross structural features of the two compound are the same.   The high
value of the R factor, however, suggests that the symmetry of $H-LiTa_3O_8$
may be lower than that of the space group Pmam reported for $LiNb_6O_{15}F$.
Single-crystal measurements do in fact show that many reflections h0ℓ
with h = 2n + 1 have appreciable intensity, thus indicating that the
structure does not contain the glide plane.   Further study on the struc-
ture of this compound by neutron single-crystal and powder techniques is
still in progress.
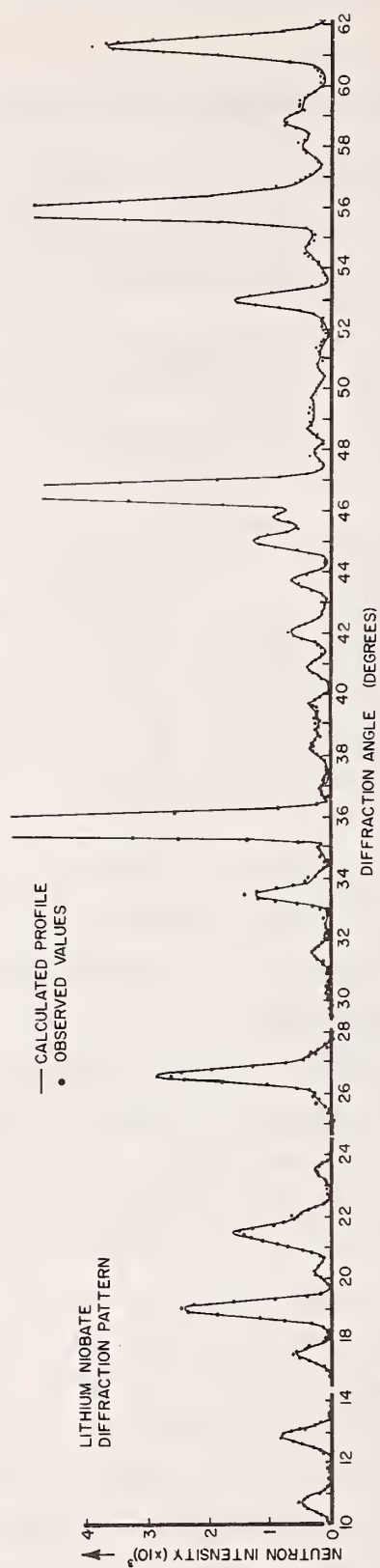
Figure 1. Observed and calculated neutron powder pattern for $LiNb_3O_8$

52
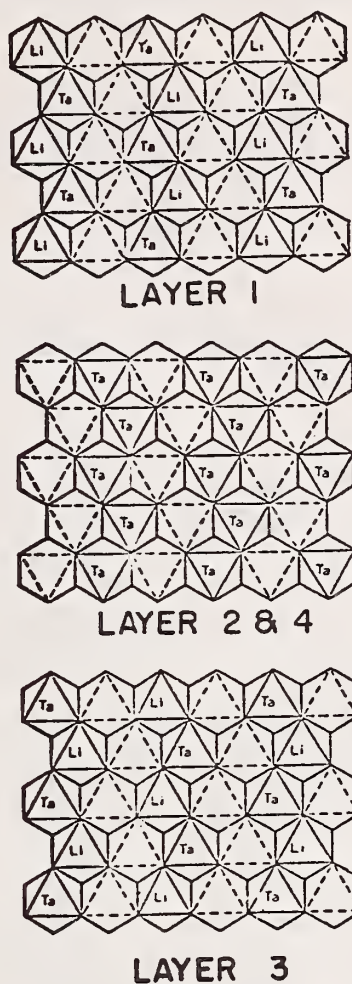
Figure 2. Layers of octahedra which build up the structure of $M\text{-}LiTa_3O_8$

Table 4. Comparison of x-rays and neutron atomic parameters for oxygen and lithium atoms in the structure of $M\text{-}LiTa_3O_8$

Atom	X RAYS				NEUTRONS			
	x	y	z	B	x	y	z	B
O(1)	0.3541(20)	0.4516(17)	0.4413(37)	0.62(28)	0.3533(5)	0.4502(5)	0.4386(11)	0.62
O(2)	0.3846(22)	0.1788(17)	0.4270(39)	0.61(27)	0.3839(5)	0.1794(5)	0.4226(10)	0.61
O(3)	0.1332(20)	0.4375(18)	0.0792(36)	0.48(26)	0.1322(5)	0.4366(5)	0.0834(12)	0.48
O(4)	0.1185(22)	0.1967(18)	0.1069(38)	0.64(28)	0.1187(5)	0.1961(4)	0.1050(10)	0.64
Li	--	-	-	-	0	0.8357(20)	1/4	0.7
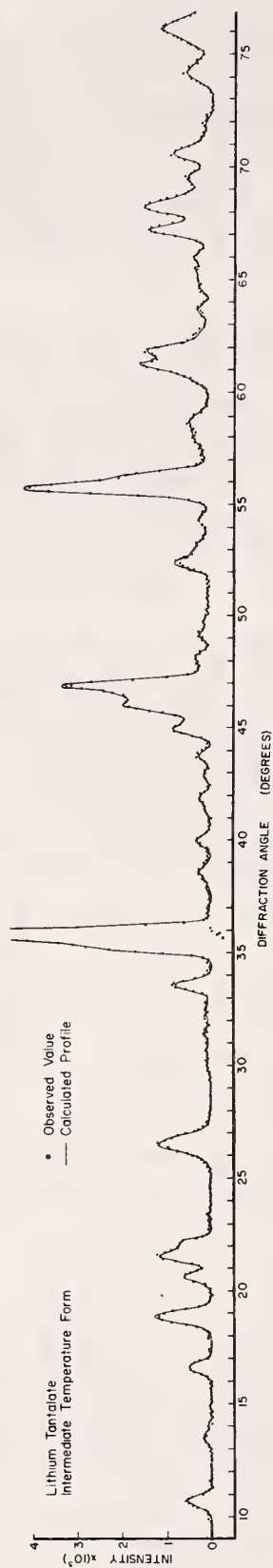
Figure 3. Observed and calculated neutron powder pattern for M-LiTa$_3$O$_8$

APPLICATION OF SIMULTANEOUS DIFFRACTION STUDIES TO THE ANALYSIS OF X-RAY SPECTRA

A. Santoro

and

R. D. DesLattes, R. LaVilla and A. Henins
(Optical Physics Division)

1.   Introduction

X-ray spectra from the sun are now being intensely studied as they are rich in structural details of importance for the understanding especially of flare phenomena. As the time of maximum solar activity approaches, large scale plans for sophisticated multi-spectral measurements are well underway. One of these, the Solar Maximum Mission (SMM), a 300 kg satellite containing more than a dozen spectrometers, is being pursued under NASA sponsorship by a group at Mullard Industries and Appleton Laboratories in England and Lockheed Research Laboratory in Palo Alto, California.

This group has asked the NBS for assistance in the quantitative characterization of the dispersion crystals and for comment on the crystallographic choices which must be made. X-ray spectroscopic resources (232.06) provided help in optimizing diffraction characteristics for the several spectral features to be studied on SMM. One additional feature of crystal choice, namely the avoidance of simultaneous diffraction, was studied at the Reactor Division (314.03).

Simultaneous, or multiple, diffraction of x-rays takes place whenever two or more sets of crystal planes are in position to diffract the incident beam. The occurrence of this effect produces complicated variations in the measured intensity of reflections (Zachariasen, *Acta Cryst.* 18, 705, 1965) and it has to be avoided in structural investigations (Santoro and Zocchi, *Acta Cryst.* 17, 597, 1964; *Acta Cryst.* 21, 293, 1966; *Acta Cryst.* 22, 331, 1967) as well as in x-ray spectroscopy work.

In what follows we will outline the method employed in this study and we will point out some properties of the diffraction geometry which may be of general interest.

2.   Method

The crystal is initially oriented so that the reciprocal lattice vector (scattering vector) corresponding to the selected "primary reflection" $h_o k_o l_o$, is perpendicular to the incident beam. The orientation needed to bring $h_o k_o l_o$ into reflecting position is then achieved by means of the appropriate rotation θ_o about the direction perpendicular to the "equatorial plane", i.e. the plane defined by incident and diffracted beams. Obviously the diffraction condition continues to be satisfied also if we rotate the crystal of any arbitrary angle ψ (azimuthal rotation about the scattering vector. Since the crystal orientation, the lattice parameters and the values of θ_o and ψ are all known quantities, it is possible to evaluate the matrix $\underset{\sim}{T}$ which transforms the coordinates $\underset{\sim}{h}$ of a reciprocal lattice point, expressed in the reciprocal lattice system, into the coordinates expressed in an appropriate Cartesian system attached to the laboratory

$$\underset{\sim}{x} = \underset{\sim}{T}\underset{\sim}{h}$$

From this equation it is easy to derive the geometrical conditions (that is the value of ψ or that of the wavelength λ) under which a second reciprocal lattice point hkl is in simultaneous diffraction with the primary reflection $h_o k_o l_o$. Starting from the same equation it is also possible to prove a number of theorems which have been found useful in interpreting the geometry of multiple diffraction and in designing experiments which minimize its effects on the measured intensities. These are the following:

  a. Simultaneous diffraction may be λ-dependent or λ-independent. (In the first case the angle ψ at which a node hkl is in simultaneous diffraction with the primary reflection $h_o k_o l_o$ is a function of λ, in the second case it is not).

GE 422 ($\bar{1}20$) $\Delta\lambda = 1.933 - 1.944$
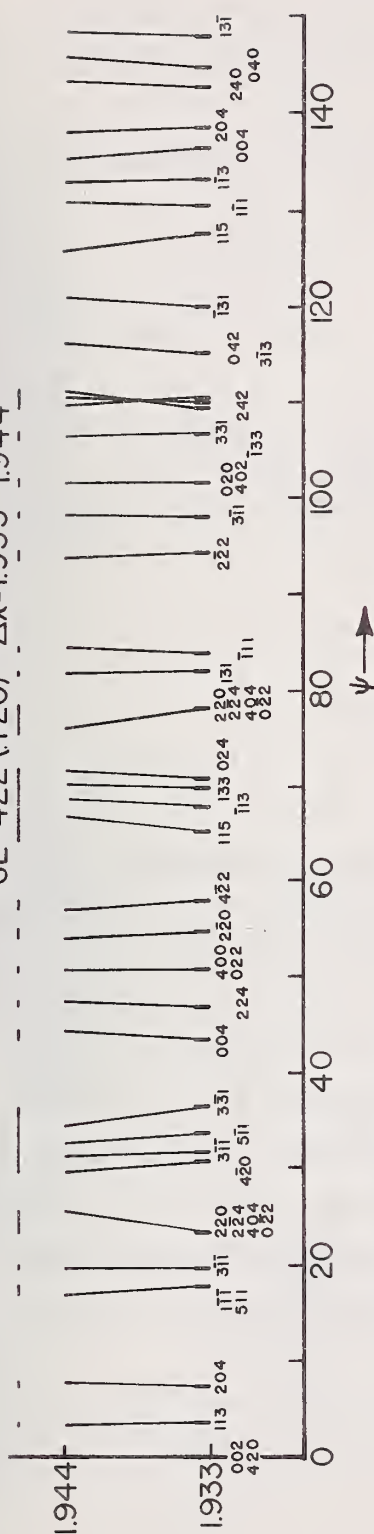
Figure 1. Simultaneous diffraction with the primary reflection 422 of a Germanium crystal and for the wavelength interval 1.933 – 1.944 Å. Regions free of multiple diffraction occur at $\psi = 12.4°$, 88.5° etc. The presence of a mirror at about $\psi = 140.75°$ is clearly shown in the diagram.

GE 220 (00l) $\Delta\lambda = 2.37 - 3.25$
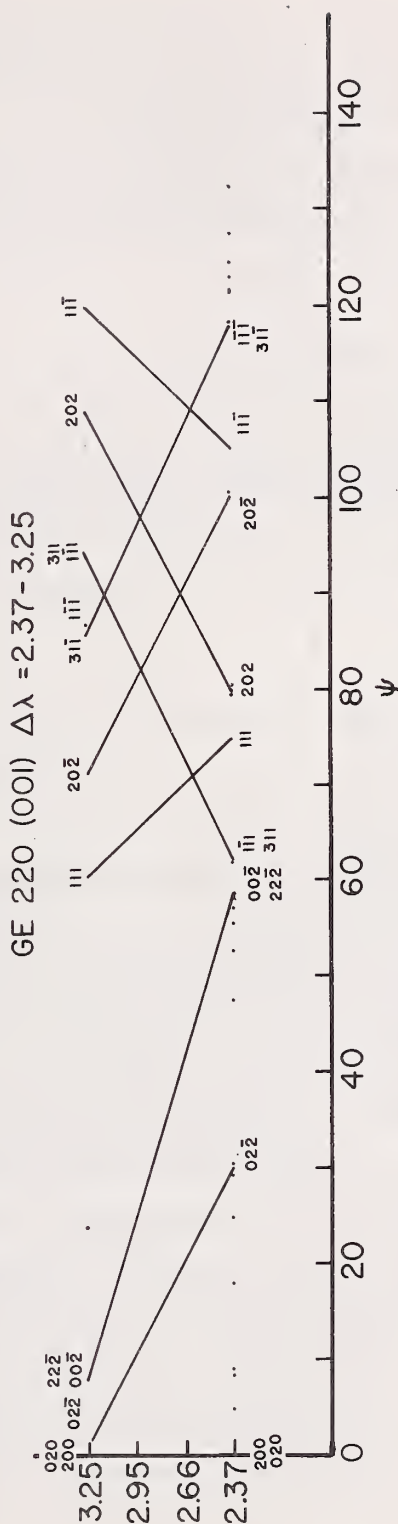
Figure 2. Simultaneous diffraction with the primary reflection 220 of a Germanium crystal and for the wavelength interval 2.37 – 3.25 Å. Due to the large $\Delta\lambda$, there are no orientations free from multiple diffraction. The diagram shows the effect of a mirror at $\psi = 90°$.

b. Simultaneous diffraction λ-independent takes place if, and only if, the points $h_o k_o l_o$ and hkl lie on a vertical net, i.e. on a net perpendicular to the equatorial plane.

c. If $h_o k_o l_o$ and hkl are in simultaneous diffraction λ independent, then also the reciprocal lattice point

$$h' = h_o - h, \qquad k' = k_o - k \qquad l' = l_o - l$$

diffracts simultaneously with hkl and $h_o k_o l_o$. In addition, the three nodes all lie on the same vertical net.

d. If $h_o k_o l_o$, hkl and h'k'l' are in simultaneous diffraction λ-independent, the net of these three nodes is rectangular.

e. If a node hkl diffracts simultaneously with the primary reflection $h_o k_o l_o$ at a value ψ of the azimuth, then the node

$$h' = h_o - h, \qquad k' = k_o - k, \qquad l' = l_o - l$$

diffracts simultaneously with $h_o k_o l_o$ at the azimuth

$$\psi' = 180° + \psi$$

3. Results

A computer program which evaluates the azimuthal coordinates ψ of multiple reflections has been developed. The values of ψ were calculated for the lower and upper limits of each wavelength interval to be studied and for each dispersion crystal employed in SMM. When these values are plotted as indicated in figure 1, one often finds orientation intervals entirely free of multiple diffraction. When possible, it is obviously desirable to choose such orientations for spectroscopy. Sometimes, however, there are no such regions, as indicated in figure 2, or the desired orientation is not accessible because of growth morphology. For these cases a second program has been developed which enumerates the Bragg angles (or wavelengths) at which trouble might be expected.

Other x-ray spectroscopy programs are benefitting from this work also. For example, the spectra of magnetically confined and laser driven

plasmas are rich in this region and need quantitative spectrophotometry.
Work done in support of the ERDA supported studies at the Princeton
Plasma Laboratory will include use of this systematic approach to the
avoidance of multiple diffraction effects. Finally, an NBS experiment
destined for installation at the Stanford Storage Ring was recently
troubled by this effect because of a failure to apply the systematic
tests in advance.

THE CONFORMATION OF PS-PMMA DIBLOCK COPOLYMER IN TOLUENE
BY SMALL ANGLE NEUTRON SCATTERING

C. C. Han
(Polymers Division)

and

B. Mozer

A deuterated polystyrene-poly(methyl methacrylate) (dPS-PMMA)
diblock copolymer and its deuterated polystyrene homopolymer precursor
were studied by small angle neutron scattering and light scattering ex-
periments using toluene as the solvent.

The radii of gyration of the deuterated PS homopolymer (M=88,000)
measured by both methods and that of the PMMA block (M=203,000) in the
diblock copolymer measured only by neutron scattering were determined as
210Å and 85Å respectively. In addition, the second virial coefficients
and the chain excluded volume exponents were also obtained.

The copolymer chain configuration in toluene at 23°C is inferred
from these measurements. It is suggested that the PMMA block forms the
interior core from which the PS block exudes out as an expanded chain.

SUMMARY OF EXPERIMENTAL RESULTS

	Molecular Wt.	$\langle R_G^2 \rangle^{1/2}$ (Å)	Excluded Volume Exponent ν	Second Virial Coefficient A_2 (mol. ml/g^2)
dPS (homo)	$(88\pm3)\times10^3$ (LS)	215±18 (LS) 210±40 (NS)	1.15~1.20 (NS)	$(5.2\pm1.0)\times10^{-4}$ (LS)
dPS (block)	$[(95\pm3)\times10^3$ (LS)]	225±40 (LS)		
PMMA (block)	203×10^3 (EA)	85±7 (NS)	1.03±.05 (NS)	
PMMA (homo)	60.6×10^3		1.11±.03 (NS)	

STUDIES ON THE STRUCTURE OF DEFECTIVE HYDROXYAPATITE

A. Santoro

and

L. Schroeder
(Polymers Division)

Structural studies of defective hydroxyapatite using the method of total profile analysis have continued in the past year. The results so far obtained do not permit to determine the nature of the defects present in the structure, mainly because a "standard" sample with which comparisons can be made is not yet available. Attempts are now being made at preparing non defective samples of the compound.

C. Interagency and University Collaborative Programs

DEUTERIUM-SITE OCCUPANCY IN THE α AND β PHASES OF TiD_x

H. Alperin
(Naval Surface Weapons Center, White Oak, MD)

and

H. Flotow
(Argonne National Laboratory, Argonne, IL)

and

J. Rush and J. Rhyne

A neutron diffraction study on polycrystalline samples of the α(hcp) and β(bcc) phases of TiDx has been completed. The objective was the determination of the sites that are occupied by deuterium atoms in each of the two phases. The compositions and temperatures chosen to achieve the α and β phases were $TiD_{0.075}$ at 375C and $TiD_{0.67}$ at 400C respectively. The results show that both phases exhibit considerable mixed – octahedral (y) – tetrahedral (1-y) site occupancy. The results are for the α-phase: $y=0.68\pm.02$ while for the β-phase: $0.15<y<0.30$. A comparison of observed and calculated intensities are given in Tables 1 and 2. The uncertainty in y for the β-phase is due to a strong correlation with the octahedral deuterium temperature factor. The site occupancy results may be correlated with the Ti-D distances for each site. In both phases it appears that the deuterium atoms predominantly occupy sites with the larger holes.

Single crystals of titanium have been obtained and diffraction measurements will be made to further refine the octahedral and tetrahedral temperature factors. Work is underway using the time-of-flight spectrometer to measure the quasielastic scattering from TiH_x in the α and β phases in order to determine the diffusion of hydrogen in the lattice. Finally we expect to measure the phonon spectra on single

Table 1. Comparison of observed and calculated neutron scattering
intensities for $TiD_{0.075}$ at 375C--α (hcp) phase.

hkl	I_{obs}	I_{calc}^a
100	51370	53024
002	54575	53068
101	199045	196319
102	21085	23269
110	34498	34694
103	48779	47774

[a]Calculated with $B^{Ti} = 1.875$, $B_D^{oct} = 4.6$, $B_D^{tet} = 3.0$ and deuterium
octahedral site occupancy, $y = 0.68$.

Table 2. Comparison of observed and calculated neutron scattering
intensities for β-phase (bcc) $TiD_{0.67}$ at 400C.

hkl	I_{obs}	I_{calc}^a
110	230700	237573
200	4529	5001
211	28822	28566
220	24936	23784

[a]Calculated with $B^{Ti} = 2.5$, $B_D^{oct} = 5.0$, $B_D^{tet} = 2.5$ and deuterium
octahedral site occupancy, $y = 0.20$.

crystals of pure α-Ti and αTiH$_{.075}$ to obtain information on how the presence of hydrogen affects the metal–metal bonds. This work has already begun with the measurements of several phonon branches for pure α-Ti at room temperature.

SMALL ANGLE MAGNETIC SCATTERING FROM A DILUTE AMORPHOUS Fe(Tb) ALLOY

H. Alperin and S. Pickart*
(Naval Surface Weapons Center, White Oak, MD)

and

J. J. Rhyne

Low temperature neutron scattering measurements on a rapidly sputtered bulk sample of composition $Tb_{0.018}Fe_{0.982}$ reveal anomalous small-angle magnetic scattering similar to that observed in the more rare earth-rich amorphous alloys $TbFe_2$ and $HoFe_2$ reported previously[1]. The data in figure 1 show a broad hump (as distinct from a sharp critical peak) about T_c (determined from magnetic measurements[2]) and the anomalously large magnetic component below T_c. Above T_c the scattering can be fitted to a Lorentzian from which we deduce a correlation length which increases from 13A at 260K to 38A at T_c. Below T_c the scattering can be fitted by the asymptotic Porod Law for a random distribution of spherical particles.

---

* Physics Dept., University of Rhode Island

1. S. Pickart, J. Rhyne and H. Alperin, Phys Rev. Lett. 33, 424 (1974); AIP Conf. Proc. 24, 117 (1975).

2. H. Alperin, J. Cullen, A. Clark AIP Conf. Proc. 29, 186 (1976).
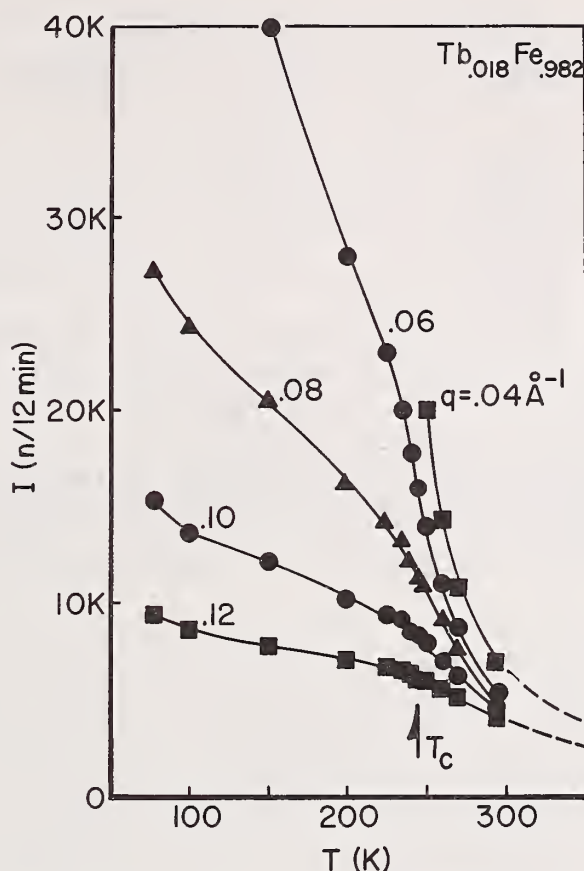
Figure 1.   Scattered neutron intensity, background subtracted as a function of temperature. The data at lower temperatures for q = .04, which are not plotted for reasons of convenience, scale very closely to the square of the observed spontaneous moment[2].

DIFFRACTION MEASUREMENTS FROM RAPIDLY SPUTTERED BULK Fe(Tb) AND Ni(Dy) ALLOY SAMPLES

H. Alperin
(Naval Surface Weapons Center, White Oak, MD.)

and

J. J. Rhyne

We have previously measured bulk samples (50 mm^3 to 150 mm^3 in volume) of Tb_xFe_{1-x} (x = 0.118, 0.25, 0.33, 0.45 and 0.75) alloys pre-
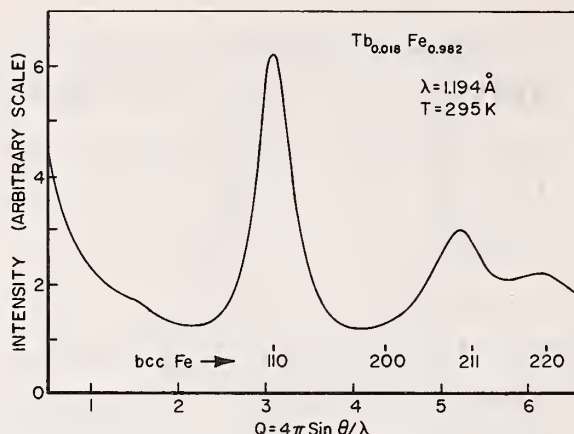
Figure 1. Diffraction pattern of amorphous $Tb_{0.018} Fe_{0.982}$ at room temperature. If the pattern were due to small polycrystalline particles of pure bcc iron the peaks would have to appear at the locations indicated.

pared by dc rapid sputtering. Diffraction patterns were found with very broadened peaks. The atomic 'structure' that can give rise to such patterns has been described as amorphous, arising from a random close packed atomic arrangement. We have now made similar measurements on the compositions $Tb_x Fe_{1-x}$ for $x = 0.018$, 0.167 and also for Ni(1wt.%Dy) which corresponds to $Dy_{0.0036} Ni_{0.9964}$. The terbuim content in the $x = 0.018$ sample was analyzed by neutron activation to an accuracy of $\pm 2\%$ by the Activation Analysis Section of the Analytical Chemistry Division. The diffraction pattern for this composition shown in figure 1, is most likely also due to an amorphous random close packed atomic arrangement. However, if one should try to attribute the broadened diffraction peaks to small-size crystalline iron particles, these particles could be no larger than an average diameter of 15A if we analyze only the broadening about the (110) Fe position. The displacement of the measured peaks from the (211) and (220) Fe positions however makes even such a crystalline interpretation doubtful. For the $x = 0.167$ composition, if the particles are crystalline they could be no larger than 10A. The Ni(Dy) sample exhibited sharp diffraction peaks indicative of a crystalline atomic structure.

NONDESTRUCTIVE DETERMINATION OF GRAIN-ORIENTATION OF METAL LINERS FOR SHAPED-CHARGE MUNITIONS

C. S. Choi and H. J. Prask
(Picatinny Arsenal, Dover, NJ)

The optimum functioning of shaped-charge ammunition requires that the projectile have essentially zero spin (i.e., axial rotation) at impact with the target. This requirement is very difficult to achieve in practice. It has been generally accepted that at relatively low spin rates ($\lesssim$ 50 r.p.s.) optimum functioning can be achieved in spite of spin if the liner cone is manufactured in a specific way. That is, by preferentially aligning the individual grains of the liner such that as the liner collapses along preferred slippage directions, a counter-rotation equal and opposite to that of the in-flight projectile is imparted to the explosive blast jet. It has also been suggested that residual stresses are induced in liners by the same manufacturing technique which produces grain orientation (i.e., shear spinning), and that it is residual stress, not grain orientation, which causes "spin compensation" in collapsing liners. The principal difficulty which has prevented the resolution of this conflict has been the lack of non-destructive test methods to measure grain orientation and residual stress, which would then allow test firing of the characterized liners.

In the present program, we have explored the feasibility of neutron diffraction as a nondestructive probe for grain orientation determination in intact, copper shaped-charge liners. Initial measurements were performed on a piece cut from a liner which had been flattened and examined by x-ray diffraction. Neutron and x-ray results were found to be comparable. Subsequent neutron diffraction studies were made on twelve intact liners from a current production batch. In figure 1 are shown pole-figure representations of the neutron diffraction results for (111) and (220) planes for two of the copper liners.
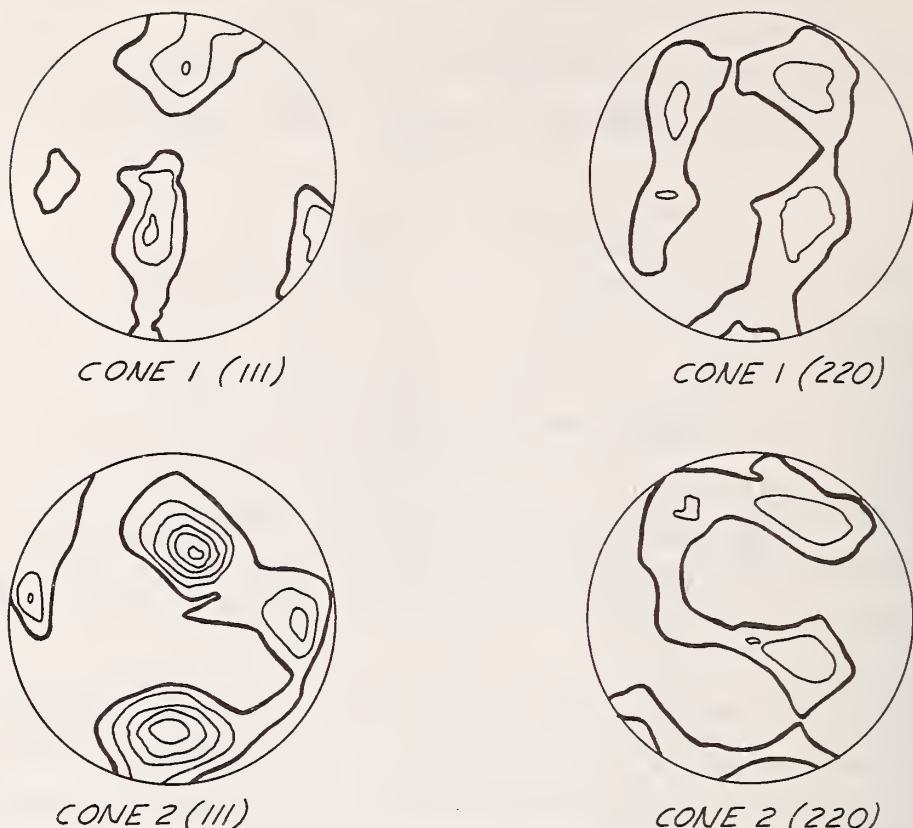
Figure 1. Pole figures for (111) and (220) grain orientation in intact shaped charge liners from neutron diffraction measurements. The heavy solid contour corresponds to "random" grain orientation; lighter counters correspond to increases in orientation by approximately 30% of random per contour.

These data represent the extremes of the differences observed for the twelve liners, which in the case of (111) reflections are rather significant. If grain orientation is the critical parameter, one would expect the performance of these two liners to be measurably different.

Further studies to establish grain orientation as a function of depth (total thickness $\sim$ 3 mm) and to examine the feasibility of nondestructive residual stress measurements using neutrons are in progress.

REINVESTIGATION OF CRYSTAL STRUCTURE OF
$\alpha\text{-}P_b(N_3)_2$
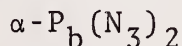
C. S. Choi
(Picatinny Arsenal, Dover, NJ)

and

E. Prince

Lead azide is a well-known primary explosive. The explosive nature of the azide compound is known to be correlated very closely with the degree of covalency in the azide bond in the crystal. Therefore, it is very important to know the structure of the azide groups and their surroundings accurately in order to understand the explosive properties. The crystal structure of $\alpha\text{-}P_b(N_3)_2$ was determined previously by using a partial three-dimensional neutron diffraction data set. The present study was aimed at improving the accuracy of the structure by collecting a complete set of three-dimensional data. A total of 1466 independent reflections were measured within the limiting sphere defined by a maximum 2Θ angle of $106°$ and a neutron wavelength of 1.226Å. With this new set of data, the refinement of the structure converged rapidly to the final discrepancy indices, $R = 0.038$ and $wR = 0.043$ for 1328 observed reflections. The structure obtained in this study is essentially the same as that of previous study, except for the detailed values of some parameters and their accuracy. The configurations of the four different azide groups in $\alpha\text{-}Pb(N_3)_2$ are given in table 1. The azide I and azide III are essentially symmetric, azide II is slightly asymmetric and azide IV is quite asymmetric. The azide structure becomes more symmetrical when the bond lengths are corrected for the effect of the thermal vibration by using the riding model.

Table 1. The structure of four different azides in α-Pb$(N_3)_2$.

Type	Bond	Bond Length ($\overset{\circ}{A}$)		N-N-N Angle ($^\circ$)
		Raw	Riding	
I	N_1-N_2	1.166(1)	1.179	177.9(2)
II	N_3-N_4	1.181(2)	1.186	178.2(1)
	N_5-N_4	1.160(2)	1.173	
III	N_6-N_7	1.172(2)	1.181	179.2(1)
	N_8-N_7	1.167(2)	1.176	
IV	N_9-N_{10}	1.191(2)	1.196	178.3(2)
	N_{11}-N_{10}	1.149(2)	1.164	

PHASE TRANSITION STUDY OF NaN$_3$ BY POWDER NEUTRON DIFFRACTION

C. S. Choi
(Picatinny Arsenal, Dover, NJ)

Sodium azide undergoes a phase transition at approximately 14 °C from β-phase (rhombohedral $R\bar{3}m$) to α-phase (monoclinic C2/m) with decreasing temperature. Iqbal and Christoe[1] have studied the phase transition by a method of polarized Raman scattering and concluded that the phase transition is a second order type. Subsequently, they proposed a mechanism for the phase transition based on the soft mode model developed by Chihara et al.;[2] the azide axis, in the phase transition, gradually changes its orientation with temperature over a wide temperature range, and this uniform tilt of the azide axis is coupled anharmonically to its librational mode in accordance with the formulas given by Chihara et al. The present study was aimed at determining the tilt of the azide axis at various temperature by the neutron powder diffraction method. Using 0.948$\overset{\circ}{A}$ neutrons, powder diffraction data of NaN$_3$ were collected at four different temperatures; 270 K, 174 K, 78 K, and 4 K, within the scanning range of 8° to 60° in

scattering angle with a 0.1° interval. The portion of the spectrum contaminated by the aluminum container was excluded from the refinement. The structure and lattice parameters were refined by the Rietveld technique of profile refinement using a program modified by Hewat. The profile residuals, R and R_w as defined by Reitveld, are 0.10 and 0.12 for 270 K, 0.067 and 0.114 for 174 K, 0.048 and 0.066 for 78 K, and 0.055 and 0.069 for the 4 K structure, respectively. The structure of α-NaN$_3$ are very similar to that of β-phase in general atomic arrangement, except for slight distortions due to a shear movement of the lattice (or β-angle changes) and an internal rotation of the azide axis. The tilt of the azide axis is the compounded effect of these two distortions.

Table 1. The distortion parameters of NaN$_3$ at various temperatures. The parameters are β for the angle of monoclinic cell, Θ for the internal rotation of the azide axis measured from the c-axis, and the tilt angle of the azide axis measured from the normal direction of the cation layer. The 300 K data refer to the equivalent monoclinic cell of the rhombohedral structure.

Temperature	β (°)	Θ (°)	Tilt(°)	Tilt(°) (soft mode Model)
300 K	112.54	22.54	0.0	0.0
270 K	110.7(1)	25.88(4)	5.2	4.4
174 K	108.63(4)	28.80(1)	10.17	9.9
78 K	107.63(1)	29.64(1)	12.01	12.2
4 K	107.46(1)	29.94(1)	12.48	12.48

The tilts of the azide axis obtained in this study agree well with those obtained by Iqbal et al. based on the soft mode model as shown in table 1. The rate of tilt is largest at near transition temperature and therefrom it decreases gradually until it saturates at near 78 K.

---

1.   Z. Iqbal and C. W. Christoe, *Solid State Commun.* <u>17</u>, 71 (1974).

2.   H. Chihara, N. Nakamura, and M. Tachiki, *J. Chem. Phys.* <u>59</u>, 5387 (1973).

QUASI-ELASTIC NEUTRON SCATTERING STUDY OF
SINGLE CRYSTAL AMMONIUM PERCHLORATE

N. J. Chesser and H. J. Prask
(Picatinny Arsenal, Dover, NJ)

The rotational motions of the ammonium ions in ammonium perchlorate (NH_4ClO_4) have been the subject of considerable study for more than a decade, primarily because this salt has been thought to provide a prototype for quasi-free rotation in an ionic solid. An earlier quasi-elastic neutron scattering (QNS) study of polycrystalline NH_4ClO_4 indicated that in the temperature range 78 to 130K the ammonium ions were reorienting via "instantaneous" 120° jumps about C_3 axes of the ion.[1] Thus three protons would move 120°, about an axis containing the nitrogen and fourth proton, to a new configuration identical to the original. A recent crystal structure determination[2] at low temperature has established that three of the four NH_4^+ protons are in non-equivalent equilibrium positions and that their thermal amplitudes differ. It would seem likely, therefore, that the jump probability for a proton is site dependent and that a QNS study of single-crystal NH_4ClO_4 might differentiate the different jump probabilities, and the present report summarizes the results of such a single crystal study. This work represents the most complex material for which QNS has been applied to establish the details of orientational disorder in a crystalline solid.

As a guide to the analysis of our experimental data, we have extended the "instantaneous" jump reorientation model of Sköld[3] to include the possibility of three different residence times, τ_i, associated with the three non-equivalent hydrogen equilibrium sites[2] of an NH_4^+ - appropriate to NH_4ClO_4. This model yields three different Lorentzian contributions and a δ-function contribution to the scattering law. Of these, the δ-function and one of the Lorentzians have structure factors independent of residence times whereas the structure factors of the second and third Lorentzians depend on the relative ratios of the residence times. Based upon average τs obtained from QNS studies of polycrystalline
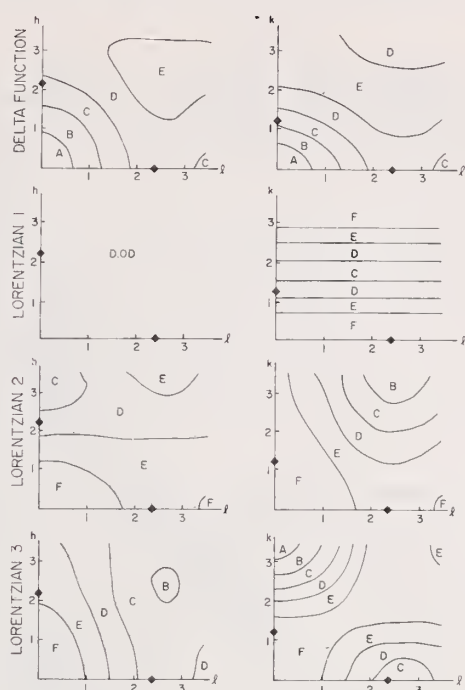
Figure 1. Intensity contour map for the $h0\ell$ and $0k\ell$ planes of NH_4ClO_4
at 120K. Areas marked A represent intensities which are, on
the average, approximately ten times those of areas marked F.
Diamonds indicate the value of Q selected to obtain relatively
pure Lorentzian contributions. While these contours are
those calculated for the residence times derived from 120K
data, they are similar to those derived for all of the tem-
peratures examined.

Table 1. Activation Energies E_o and Arrhenius Prefactors τ_o for each
atom.

Hydrogen Site	E_o (kcal/mole)	τ_o (psec)
1	.58±.04	.15±.03
2	.61±.04	.15±.03
3(3')	.52±.05	.28±.03
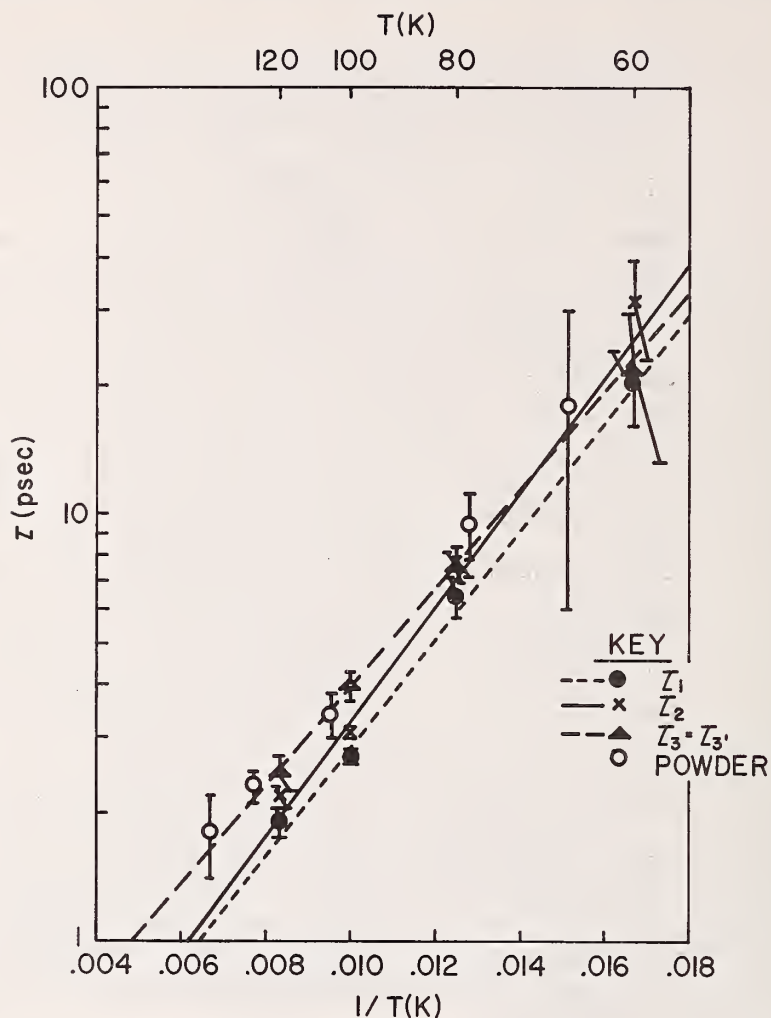
Figure 2. Residence times derived from analysis of the Lorentzian widths (see text). The lines are obtained under the assumption of an Arrenhius temperature dependence for the residence times ($\tau = \tau_o \exp(E_o/T)$ for each proton. Parameters are listed in table 1. Powder data are from reference 1.

1. H. J. Prask, S. F. Trevino and J. J. Rush, J. Chem. Phys. **62**, 4156 (1975).

2. C. S. Choi, H. J. Prask and E. Prince, J. Chem. Phys. **61**, 3523 (1974).

3. K. Skold, J. Chem. Phys. **49**, 2443 (1968).

4. V. F. Sears, Adv. Phys. **24**, 1 (1975).

NH_4ClO_4 and the ratios of librational amplitudes inferred from the low temperature neutron diffraction study[2] the structure factor contour map of figure 1 is obtained.

Constant Q scans of the quasielastic scattering were made for single crystals[3] of NH_4ClO_4 using a triple axis spectrometer configured such that FWHM (ful-width-at-half-maximum) $\simeq 0.1$ meV. Measurements were made at temperatures of 60 to 120K, at the reciprocal lattice points indicated in figure 1.

The data were fit using a non-linear least squares fitting routine with six adjustable parameters: the Lorentzian width, Lorentzian and δ-function intensities, "thermal" (i.e. analyzer efficiency dependent) and "fast" (i.e. flat) neutron background levels, and offset of the peaks from the nominal elastic position. The calculated curves were folded with the appropriate Gaussian resolution function and corrected for analyzer efficiency ($K_f^3 \cot\theta_A$).

From the structure factor map and the limitation that the model requires the width of Lorentzian two to be greater than that of Lorentzian three, residence times for the different sites were obtained at each temperature as shown in figure 2. Assuming Arrenhuis behavior, activation energies and prefactors as shown in table 1 are obtained. The results shown in figure 2 and table 1 clearly indicate the aniso-tropic character of ammonium uon reorientations in NH_4ClO_4. Work is in progress to further examine this behavior.

REINVESTIGATION OF THE CRYSTAL STRUCTURE OF NH_4ClO_4 AT 298 K

C. S. Choi and H. J. Prask
(Picatinny Arsenal, Dover, NJ)

and

E. Prince

A refinement of the structure of ammonium perchlorate at room temperature has been reported by Peyronel and Pignedoli,[1] who concluded that the structure cannot be refined in the centrosymmetric space group Pnma, but can be refined in the space group $Pna2_1$. Since this conclusion is in disagreement with our study at low temperature using neutron diffraction data, we have performed further least-squares refinement of the room temperature structure in the centrosymmetric space group Pnma using their published data. Two cycles of refinement with isotropic temperature factors, followed by three more cycles of refinement with anisotropic temperature factors and an isotropic secondary extinction parameter, reduced the R indices to $R_w = 0.044$ and $R = 0.049$ for the 800 observed reflections. A comparison of this centrosymmetric structure result ($R = 0.044$ for the 35 parameters) with their acentric structure refinement ($R = 0.055$ for the 55 parameters) shows clearly that Pnma is the correct space group for NH_4ClO_4 at room temperature as it is at lower temperatures. The bond parameters and rigid body motions of the perchlorate group obtained in this study are given in table 1. The librational motion of the perchlorate group, as obtained from the rigid body refinement, is almost isotropic and causes the apparent Cl-O bond length to be shortened by about $0.02\overset{\circ}{A}$. The translational motion, however, is extremely anisotropic and closely resembles the thermal ellipsoid of the nitrogen atom of the ammonium group.

INTERAGENCY AND UNIVERSITY COLLABORATIVE PROGRAMS

Table 1. The bond parameters and rigid body motions of the perchlorate group.

Bond length (A)	Uncorrected (A)	Corrected (A)
Cl-O(1)	1.432(3)	1.452
Cl-O(2)	1.424(3)	1.445
Cl-O(3)	1.442(2)	1.462

Bond angle (°)	Uncorrected (°)	Corrected (°)
O(1)-Cl-O(2)	111.3(2)	111.2
O(1)-Cl-O(3)	108.7(1)	108.7
O(2)-Cl-O(3)	109.7(1)	109.7
O(3)-Cl-O(3)	108.6(2)	108.6

Principal axis	Amplitudes r.m.s. (A)	Directions based on crystal system		
		α (°)	β (°)	γ (°)
T(1)	.314	89.	0	1.
T(2)	.171	1.	0	91.
T(3)	.168	0	1.0	0
	r.m.s. (°)			
L(1)	7.1	0	1.0	0
L(2)	6.9	138.	0	132.
L(3)	6.5	48.	0	138.
N-atom				
U(1)	.325(3)	88.(1)	90	2.(1)
U(2)	.191(3)	90	180	90
U(3)	.179(3)	2.(1)	90	92.(1)

---

1.   G. Peyronel and A. Pignedoli, *Acta Cryst.* B31, 2052 (1975).

SMALL ANGLE SCATTERING: INSTRUMENT AND APPLICATIONS

C. S. Schneider

(U. S. Naval Academy, Annapolis, MD)

The double perfect crystal diffractometer has been considered for measuring the scattering of thermal neutrons from a Christiansen filter to determine the scattering amplitude[1,2] of the powder atoms. The scattered intensity, as a function of the difference ΔNb for powder and liquid, changes in form with the phase shift across the particle, $\phi = 2\delta kR = 2\lambda R\Delta Nb$ and the probability of scattering from particles in the sample, $P = N_p \sigma_p x$ where x is the powder thickness. In the single diffraction region $\phi < 1$ and $P \doteq x\phi^2/4R < 1$ for a packed powder of particle radius R.   Thus

$$I_1 = PfI_o = (\Delta Nb)^2\lambda^2 xRfI_o$$

where I_o is the central peak intensity and $f \leq 1$ accounts for absorption $e^{-\mu x}$ and slight broadening from the initial resolution to λ/R. When P exceeds unity the central peak is completely diffracted and multiple diffraction begins causing reduction in the intensity seen at the base of the central peak: in region two where $\phi \leq 1$ and $P \geq 1$

$$I_2 = fI_o/\sqrt{P} = fI_o/\lambda\sqrt{xR} \; \Delta Nb.$$

Finally, as ϕ exceeds unity the scattering becomes multiple refractive being broadened through roughly $\lambda^2\sqrt{P} \; \Delta Nb/2\pi$ where $P = x/R$.   Thus

$$I_3 = f'I_o/\lambda\sqrt{xR} \; \Delta Nb$$

continuing the $(\Delta Nb)^{-1}$ decrease with a small change in coefficient f'.

The precision of using the double crystal diffractometer to determine Nb by finding the center of equal intensities in region one from the plot in figure 1, is one part in $2\sqrt{N_o}$ where N_o is the total counts recorded. In one day's counting using perfect Ge crystals, $\lambda = 0.4$ nm, $R = 40$ μm and $x = 1$ mm for highly absorbing powders, the precision approaches a few parts per thousand.

Because a rapidly decreasing tail of the resolution in a diffracto-
meter is necessary to observe small angle scattering, which decreases as
θ^4, Darwin reflectivities are not ideal with their θ^2 decrease soon over
powering the sample scattering. Bonse-Hart triple reflection monochro-
mator and analyzers have been made of Ge single crystals with the hope
of exploiting their θ^6 tail drop-off, but the modest peak intensities of
10^4 n/min made the advantage marginal. Several modifications have been
considered: first, highly assymetric channel cutting (beam incident
upon monochromator nearly parallel to the channel) can largely reduce
the rocking width but the intensity would stay nearly the same.

Second, inducing thermal gradients perpendicular to the reflecting
planes can broaden the integrated reflectivity[3] to $\frac{\Delta d}{d} = \alpha \, \Delta T$ where α is
the thermal expansion coefficient and ΔT the temperature difference
across the crystal. Due to the small value of α, the large thermal con-
ductivity and the large temperature dependence of α, power densities of
20 W/cm^2 did not cause a significant reflectivity increase from Si (111)
planes. The techniques of adhering a graphite wafer to the back surface
and preparing a resistive pathway proved a very effective method of
applying several hundred watts to the crystal. Air jet cooling appears
sufficient but is not highly uniform.

Finally, strain induced reflectivity[4] is being intensively studied
with a strained perfect crystal spectrometer recently fabricated, with
reversible dialable strain normal to the reflecting plane

$$e_{max} = \frac{\Delta d}{2d} \quad \sigma = \frac{\sigma t}{P}$$

existing furthest from the neutral axis of the crystal sheet where σ is
Poisson's ratio. Slices of both Si and Ge have been optically polished
and their curvatures measured as a function of the strain device micro-
meter reading, by observing the focussing of a nearly parallel laser
beam. Anticlastic (saddle shaped) curvature is 25 percent of the ap-
plied curvature between constraint lines. Strain is applied vertically
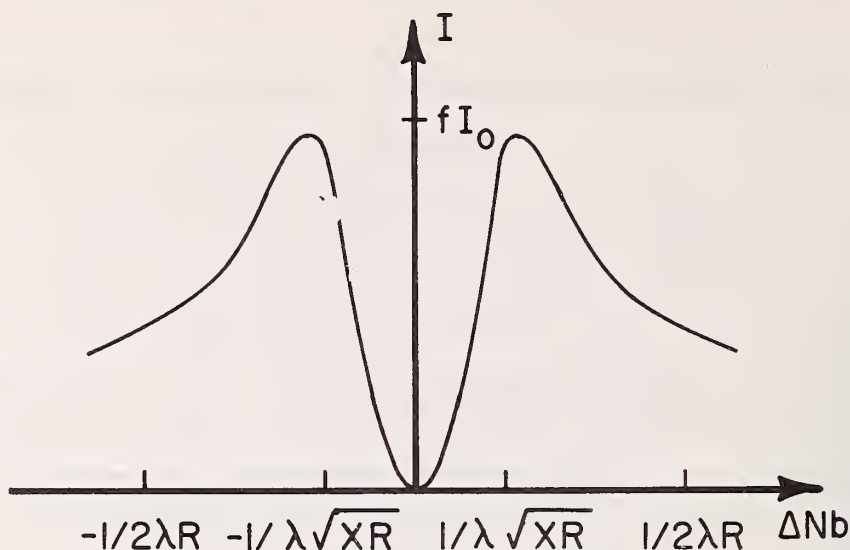
Figure 1.   Intensity scattered by a Christiansen filter as viewed at
            the base of the central peak in the double perfect crystal
            diffractometer.

so that the defocussing of the double crystal diffractometer is mini-
mized: two smearing effects are present. First is the permanent
smearing due to finite horizontal collimation β_H and second crystal cur-
vature, $1/\rho_{2H}$:

$$\Delta\theta_1 = \beta_H \; x \; /\rho_{2H}\textbf{:}$$

where x is the separation of monochromator and analyzer crystals. Sec-
ond is the relative curvature smearing which can be eliminated by setting
$\rho_{2H} = \rho_{1H}-2x$, the focus condition:

$$\Delta\theta_2 = \frac{W_1}{\rho_{1H}\rho_{2H}} (\rho_{2H}-\rho_{1H}+2x)$$

where W_1 is the width of the monochromator crystal. If the smearing is
not to affect the induced mosaic, $\Delta\theta = 2ef \tan\theta$ where $f\leq1$ is due to
dynamical effects[5] then in the focussed condition for $\rho>>x$,

$$\Delta\theta = ftt an\theta/\rho > \Delta\theta_1 = \beta_H x/\rho_H$$

or $t>\beta_H x \cot\theta \rho_v/\rho_H f$. Since $\rho_v/\rho_H \leq .25$ and $\beta_H = 0.01$ and x = 50 cm is
ample sample and shielding space, then $t\geq1.2$ mm/f. Present studies on

80
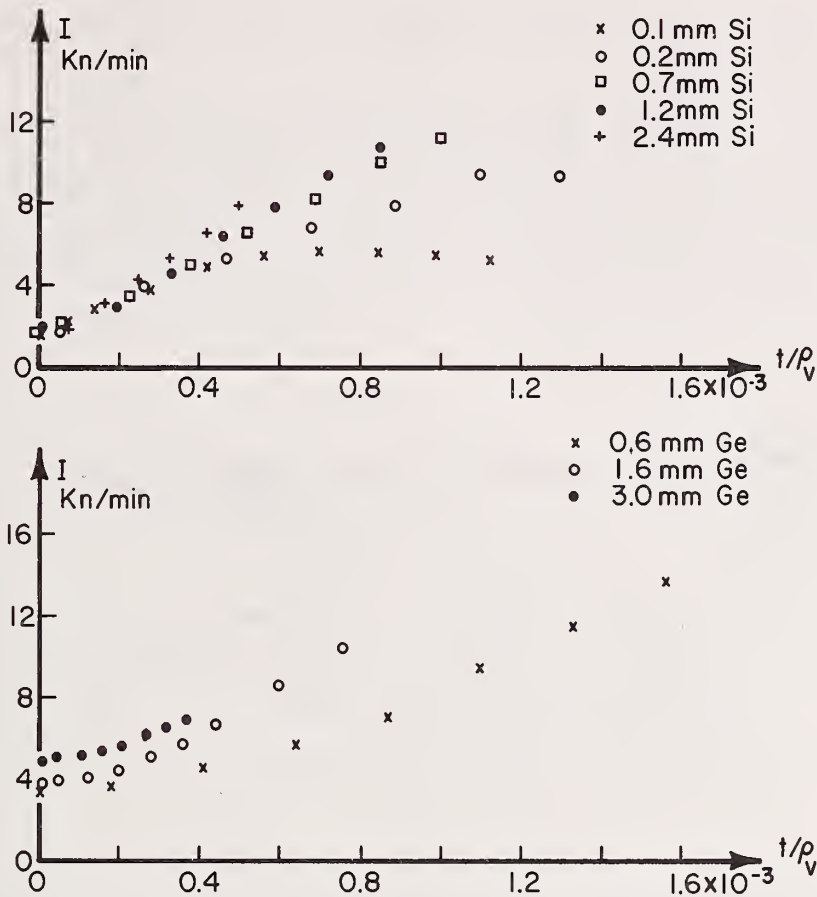
Figure 2.   Intensity reflected from various thicknesses of 18x25 mm
            area Ge (some imperfect) and Si crystals. Note saturation
            of thin crystal reflectivity.

piezoelectrically strained crystals[6,7] should eliminate focussing
problems.

      Deeper penetration of the beam into a mosaic or strained crystal
also requires a minimum thickness to reflect fully. This thickness is
roughly one millimeter as above and can be extracted from the intensity
measurements made with the Si and Ge crystals on the strain device. The
intensity saturates either due to beam penetration of the thin crystals
or to yield of the thicker crystals, which was at a strain of roughly

10^{-3}, corresponding to a few minutes arc mosaic. Preliminary data is shown in figure 2.

Insertion of the 2 mm thick amorphous $TbFe_2$ sample into the beam of the perfect crystal diffractometer caused severe attenuation, largely from scattering. This suggests the need for the broader resolution of the bent crystal diffractometer. Critical scattering in iron is also under consideration as the very fine q resolution allows direct observation of long correlation lengths.

1.   L. Koester and H. Ungerer, *Z. Physik*, 219 300 (1969).

2.   L. Koester and K. Knopf, *Z. Naturforsch* 262, 391 (1971).

3.   B. Alefeld, *A. Physik*, 228 454 (1969).

4.   A. Boeuf and F. Rustichelli, *Acta Cryst.* A30, 798 (1974).

5.   M. Kuriyama and T. Miyakawa, *Acta Cryst*, A26 667 (1970).

6.   T. F. Parkinson and M. W. Moyer, *Nature*, 211, 400 (1966).

7.   A. G. Klein et al., *Appl. Phys. Letters*, 10, 293 (1967).

STRUCTURE OF THE ANTIFERROELECTRIC PHASE OF COPPER FORMATE TETRAHYDRATE

M. I. Kay
(Puerto Rico Nuclear Center, Mayaguez, PR)

and

E. Prince

A three-dimensional neutron diffraction data set was collected from a crystal of copper formate tetrahydrate in the antiferroelectric phase at 77 K. The antiferroelectric phase is characterized[1] by small deviations, in alternate unit cells, from more symmetric positions in the room temperature, paraelectric phase. Consequently, reflections with odd values of ℓ are much weaker, on the average, than reflections with even values of ℓ. Nevertheless, some of the odd ℓ reflections

have appreciable intensity. Attempts to refine the structure using conventional least-squares techniques have met with difficulties, particularly with respect to reflections of the class 5, k, ℓ with ℓ odd. There may be features in the structure not included in the model which have a particularly strong effect on these reflections. Work is continuing on refinement of the structure using robust/resistant methods.

---

1. M. I. Kay and R. Kleinberg, *Ferroelectrics*, <u>4</u>, 147 (1972).

ACTIVATION ANALYSIS: SUMMARY OF 1976 ACTIVITIES

Harry L. Rook and Thomas E. Gills

(Analytical Chemistry Division)

This summary of the activities of the Activation Analysis Section covers the period of July 1975 to June 1976. During this period the Section has continued its efforts to attain a high degree of versatility in activation analysis and has directed efforts toward developing a greater expertise in multielemental analysis particularly coupled with automation and computer data reduction. In addition, research is continuing in the area of the investigation of parameters which affects accuracy and precision in activation analysis.

While the majority of the activation analysis work is in support of the Analytical Chemistry Division's programs, a large portion of the Section's activities this year has been spent in service analyses for organizations outside the Bureau of Standards and for groups within the Bureau of Standards. Such cooperation affords an opportunity to transfer analytical capabilities or expertise to the analytical community.

The Activation Analysis Section has at present eleven members and has programs in a variety of areas related to the trace elemental characterization of materials. These areas include research projects, SRM certification analyses and service analyses. Summaries of the work in these areas are included.

1.   Basic Research in Activation Analysis
    a. A Method for the Determination of Iodine in Biological and
        Environmental Matrices
        H. L. Rook

Iodine is an element with excellent intrinsic sensitivity when determined by thermal neutron activation. However, in most real samples,

the preponderance of chlorine and bromine, relative to iodine, makes the direct determination of iodine virtually impossible. Over the past 20 years, there probably have been as many publications on the separation of iodine as there have been for any other radionuclide. Upon review, however, the methods are essentially the same. After irradiation, the samples are subjected to a rapid destructive process to free the iodine from the matrix and then the iodine is separated from the other halides either by liquid-liquid extraction or by liquid ion exchange. Both of these procedures are, however, rather complex and do not effect a complete separation of the halides in one pass. Also, most of the separations are not quantitative in the recovery of iodine, thus, they require a radiochemical yield determination, with its associated problems and additive errors.

The best assessment of the present ability of NAA to determine iodine in real matrices is the published results of iodine in Bowen's Kale and in certain NBS SRM's such as Orchard Leaves, Bovine Liver and Coal. These matrices have been widely studied and numerous publications have appeared with data on their trace element compositions. In Bowen's Kale, no consensus iodine result was obtained, because values reported by cooperating laboratories varied by more than two orders of magnitude. In the NBS SRM's, no iodine values have appeared in open literature, except on Coal, and they appear to be in error.

In the work presented here, a simple, rapid procedure is developed for the quantitative determination of iodine in botanical, biological and environmental matrices.

For the separation of iodine from general matrix activity, the sample is burned in a flowing oxygen atmosphere using a quartz combustion tube, similar to the one described for mercury separations. Following combustion, the sample is heated to 1100° C with a resistance oven to completely distill the volatile elements. During this process, the iodine is separated from the chlorine and bromine, in the gas phase, by a trap containing hydrated manganese dioxide (HMD). A second trap,

of silvered glass wool, is placed downstream from the HMD trap to collect the iodine. The HMD trap, heated to 80° C, has been found to completely remove chlorine while quantitatively passing iodine through to the final collector trap. With this separation system, samples can be processed in 10-15 minutes with separations of greater than 10^6 for chlorine and 10^4 for bromine.

The described procedure has been used for the determination of iodine in numerous new and old SRM's at the NBS. Table 1 gives some representative data on SRM 1571, Orchard Leaves. From this work, it is estimated that $<10^{-9}$ g of iodine can be easily determined in real matrices.

Table 1. Iodine Concentration in SRM 1575 Orchard Leaves

Sample #	μg/g Iodine	Sample #	μg/g Iodine	Mean
1	0.176	5	0.160	
2	0.165	6	0.166	
3	0.171	7	0.153	
4	0.180			0.167 ± 0.009

b. The Measurement of Radial Efficiency Gradients in Ge(Li)
    Gamma Detectors
    R. M. Lindstrom

In the decade since the introduction of lithium-drifted germanium detectors, their availability from commerical suppliers with steadily increasing counting efficiency has led to their nearly universal use in measuring gamma-rays from radioactive substances. The rapid replacement of the sodium iodide scintillation detector for gamma assay is due almost entirely to the forty-fold sharper energy resolution of the newer detectors. In addition to assuring qualitative identification of gamma emitters, this resolution allows a forty-fold reduction of the background

area under a peak, with the result that despite a two to ten-fold decrease in counting efficiency the Ge(Li) detector is still superior to NaI for quantitative determination.

In order to minimize the counting time required for a given statistical precision, the analyst is often impelled to place the source close to the detector, often in contact with the end cap. But, because of the small size of the crystal, small differences in shape or positioning of the counting sample compared to a standard may lead to significant differences in counting efficiency. It is the intent of the present work to examine this position sensitivity where the source is in contact with the detector can. With a ^{137}Cs point source directly on the vacuum can of 80 cm^3 Ge(Li) detector, the radial gradient in efficiency (i.e., across the can) is 1.6%/mm at r = 10 mm; this is three times the efficiency gradient of a 7.6 x 7.6 cm NaI(Tl) detector. The present work extends these considerations to different detector configurations.

c. Selective Radiochemical Separation for the Activation Analysis
    of Biological Standard Reference Materials
    T. E. Gills

New biological materials such as Tomato leaves, Pine Needles and Spinach are currently being characterized at the National Bureau of Standards as part of the Standard Reference Materials Certification Program. Of the elements whose concentrations are usually certified, Copper, Arsenic, and Antimony could be determined accurately and precisely by activation analysis if sensitivity were the only consideration. However, the matrix radioactivities in most cases prevent instrumental determination of those elements or nuclides. The most useful (n,γ) reactions involve short-lived nuclides of Cu, As and Sb thus requiring chemical separation of those elements from the activated matrix. Separation procedures by Kosta et. al. for Cu, As, and Sb are capable of producing accurate results at the sub-ppm level of concentration. However, such procedures are highly

dependent upon the pH of the extraction system and are not easily adaptable to multielemental analyses.

Among possible radiochemical procedures and reagents for group separation of elements, inorganic ion exchangers have received increased interest arising from the high selectivity which can often be obtained by their use. Furthermore, by separating elements in groups instead of individually, and utilizing the high resolution of semiconductor detectors, simple, low cost and rapid analyses can be achieved.

Table 1

A Comparison of NAA Results Using The Described
Separation Procedure to other Independent Methods

Code	Element	Spinach	Pine Needles	Tomato Leaves
1	Cu	$10.8 \pm .2$	$2.98 \pm .16$	$11.1 \pm .2$
4	Cu	$12.7 \pm .4$	$3.2 \pm .4$	$11.5 \pm .2$
3	Cu	11.5	2.9	10.6
1	As	$.12 \pm .01$	$.20 \pm .02$	$.23 \pm .03$
2	As	$.17 \pm .05$	$.21 \pm .04$	$.29 \pm .05$
1	Sb	$.043 \pm .004$	$.22 \pm .01$	$.12 \pm .03$

Codes: 1 - Neutron Activation Analysis with Chemical Separation.

2 - Colorimetry.

3 - Isotope Dilution Spark Source Mass Spectrometry.

4 - Atomic Absorption Spectrometry.

This work involved the use of two chromatographic columns separately filled with Cuprous Chloride and Tin Dioxide. The columns were placed in series to provide a selective separation procedure for Cu, As and Sb from neutron activated biological materials. This separation scheme, was initially tested by reanalyzing previously certified NBS Orchard Leaves (1577). The procedure was then used to determine Cu, As, and Sb in new proposed Standard Reference Materials: Spinach, Pine Needles and Tomato Leaves. A comparison of NAA results using this procedure to other independent methods is given in table 1.

d. Evaluation by Activation Analysis of Elemental Retention in
   Biological Samples After Low Temperature Ashing
   G. J. Lutz, J. S. Stemple and H. L. Rook

Low temperature ashing (LTA) is the low temperature ($\sim$100° C) decomposition of organic or biological samples using atomic oxygen produced by an electrodeless radio-frequency discharge. There are a number of advantages in using LTA as the first step in a general analytical method such as the avoidance of contamination during wet or high temperature ashing. With respect to activation analysis, freeze-drying followed by LTA has the advantage that with the elimination of organic carbon, the possibility of charring a sample with a very high neutron flux is removed. In addition, wet digestions can be substantially speeded up and hence short-lived nuclides can be more readily separated for counting.

The possibility exists in the LTA method of the loss of some volitile elements during ashing. We have studied, using activation analysis, loss or contamination of trace elements during LTA.

A commerical model LTA apparatus capable of 100 watts forward power was used in these experiments. A schematic of the apparatus is shown in figure 1. The sample was placed in a borsilicate glass ashing chamber which was briefly rotated by hand to induce the organic sample to spread as evenly as possible on the inside surface. The cold trap was filled

with crushed dry ice (liquid nitrogen would condense explosive ozone). The system was pumped down to 1.3 - 2.6 Pa (10-20 millitorr). The oxygen flow rate was adjusted so as to maintain a pressure of 13-40 Pa (100-300 millitorr). Forward power was usually set to the maximum of 100 watts. Tuning to optimum was accomplished by observing the maximum intensity in discharge glow in the tube.

Preliminary experiments involving addition of tracers to biological materials and determining retention of each isotope after ashing verified previously published data and served to establish and perfect the basic ashing technique. After these experiments, it was decided to study three NBS Standard Reference Materials in detail: 1571-Orchard Leaves, 1577-Bovine Liver, and 1632-Trace Elements in Coal.

Samples of about one gram were ashed for a period of several hours. The relative amounts of the elements in ashed and unashed samples were determined by nondestructive neutron activation analysis with the NBS 10 megawatt nuclear reactor and photon activation analysis with the NBS electron linear accelerator. Suitable irradiation and counting schedules were arranged to detect and quantify both long- and short-lived activities.

In the activation analysis experiments, the losses of iodine, bromine, chlorine and mercury in addition to carbon were observed.

Figure 2 shows, in the format of the periodic chart, the elements detected and not lost during ashing in all experiments. The symbols in the individual square of each element, OL, C and BL stand for orchard leaves, coal and beef liver, respectively, in which the element was determined. In addition, some elements reported retained in the literature determined by neutron activation analysis, atomic absorption spectrometry, or spectrophotometry are included.

It is also significant to note that, equal in importance to loss of trace elements, there was no pick-up of contamination during the ashing process as would be evidenced by an increase in the amount of the element after ashing. This is in spite of the fact that only very ordinary precautions were taken to guard against contamination during cleaning of the

borosilicate glass ashing tube with ordinary laboratory detergent follow-
ed by rinsing with water, hot dilute hydrochloric acid and finally
deionized water and drying in an oven at 110° C.
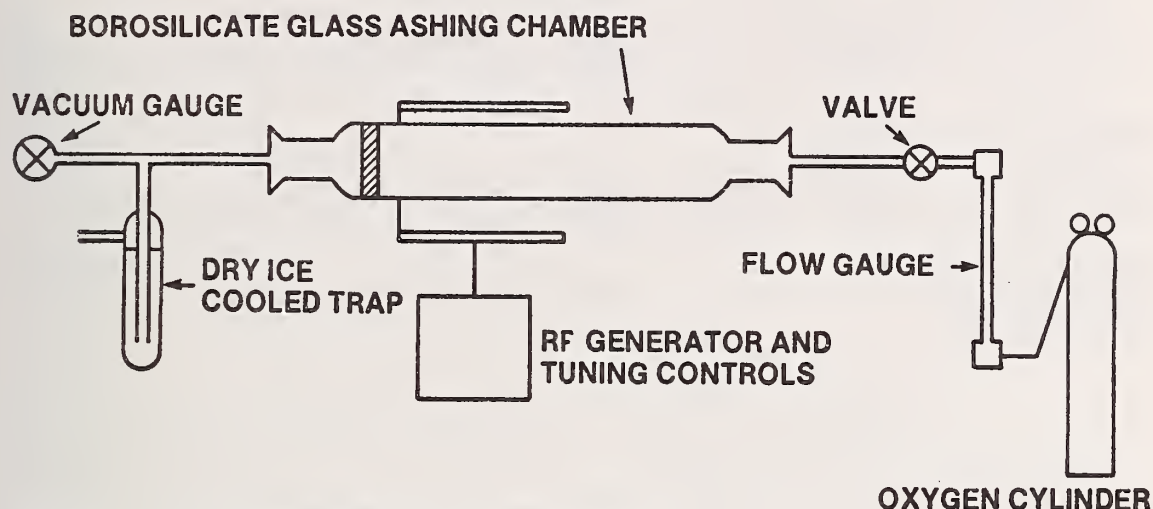
Figure 1.   Block diagram of LTA apparatus.

2.   Cooperative Research Projects

   a.   The Determination of the Absorption of Metallic Ions on Tooth
        Tissue

        The American Dental Association Health Foundation Research Unit
at NBS (ADA-NBS) is involved in a research effort to improve adhesive
bonding between hard tooth tissues and materials for use in preventive
and restorative dentistry. The initial direction of this project is to
determine which candidate metallic ions, are the best suited to serve as
a mordant to improve the adhesion of dental resins and composites to hard
tooth tissues. Success in this objective could save millions of teeth
annually from decay and the costly procedure of drilling and filling with
expensive silver alloy restorations.

        Neutron activation analysis is currently being used to determine
the concentration of four elements (Al, Cu, Fe and Zn) in hard tooth

Table 1. Trace Element Variations in a Whole Bovine Liver Compared to Replicate Analysis of NBS Bovine Liver.

	Average Concentrations [ppm]							
	As	Se	Cu	Co	Fe	Zn	Mo	La
Whole Bovine Liver n = 12 (2-gram samples) (wet wt.)	.004+.001 (25%)	<.1	25.9+2.8 (11%)	.056+.003 (6%)	240+18 (8%)	42+5 (12%)	1.3+.2 (15%)	1.7+.3 (18%)
NBS Bovine Liver Standard n = 6 (gm dry wt.)	.055+.003 (5%)	1.2+.1 (8%)	193+14 (7%)	.18+.01 (6%)	.027+.002 (7%)	125+5 (4%)	3.0+.3 (10%)	---
NBS Certified Certificate Value or recommended Interim Value	.055	1.1+.1	193+10	.18	.027+.002	130+10	3.2	---

Figure 2. Elements retained during LTA.

tissue. Metallic salts of these four metals were chosen to study as
mordants (chemicals which serve to fix a colorless surface active coupling
agent on the surface of enamel or dentin) because ions of these metals
form more stable chelates with organic completing compounds than calcium
ions, which are dominant in tooth tissue. Improved bonding might be
obtained if appropriate metal cations are placed on the tooth surface,
and in effect replace or supplement calcium ions as sites for bonding
by means of chelating or coupling agents.

The results obtained in this study will be published later in
cooperation with the ADA-NBS.

3. Analytical Research Applied to Specific NBS Programs
   a. The Use of Neutron Activation Analysis in the Evaluating of
      Sampling, Storage and Analysis of Samples for the National
      Banking System*
      T. E. Gills and L. T. McClendon

When reviewing the literature for trace element concentrations in
similar biological materials the range of the results are enormous.
Several orders of magnitude in analytical data are not uncommon, even
from laboratories using comparable (though not ridgidly standardized)
techniques for biological materials. The need to make accurate and pre-
cise measurements of selected metals in biological samples such as
human, plant and animal tissue is important to agencies who have the
responsibilities to monitor trace element pollution trends and establish
pollution guidelines. The National Bureau of Standards (NBS) has been
cooperating with the Environmental Protection Agency (EPA) in the
evaluation and improvement of methods for sampling and storage of envir-
onmental and biological materials. This research is in support of the
proposed National Environmental Specimen Bank (NESB). It is the purpose
of NESB to preserve samples for long periods so that retrospective
analyses can be made.

One important part of this research is to gain a better understanding of trace element variations within whole organs or tissue biopsies. Since many of the biologically active elements are present at the ultra trace levels, the utmost in analytical sensitivities are necessary to study and evaluate many of these trace elements. Neutron activation has been extensively used in this study due to its sensitivity and specificity for many elements in a variety of matrices. A typical analysis of a fresh whole bovine liver compared to an NBS SRM (liver matrix) is given in table 1 as an illustration of elemental variation within a tissue compared to analytical variability.

b. Prompt-Gamma Activation Analysis

R. M. Lindstrom, W. B. Walters*, and W. Zoller*

In the past year, a cooperative venture was initiated between the University of Maryland nuclear and atmospheric chemistry group and the Activation Analysis Section to design and evaluate a prompt-gamma-ray counting facility dedicated to chemical analysis. The intense, well-thermalized neutron flux available in the National Bureau of Standards Reactor (NBSR) makes it likely that this prompt-gamma facility will be the best ever operated for analytical usage.

After examining several possible ports, it was decided that a vertical beam tube in the reflector could offer the best combination of high flux ($\sim 2.2 \times 10^8/cm^2$ sec) good thermalization ($CR_{AU} \sim 20$) and low flux of scattered gamma-ray. A thimble and shutter have been designed by R. S. Carter and J. Sturrock for insertion into V5 and is currently being fabricated in the NBS Shops. An order has been placed for a large computer-based multiparameter pulse height analyzer, and designs for the target holder and beam stop, primary Ge(Li) gamma-ray detector and split-annulus coincidence detector are being completed. Initial experiments are planned for early in 1977.

c. A Study of Lithium Uptake and Location in the Brain Using the
Nuclear Track Technique

B. S. Carpenter, D. Samuel, I. Wassermann and A. Yuwiler

It is well established that lithium salts are a most effective
treatment for some mental disorders, particularly for mania and forms of
depression. In spite of their widespread use, both therapeutically and
prophylactically, their mode of action is still poorly understood. One
aspect of lithium treatment in man seems to be its mono- and bi-polar
forms. An understanding of the neurochemistry and psychopharmacology of
this disease may help in the understanding of other forms of mental dis-
order. In spite of research on the effect of lithium electrolytes, on
various neurotransmitters and other biochemical systems, little is known
about their mode of action or their distribution in mammalian brains.
One reason is the absence of a suitable, sufficiently long-lived radio-
active tracer which would enable the site and rate of turnover release
of lithium to be studied by classical biochemical techniques of labeling,
autoradiography, *etc*. A second problem is the difficulty of studying,
in vivo, metabolic processes in the brain, and the dearth of suitable
animal models of affective mental disorder.

In order to determine the lithium concentration, rate of uptake and
location in the brain, rats were injected interperitoneally with doses
of 99.6% enriched $^6Li_2CO_3$ in an inert carrier (carboxymethyl cellulose).
The doses of $^6Li_2CO_3$ varied from 50 to 100 mg/kg body weight. The rats
were sacrificed at 0, 0.5, 1, 3, 5, 8, 12, 24, and 48 hours after injec-
tion. The brains were then excised, fixed, and two sections made:
(a) a transverse section through the hypothalamus region and (b) a trans-
verse section through the pons. These sections were sandwiched between
dyed cellulose nitrate (CN) detectors and prepared for thermal neutron
irradiation. The tissues were irradiated for 90 seconds (1.33×10^{13}
$n \cdot cm^{-2} \cdot s^{-1}$) to produce α-tracks in the CN detectors from the $^6Li(n,\alpha)^3H$
reaction. The tissues were separated from the detectors and the CN de-
tectors were etched in a caustic solution. The entire area that the

brain tissues occupied on the detector was scanned, ∿13 mm by 19 mm for
each detector, by the use of an optical light transmission microscope.

Visual observation of the α-track density indicated that the
lithium was dispersed between the cortical and the subcortical regions
nonuniformly. The distribution of the track densities in the tissues
is believed to be indicative of the fact that the Li is not bound chemi-
cally in the brain to plasma protein, but remains free in plasma water.

Microscopically, the results of lithium uptake study showed that Li
reach its maximum concentration level in both the hypothalamus and the
pons region of the brain 8 hours after injection of the Li_2CO_3. Finally,
from this study the biological half-life of Li in the brain was deter-
mined by assuming they followed a first order exponential decay 12 hours
after injection. The Li biological half-life in the hypothalamus region
was found to average 29.4 ± 2.9 hours. This value is in close agreement
with the 30.9 hour value obtained from Ebadi, *et al*, data. The half-
life in the pons region was longer, 132.5 ± 17.2 hours. There are no
other results available on the biological half-life of Li in the pons
region.

4.   Analytical Support for the SRM Program

    a.   Standard Reference Materials

Much of the Section's efforts have been in support of the Standard
Reference Materials Certification Program. A wide variety of SRM's were
analyzed by NAA and the table below lists those in which activation
analysis was responsible for a significant fraction of the trace element
certification data.

Table 1

	Matrix	SRM/Reference Sample Name
(a)	Copper	Copper Benchmark
(b)	Food Grain	{ Wheat Flour Rice Flour
(c)	Body Fluids	{ Serum Freeze-Dried Urine
(d)	Water	Toxic Metals in Water
(e)	Botanicals	{ Spinach Tomato Leaves Pine Needles
(f)	Biological	Brewer's Yeast
(g)	River Sediment	Sediment
(h)	Rock	Obsidian Rock

b. SRM Feasibility Studies - SRM Mixing

R. M. Lindstrom, B. S. Carpenter and S. S. Fine

The intent of the project was to establish and test procedures by which an analyst can prepare from two different SRM's a standard sample of known intermediate composition.

The first pair of SRM's examined was pine needles and tomato leaves due to their similar particle size and density and their dissimilar trace element content. Mixing known (weighed) proportions of these two materials and analyzing each of nine mixes resulted in a satisfying predictability of concentration.

Similar mixtures have been made from pine needles and river sediment, a pair of materials that might be expected not to mix well nor stay homogeneous once blended. These experiments should give an indication of how well the simple procedures used here can be expected to predict the composition of mixtures. The final output of the work, to be completed during the transition quarter 1976, will be a manuscript describing the experiments and detailing expected variations in resultant compositions.

5.   Service Analyses

In addition to analyses on SRM's, a large number of analyses were made on non-SRM Materials. These include cooperative analyses, where the analyses were made on samples furnished by other laboratories in the past year. The following analyses were done:

1. Mercury in Soil and Calcium Chloride - G. J. Lutz, H. L. Rook
2. Mercury in Sea Water - G. J. Lutz, H. L. Rook
3. Trace Elements in Antimony Trioxide - R. M. Lindstrom, S. Fine
4. Platinum in Iron Oxide - T. E. Gills, H. L. Rook
5. Impurities in Lithium Hydroxide - T. E. Gills
6. Trace Elements in Raney Nickel - R. H. Filby
7. Trace Elements in Fiber Samples - R. M. Lindstrom, S. H. Harrison
8. Titanium in Sapphire - G. J. Lutz
9. Analysis of Gold Films - S. H. Harrison, R. M. Lindstrom
10. Trace Metals in Polyethylene Inplant Standards - T. E. Gills
11. Trace Elements in Dental Materials - L. T. McClendon, T. E. Gills
12. Boron in Silicon Detectors - B. S. Carpenter

6.   Facilities

Two major enhancements to our ability to analyze large numbers of samples were added in the past year. First, our two best Ge(Li) detector-analyzer systems were equipped with automatic sample changers (Ref: Shideler and Suddueth, in prep.), allowing unattended counting of many samples over evenings and weekends. The two sample changers are electrically similar in operation, but mechanically different so as to handle 55 mm x 12 mm petri dishes with one system and 20-ml scintillation counting vials with the other. The first system offers the ability to count samples at 5 to 10 cm from the detector face, as well as at 1 cm.

The second major strengthening of the analytical system is the addition of several additional capabilities to QLN1, the activation analysis computer code written and maintained for this Section under contract by H. P. Yule of the NUS Corporation. These features include the quantitative as well as qualitative use of the code's multiplet resolution abilities, and the estimation of upper limits for components sought but not found. The code will now handle up to 4096 channels of data per spectrum.

FILTERED BEAMS

R. B. Schwartz and I. G. Schroder
(Nuclear Sciences Division)

A 136 cm long silicon filter was placed in through tube GT-2, viewing a graphite scatterer placed at the center of the tube. This
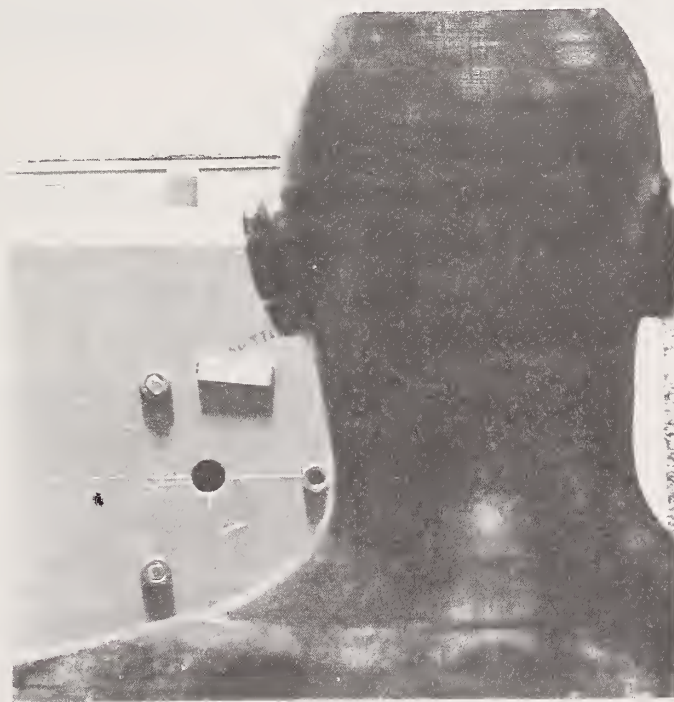

Figure 1. "Phantom" in position in front of the 2 keV beam.

arrangement produces an intense collimated beam of 144 keV neutrons. The addition of ∿ 3 cm of titanium removed a low-energy contaminant peak, resulting in an essentially pure beam of 144 keV neutrons. The beam intensity is ∿ 3×10^6 neutrons/s, in an one-inch diameter beam. The gamma ray contamination is ∿ 30 mR/hr. This 144 keV beam, together with the very pure 2 keV and 25 keV filtered beams, gives the NBS Reactor a unique facility for instrument and dosimeter calibration in the keV neutron energy range.

Typical uses for the facility include testing the response of albedo dosimeters by placing them on our anthropomorphic phantom and irradiating them under carefully controlled conditions in the various beams. Figure 1 shows the phantom in position in front of the 2 keV beam during such an irradiation.

INTERCOMPARISON OF FISSION RATE MEASUREMENTS: KARLSRUHE REACTOR PHYSICS AND LOS ALAMOS RADIOCHEMISTRY

D. M. Gilliam
(Nuclear Sciences Division)

Fission rate measurement scales at two laboratories engaged in quite different branches of nuclear energy development have been inter-compared via NBS initiative and cooperative execution. The Reactor Physics Group at GfK (Gessellschaft für Kernforschung) in Karlsruhe, Germany, submitted fissionable deposits for direct comparisons with NBS reference deposits, and the Radiochemistry Group at Los Alamos participated in joint fission rate measurements with NBS at Los Alamos. For the basic uranium fissionable isotopes, both laboratories are with-in 2% of the NBS fission rate measurement scale. This is marginally adequate for some programmatic goals; more serious, however, is a discrepancy between Los Alamos and NBS of nearly 6% for Pu-239 fission rate measurements.

NON-RRD NBS PROGRAMS

With the cooperation of Dr. Werner Scholtyssek of GfK, fissionable deposits of U-235, Pu-239, and normal uranium were sent to NBS for comparisons with the corresponding NBS reference deposits. The mass assay of the NBS reference deposits has been described in detail by Grundl, et al.[1] The GfK deposits were received and maintained in sealed fission chambers of the type used at Karlsruhe. The NBS reference deposits were mounted in nearly identical gas flow chambers. Both chambers were of the parallel plate type with the deposit positioned flush against a thin aluminum wall. The chambers were mounted so that the two deposits would be back-to-back with only the thin aluminum walls separating them. In this configuration, the chambers were positioned so that the deposits were at the center of a 4-cm-wide beam from the thermal column. The angle between the beam axis and the deposit normal was not determined to high precision, but a very accurate 180° rotation was possible by alignment of the holder base against a fixed plate on the supporting table. The relative fission rates from the two orientations were averaged in the following way:

$$(\dot{F}_{GfK}/\dot{F}_{NBS})_{AV} = \sqrt{(\dot{F}_{GfK}/\dot{F}_{NBS})_{\theta} \quad (\dot{F}_{GfK}/\dot{F}_{NBS})_{\theta+180°}}$$

where θ is the angle between the beam axis and the chamber axis. A choice of $\theta = 55°$ was made for the final deposit comparisons, based on

Table 1. Variation of the orientation in the beam.

θ	$(\dot{F}_{GfK}/\dot{F}_{NBS})_{\theta}$		$(\dot{F}_{GfK}/\dot{F}_{NBS})_{\theta+180}$		$(\dot{F}_{GfK}/\dot{F}_{NBS})_{AV}$	
70°	1.3235	± .0004	1.062	± .001	1.185	± .001
55°	1.267	± .001	1.108	± .001	1.185	± .001
35°	1.2446	± .0006	1.1334	± .0005	1.188	± .001
20°	1.215	± .002	1.136	± .003	1.175	± .003
0°	1.385	± .001	1.137	± .001	1.255	± .001

---

the data of table 1 for enriched uranium deposits at a variety of angles. Consistency with ± 0.25% is seen over the range 35° to 70°. The odd ratios at small angles are not at all surprising, since gross scattering effects from insulators, cables, support structures, and the gas line are expected at these angles.

Table 2 shows the results of the comparison and the estimated uncertainties. The largest uncertainties were the quoted errors (1.2% to 1.5%) for the NBS reference deposits themselves.[1] Other systematic errors contributed about 0.5% uncertainty or less.

Table 2. Comparison of results.

Principal Isotope	Mass Determined by NBS μg	Mass Determined by GfK μg	Mass Scale Ratio GfK/NBS
U-238	325.1 ± 1.6%	325	0.9997
U-235	309.4 ± 1.3%	311	1.0052
Pu-239	28.62 ± 1.3%	28.98	1.0126

The intercomparison of absolute fission rate measurements between NBS and the Radiochemistry Group responsible for weapons diagnostics at Los Alamos Scientific Laboratory (LASL) was carried out at LASL. After calibrations and temperature effects testing at the National Bureau of Standards Reactor, double fission chambers developed at NBS were operated in the BIG-10 critical facility at LASL simultaneously with the irradiation of an activation fission foil pack which was later destructively analyzed by the Radiochemistry Group. Table 3 shows the results of the comparison. The striking discrepancy in Pu-239 fission rates is receiving careful study by both groups.

Table 3. Fission rates (per nucleus) in BIG-10 test C-LASL.

| | Isotope Studied | | | |
	U-235	U-238	N_p-237	Pu-239
NBS Measurement (10^{-15} sec^{-1})	110.4±1.5%	4.14±1.8%	35.2±1.9%	132.3±1.6%
LASL Measurement (10^{-15} sec^{-1})	112 ±1.6%	4.21±3.8%	35.3±5%	140 ±2%
LASL/NBS	1.014	1.017	1.003	1.058

---

1. J. A. Grundl, D. M. Gilliam, N. D. Dudey, and R. J. Popek, "Measurement of Absolute Fission Rates," *Nuclear Technology* <u>25</u>, 237 (1975).

PRECISION MEASUREMENT OF THE WAVELENGTH OF NUCLEAR GAMMA LINES AND THE COMPTON WAVELENGTH OF THE ELECTRON

R. D. Deslattes, E. G. Kessler,
W. C. Sauder, and A. Henins
(Optical Physics Division)

The wavelengths of nuclear γ-lines and the Compton wavelength of the electron are being measured in terms of the wavelength of a molecularly stabilized visible laser. The wavelength measurements use a two crystal transmission spectrometer equipped with angle-measuring interferometers to determine the crystal diffraction angles. The γ-rays are diffracted by nearly perfect Ge and Si crystals whose spacings have been accurately measured in terms of the above-mentioned stabilized laser. A more detailed description of the experimental procedure has been given in other reports.[1,2]

Our activity over the past year has been primarily centered in three areas: (1) the reduction of systematic uncertainties associated with the vertical divergence correction, the angle interferometer calibration, the temperature sensitivity of the angle interferometers, and the crystal lattice spacing; (2) the irradiation of several

γ-sources of Au-198 and Ir-192 and the measurement and data analysis of the wavelengths of the associated γ-radiations; and (3) the design and manufacture of a transfer cask for nuclear γ-sources and the design of a transfer cask for the Compton wavelength measurement.

1. Reduction of Systematic Uncertainty

Several new Soller collimators have been manufactured which allow the vertical divergence correction to be varied and be more accurately calculated.

The interferometers have been recalibrated under more controlled conditions to obtain an interferometer constant accurate to 0.06 ppm. The calibration procedure involves summing to closure measurements of the interfacial angles of a 72-sided optical polygon and provides absolute angle measuring capability.

One of the angle interferometer zeroes was found to drift with temperature. This drift resulted from a temperature sensitive dove prism in the interferometer which has now been replaced with good effect. An interferometer design which eliminates the dove prism is planned for the future. Temperatures are controlled to better than 0.01 °C so that sub ppm measurements are possible even with the present interferometer.

The crystal lattice spacing was determined by first measuring the spacing of a standard Si crystal by simultaneous optical and x-ray interferometry.[3] Then, the ratios of the lattice spacings of this standard Si crystal and of the crystals used for γ-ray diffraction are measured. This transfer has been completed to the 0.5 ppm level. However, γ-ray wavelengths measured with Ge and Si crystals differ by 1 to 2 ppm as indicated below. An unknown systematic error of this magnitude is thus associated with the crystal lattice measurements or the γ-ray angle measurements. This systematic error is under investigation.

2. γ-ray Measurements

Three Au sources were irradiated with activities up to 4×10^3 Ci. These sources were used for measurement of the wavelength of the 412 keV Au-198 line. Measurements were obtained for diffraction with Ge crystals in two orders and Si crystals in three orders. Measurements in different orders are consistent. However, wavelengths measured with Si crystals are approximately 2 ppm larger than those measured with Ge crystals.

A 2×10^3 Ci Ir-192 source was produced and used for measurement of eight γ lines (205, 295, 308, 316, 468, 588, 604, 612 keV) by diffraction with Ge crystals in two different orders. Five of these lines were used in two tests of consistency by the combination principle (295 + 316 = 612 keV and 295 + 308 = 604 keV). Closure was found within 0.5 ppm. The wavelengths of four other lines (136, 416, 484, and 884 keV) were determined by use of the combination principle. The strongest four lines (295, 308, 316, and 468 keV) were also measured using Si crystals. Wavelengths measured with Si crystals are approximately 1.5 ppm larger than those measured with Ge crystals.

Although there is a 1 to 2 ppm unknown systematic associated with our wavelength measurements, our results are nonetheless 10 times more accurate than previous results.[4] A detailed summary of all our γ-ray measurements will appear shortly in reference 5.

3. Design and Manufacture of Transfer Casks

A 41 cm diameter transfer cask for intense (several kilo-Ci) nuclear γ sources was designed and constructed. The cask allows convenient irradiation of samples from the vertical ports on the NBSR.

A large diameter transfer cask for a multi kilo-Ci Cu-64 source has been designed and is under construction. This source will serve as a positron emitter in the measurement of the Compton wavelength of the electron.

1. R. D. Deslattes, E. G. Kessler, W. C. Sauder, and A. Henins, *Atomic Masses and Fundamental Constants 5*, J. H. Sanders, A. H. Wapstra, eds., Plenum Press, New York, p. 48 (1976).

2. R. D. Deslattes, E. G. Kessler, W. C. Sauder, and A. Henins, Nat. Bur. Stand. (U.S.), Tech. Note 896, 114 (Jan. 1976).

3. R. D. Deslattes and A. Henins, *Phys. Rev. Lett.* <u>31</u>, 972 (1973).

4. R. G. Helmer, R. C. Greenwood, and R. J. Gehrke, *Atomic Masses and Fundamental Constants 5*, J. H. Sanders, A. H. Wapstra, eds., Plenum Press, New York, p. 30 (1976).

5. R. D. Deslattes, *Proceedings of the School of Physics, 'Enrico Fermi'*, Metrology and Fundamental Constants Course (1976). Preprints will shortly be available.

E. Summary of Reactor Operations

Operating productivity and fuel utilization efficiency for the past year were the best in the history of the facility. The newly installed heat exchangers functioned well. Otherwise, this operating cycle was uneventful. Four papers dealing with the operation of the NBSR were presented at the August 1975 meeting of the Reactor Operations Division of the American Nuclear Society.

A summary of the overall operating statistics for this and previous years is presented in the following table.

NBSR Operating Summary

	1973	1974	1975	1976
Reactor Operations to date, MWh	229,000	290,000	328,000	396,000
Reactor Operations for year, MWh	67,000	61,000	38,000	68,000
Hours Reactor Critical	7,000	6,600	3,900	6,900
Number of Days at 10 MW	279	254	157	283
On-line Time at 10 MW	77%	70%	43%	78%
Number of fuel elements used	28	24	16	24
Average U-235 Burnup	52%	54%	53%	55%
Number of Refueling Operations	7	6	4	6
Number of Unscheduled Shutdowns	14	6	0	2
Number of Irradiations	4,300	3,000	1,550	2,360
Irradiations, Total Hours	5,250	4,300	1,800	7,250
Hours per irradiation	1.2	1.4	1.2	3
Number of Visitors	3,000	5,000	3,000	7,000

ACTIVATION ANALYSIS PROGRAM OF THE
FOOD AND DRUG ADMINISTRATION AT THE NBSR

J. T. Tanner and M. H. Friedman
(Food and Drug Administration, Washington, DC)

1.   Analysis of Chlorine in Japanese Rice Oil

During 1968 an incident in Japan (the so-called "Yusho" poisoning) resulted in the contamination of a large quantity of rice oil with poly-chlorinated biphenyls (PCB). Several people died and many were injured ppermanently as a result of consuming this contaminated cooking oil. The FDA has recently been reviewing regulations governing the amount of PCB allowable in foods. Since much of the data on the effect of PCB on man was gathered as a result of this accidental contamination incident in Japan, it was very important that there be an accurate analysis of this oil for PCB.

A sample of this rice oil was analyzed at the FDA headquarters laboratory for PCB's and compared with an earlier analysis of PCB done in Japan. The results differed by almost a factor of two. The analytical procedure used by FDA was the official method of analysis for PCB currently listed by the A.O.A.C. The Japanese data were based on earlier methodology and on neutron activation analysis for total chlorine.

In support of the pesticide analysis unit of FDA, the NAA unit analyzed the contaminated oil for chlorine. The NAA results supported the original Japanese analysis. Since control rice oil contained virtually no chlorine, the chlorine detected was assumed to be bonded to the PCB (approximately 50% chlorine) or another yet unknown contaminant.

To resolve the factor of two discrepancy, the pesticides unit then succeeded in separating the chlorine containing compounds by adsorption chromotography and GLC into two fractions. One fraction contained PCB and results from NAA chlorine determination and the A.O.A.C. PCB method were equivalent. The second fraction was a group of later components

from a GLC column and contained an equivalent amount of chlorine. This resolved the factor of two discrepancy between analyses at FDA and in Japan. To date, the other chlorine containing compound(s) have not been identified.

2.   Analysis of Animal Waste Material

Recently it has become common practice to use animal waste as a feed ingredient for animal feeds. This practice has been approved by

Table 1. Elemental concentration of animal waste material (µg/g)

Element	Dried Cattle Manure (low fiber)	Dried Cattle Manure (high fiber)	Dried Processed Waste Pellets	Dried Poultry Waste (with litter)	Dried Poultry Waste	Dried Sewage Sludge
Fe	2394±444	4565±611	1890±125	895±84	1838±14	15414±444
Zn	109±11	79±10	69±3	165±3	140±12	1752±113
Rb	19±2	37±1	14.7±0.2	8.8±1.1	12.7±1.3	32±11
Co	1.7±0.5	2.2±0.5	1.1±0.2	2.0±0.3	1.2±0.1	7.1±2
Sb	0.28±0.02	0.29±0.05	0.22±0.02	0.37±0.02	0.38±0.02	6.3±1.8
Br	29±4	29±2	56±3	9±2	20±2	30±3
Cr	20±7	31±9	5±1	6±1	4.9±0.3	280±105
Se	0.5±0.2	0.6±0.1	0.29±0.01	0.4±0.1	0.7±0.2	4.8±1.2
Ba	0.09±0.02	0.17±0.01	0.07±0.01	<0.2	<0.1	0.8±0.2
Sc	<0.7	<2	<0.4	0.19±0.02	0.3±0.1	---
Cs	0.13±0.02	0.33±0.05	0.25±0.06	0.06±0.02	0.10±0.04	0.58±0.03
La	2.6±0.4	11±1	2.5±0.5	2.4±0.4	1.9±0.2	27±8
Eu	0.13±0.02	0.5±0.2	0.09±0.03	0.05±0.02	0.07±0.03	0.6±0.1
V	1.6±0.4	9±5	2±1	2.9±0.3	2.9±0.3	21±2
Ca	10500±700	10500±700	12500±2000	48000±3000	62000±7000	27000±6000
Cl	7800±600	6050±1300	5200±400	3400±100	5300±400	570±100
Al	6300±300	12000±5000	2600±600	1070±15	2400±100	19000±900
Mg	2300±800	2900±700	4000±500	3200±1000	3600±400	4000±2000
Cu	<100	<100	<50	<50	<100	500±60
Mn	40±17	103±9	57±6	130±50	160±20	210±40
Na	5600±700	6800±1500	3300±900	1600±400	3500±900	3400±800
K	21000±8000	16000±4000	20000±4000	15000±3000	15000±3000	14000±7000
As	<1.4	<1.6	<1.2	<1.2	<1.4	4±1

*The above samples were collected from the feed lots (except sludge) and air dried. The sludge was also air dried.

seven states for animals in intrastate commerce, but has not been approved by FDA for animals in interstate commerce. In order to establish base line information about trace metals in typical animal waste products, samples of dried waste from animals with a known diet history and a sample of processed waste pellets composed of a mixture of animal feed and dried animal waste were obtained for analysis. In addition a sample of sewage sludge, which is being tested as an animal feed ingredient on an experimental basis, was analyzed. The results of these analyses are given in table 1. The high levels of many metals in both animal waste products and sewage sludge indicate that the practice of using animal waste or sewage sludge as animal feed ingredients should be carefully evaluated before being fully sanctioned.

IMPROVED MATERIAL FOR SOLAR ENERGY CELLS

T. M. Raby

Neutron Transmutation Doped (NTD) silicon is beginning to assume a position of major importance in the semiconductor device field and may have wide ranging application in the development of solar energy cells.

It has been recognized in recent years that silicon is almost an ideal material for transmutation doping. Normally available silicon contains 3% Si-30 which transmutes to P-31 on the capture of a thermal neutron. This process produces a uniform concentration of phosphorus, a paramount factor in the material's performance and use.

The NBS reactor, with its extensive and versatile facilities and its intense highly thermalized neutron flux, is ideally suited for transmutation doping of materials. Over the past several months, together with the Oak Ridge National Laboratory, numerous silicon samples have been irradiated at the NBS reactor. Extensive research is currently being carried out to study the use of NTD silicon in power

devices and solar cells and to expand its application into other semi-
conductor fields. The success of this work could mark a new era in the
use of reactor produced materials in important energy fields.

ATF'S FORENSIC ACTIVATION ANALYSIS PROGRAM

C. M. Hoffman
(U.S. Treasury Department, Washington, DC)

Although the use of NAA for detecting barium and antimony in gun-
shot residues has been replaced by flameless atomic absorption spectro-
photometry, NAA still plays a valuable role in the analysis of trace
evidence. The method's sensitivity and non-destructive nature make the
technique very attractive for the analysis of certain types of physical
evidence commonly found at crime scenes.

During the past year, our Laboratory used NAA to examine evidence
in 175 cases. This evidence consisted of hair, paint, glass, soil and
metal particles.

The conclusions drawn by a Laboratory examiner concerning the re-
lative origins of questioned and known evidentiary materials depends
upon the analytical background data available for the type of material
under examination. Characterization of the material requires that a
significant quantity of data be available for this evaluation. Studies
of various materials, such as paint and glass, are being conducted by
our laboratory scientists to meet this need. For example, glass samples
which cannot be discriminated by their refractive index, density or ele-
mental composition as determined by x-ray flourescence, will be studied
by NAA to assess the worth of this method as it applies to this type of
problem.

LUNAR SAMPLE ANALYSIS FOR 20 TRACE ELEMENTS

E. Anders
(University of Chicago, Chicago, IL)

During the last year, numerous samples were analyized for 20 trace elements (Ag, Au, Bi, Br, Cd, Cs, Ge, In, Ir, Ni, Os, Pd, Rb, Re, Sb, Se, Te, Tl, U and Zn) by radiochemical neutron activation using the NBS Reactor. This is part of a continuing extensive program to determine the origin and constituents of lunar samples. The analysis involved trace levels as low as one part in 10^{15} and will be compared with those obtained from meteorite specimens.

ACTIVATION ANALYSIS PROGRAM OF THE U. S. GEOLOGICAL SURVEY

J. J. Rowe and P. A. Baedecker

(U. S. Geological Survey, Reston, VA)

Activation analysis is being applied by the Radiochemistry Project, Reston to the determination of trace concentrations of elements in geological materials. The technique is used for the analysis of rocks, minerals, waters and coals for geochemical studies related to ore formation, magmatic differentiation, hydrothermal alteration and transport, energy reserves and environmental problems.

Coals are being analyzed as part of a program to study the trace element content of U. S. coals. More than 1000 coal samples per year are being analyzed for 24 elements. This is possible through the use of automated counting equipment and computer data reduction. The system operates 24 hours per day, 7 days per week to collect gamma ray spectra onto magnetic tape. Samples are counted 4 days after irradiation and then again 6 weeks later. The data from the two counts are processed by computer to provide the final analytical report (Table 1). Through the use of epithermal neutron irradiations at the JEEP reactor, Kjeller, Norway we were able to instrumentally determine U, Sr, Mo, and Ni and

INSTRUMENTAL NEUTRON ACTIVATION ANALYSIS SUMMARY REPORT

JOB NUMBER: AH29
SUBMITTED BY: JACK H. MERLIN
ANALYST: LILLIE JENKINS
IRRADIATION NUMBER: S-102
SAMPLE DESCRIPTION: COALS

SAMPLE:	W1910700 AL-1 ( )	W1910710 AL-2 ( )	W1910720 AL-3 ( )	W1910730 AL-4 (A)	W1910730 AL-4 (B)	W1910730 AL-4 (C)	W1910740 AL-5 ( )	W1910750 AL-6 ( )	W1910760 AL-7 (A)	W1910760 AL-7 (B)
WEIGHT:	0.10215	0.10780	0.10574	0.10672	0.12126	0.13285	0.10277	0.12059	0.10753	0.12266
FE (%)	1.30	1.19	0.81	1.99	1.94	2.00	0.79	1.36	0.47	0.55
SIGMA(%)	1(2)	1(2)	1(2)	1(2)	1(2)	1(2)	1(2)	1(2)	1(2)	1(2)
AS (PPM)	19.2	43.9	10.7	57.1	60.6	63.1	17.8	12.5	8.8	11.3
SIGMA(%)	1(1)	1(1)	1(1)	1(1)	1(1)	1(1)	1(1)	1(1)	1(1)	1(1)
BA (PPM)	319	109	648	414	429	426	339	284	176	237
SIGMA(%)	9(1)	13(1)	3(1)	4(1)	4(1)	3(1)	4(1)	5(1)	7(1)	4(1)
BR (PPM)	2	4	2	9	9	9	1	4	2	2
SIGMA(%)	3(1)	1(1)	3(1)	1(1)	1(1)	1(1)	2(1)	2(1)	2(1)	2(1)
CO (PPM)	6.3	3.4	6.6	2.4	2.3	2.4	5.7	5.2	4.2	4.4
SIGMA(%)	7(2)	7(2)	7(2)	3(2)	2(2)	1(1)	1(2)	2(2)	2(1)	2(1)
CR (PPM)	39.9	21.0	30.7	16.4	16.8	16.5	9.1	22.9	12.9	11.8
SIGMA(%)	5(2)	6(2)	3(2)	8(2)	5(2)	5(2)	6(2)	4(2)	7(2)	6(2)
CS (PPM)	2.8	1.4	1.8	1.2	1.0	1.0	0.4	1.5	0.7	0.7
SIGMA(%)	6(2)	6(2)	5(2)	7(2)	8(2)	6(2)	6(1)	5(2)	8(2)	6(2)
HF (PPM)	2.0	0.7	2.1	1.0	0.9	0.8	0.5	1.6	0.5	0.5
SIGMA(%)	8(2)	3(2)	2(2)	3(2)	7(2)	2(2)	3(2)	2(2)	4(2)	4(2)
RB (PPM)	< 50	< 23	< 31	< 24	< 17	< 15	< 25	< 25	< 19	< 14
SIGMA(%)	0(1)	0(1)	0(1)	0(1)	0(1)	0(1)	0(1)	0(1)	0(1)	0(1)
SB (PPM)	1.33	2.57	0.61	1.39	1.36	1.56	0.31	1.29	1.50	1.61
SIGMA(%)	3(2)	1(2)	4(2)	2(2)	2(2)	1(2)	5(2)	2(2)	2(2)	2(2)
SE (PPM)	5.5	2.6	5.2	4.2	3.3	3.5	3.0	6.0	2.2	2.2
SIGMA(%)	6(1)	9(1)	6(1)	5(1)	15(2)	9(2)	17(2)	9(2)	9(1)	7(1)
TA (PPM)	0.48	0.13	0.51	0.24	0.23	0.24	0.09	0.61	0.10	0.10
SIGMA(%)	5(1)	16(1)	5(1)	7(1)	6(1)	6(1)	15(1)	9(2)	15(1)	16(1)
TH (PPM)	7.7	1.7	6.2	3.0	3.0	3.1	1.3	4.4	2.2	2.2
SIGMA(%)	4(1)	6(1)	4(1)	8(1)	4(1)	5(1)	29(1)	5(1)	6(1)	8(1)
ZN (PPM)	< 41	13	17	13	11	13	8	17	12	11
SIGMA(%)	2(1)	3(1)	3(1)	3(1)	3(1)	2(1)	4(1)	2(1)	3(1)	3(1)
W (PPM)	0.99	2.37	1.22	0.92	0.86	0.82	0.38	1.04	0.74	0.65
SIGMA(%)	5(1)	5(1)	4(2)	6(1)	6(1)	6(1)	4(1)	6(1)	6(1)	6(1)
SC (PPM)	8.69	4.78	6.43	3.73	3.61	3.59	1.69	5.16	4.22	4.12
SIGMA(%)	1(2)	1(2)	1(2)	1(2)	1(2)	1(2)	1(2)	1(2)	1(2)	7(1)
LA (PPM)	24	6	21	11	11	11	9	14	10	10
SIGMA(%)	1(1)	1(1)	1(1)	1(1)	1(1)	1(1)	1(1)	1(1)	1(1)	1(1)
CE (PPM)	48	14	41	21	19	19	15	27	21	19
SIGMA(%)	4(2)	4(2)	4(2)	5(2)	3(2)	4(2)	4(2)	4(2)	3(2)	2(2)
SM (PPM)	3.7	1.2	3.3	1.7	1.7	1.7	1.4	2.3	2.2	2.1
SIGMA(%)	1(1)	1(1)	1(1)	1(1)	1(1)	1(1)	1(1)	1(1)	1(1)	1(1)
EU (PPM)	0.96	0.21	0.68	0.30	0.30	0.32	0.26	0.54	0.43	0.46
SIGMA(%)	7(2)	3(1)	7(2)	2(1)	5(1)	7(2)	2(1)	7(2)	7(2)	6(2)
TB (PPM)	0.49	0.15	0.39	0.22	0.21	0.21	0.14	0.31	0.31	0.35
SIGMA(%)	7(1)	12(1)	7(1)	11(1)	11(1)	10(1)	9(1)	8(1)	7(1)	16(2)
YB (PPM)	1.4	0.6	1.3	0.7	0.6	0.6	0.5	1.1	0.9	0.8
SIGMA(%)	8(2)	8(2)	9(2)	10(2)	8(2)	7(2)	10(2)	6(2)	9(2)	7(2)
LU (PPM)	0.22	0.16	0.24	0.12	0.13	0.12	0.08	0.19	0.15	0.15
SIGMA(%)	18(1)	10(1)	9(1)	15(1)	20(1)	12(1)	18(1)	11(1)	11(1)	12(1)

ERROR LIMITS ARE ONE STANDARD DEVIATION BASED ON COUNTING STATISTICS ALONE
NUMBER IN PARENTHESES IS NUMBER OF INDIVIDUAL RESULTS, BASED ON REPETITIVE COUNTS, AVERAGED TO YIELD EXPRESSED RESULT

INSTRUMENTAL NEUTRON ACTIVATION ANALYSIS SUMMARY REPORT

JOB NUMBER: AD-74   SUBMITTED BY: SMITH   ANALYST: BAEDECKER

IRRADIATION NUMBER: 94,117   SAMPLE DESCRIPTION: VALLES MTNS. N.M.

SAMPLE:	W176910 71-15	W176911 71-16	W176912 71-17	W176913 71-18	W176914 71-19	W176915 71-20	W176916 71-21	W176917 71-22	W176918 71-23	76-50
WEIGHT:	0.10684	0.11174	0.12156	0.11953	0.09830	0.12882	0.12996	0.11413	0.12181	0.19069
FE (%)	1.29	1.24	1.19	1.15	1.19	0.97	1.00	0.98	0.99	1.07
SIGMA(%)	1(2)	1(2)	1(2)	1(2)	1(2)	1(1)	1(1)	1(1)	1(1)	1(2)
BA (PPM)	207	170	205	218	174	163	148	143	133	159
SIGMA(%)	8(1)	9(1)	7(1)	7(1)	10(1)	9(1)	9(1)	11(1)	11(1)	7(1)
CD (PPM)	0.4	0.5	0.6	0.6	0.4 <	1.1 <	1.1 <	1.0	0.5	0.5
SIGMA(%)	7(1)	6(1)	13(2)	13(2)	7(1)	9(1)	0(1)	0(1)	0(1)	31(2)
CR (PPM)	6.9	3.5	6.2	5.2	3.1	1.4	3.1	3.2	3.1	6.7
SIGMA(%)	13(1)	10(1)	18(1)	19(1)	18(1)	10(1)	0(1) <	0(1) <	0(1)	4(1)
CS (PPM)	9.6	10.0	11.0	10.2	10.6	10.1	10.0	10.4	10.3	6.0
SIGMA(%)	3(2)	3(2)	2(2)	3(2)	3(2)	6(1)	2(1)	6(1)	6(1)	3(2)
HF (PPM)	14.7	13.8	13.1	13.5	13.5	12.3	12.1	12.3	12.6	7.2
SIGMA(%)	1(2)	1(2)	1(2)	1(2)	1(2)	1(1)	1(1)	1(1)	1(1)	1(2)
RB (PPM)	302	313	301	314	289	342	340	334	351	139
SIGMA(%)	5(2)	5(2)	2(2)	2(2)	5(2)	4(1)	4(1)	4(1)	4(1)	6(2)
SB (PPM)	1.0	0.8	0.6	0.5	0.5	2.4	2.5	2.3	2.3	0.2
SIGMA(%)	16(2)	9(1)	10(1)	11(1)	12(1)	0(1) <	0(1) <	0(1) <	0(1)	14(1)
TA (PPM)	12.53	11.49	11.08	12.03	11.04	15.94	15.69	15.69	15.90	3.52
SIGMA(%)	1(2)	1(2)	1(2)	1(2)	1(2)	2(1)	2(1)	1(1)	1(1)	1(2)
TH (PPM)	39.3	35.9	36.1	36.9	35.1	44.7	45.3	45.4	44.5	13.7
SIGMA(%)	1(2)	1(2)	1(2)	1(2)	1(2)	2(1)	2(1)	2(1)	2(1)	2(2)
ZN (PPM)	129	195	122	127	111	89	85	79	82	57
SIGMA(%)	2(1)	2(1)	2(1)	2(1)	3(1)	3(1)	3(1)	4(1)	3(1)	2(1)
ZR (PPM)	338	377	346	320	304	329	279	295	298	234
SIGMA(%)	7(1)	6(1)	7(1)	6(1)	8(1)	6(1)	8(1)	7(1)	7(1)	6(2)
SC (PPM)	1.02	0.94	0.87	0.83	0.87	0.54	0.55	0.55	0.54	1.36
SIGMA(%)	1(2)	1(2)	1(2)	1(2)	1(2)	2(1)	2(1)	2(1)	2(1)	1(2)
LA (PPM)	74	67	69	68	73	47	50	49	48	72
SIGMA(%)	1(1)	1(1)	1(1)	1(1)	1(1)	1(1)	1(1)	1(1)	1(1)	1(1)
CE (PPM)	136	133	139	132	139	109	111	113	111	114
SIGMA(%)	1(1)	1(3)	1(3)	1(3)	1(3)	2(2)	1(2)	1(2)	2(2)	1(3)
ND (PPM)	62	55	52	52	62	48	54	50	49	49
SIGMA(%)	6(3)	7(3)	7(3)	7(3)	7(3)	6(2)	6(2)	6(2)	7(2)	4(3)
SM (PPM)	15.6	14.2	14.0	13.8	14.8	13.9	14.7	14.7	14.4	9.2
SIGMA(%)	2(1)	2(1)	1(1)	2(1)	1(1)	1(1)	2(1)	1(1)	1(1)	2(1)
EU (PPM)	0.12	0.10	0.09	0.17	0.10	0.06	0.06	0.06	0.06	0.31
SIGMA(%)	17(2)	13(2)	16(2)	16(2)	18(2) <	0(1) <	0(1) <	0(1)	34(1)	4(2)
TB (PPM)	3.25	2.92	2.80	2.87	2.83	2.70	2.72	2.85	2.69	1.38
SIGMA(%)	2(2)	2(2)	2(?)	2(2)	2(2)	4(1)	4(1)	3(1)	4(1)	3(2)
YB (PPM)	13.1	12.7	12.2	12.9	12.6	12.3	12.0	12.2	11.6	4.5
SIGMA(%)	1(2)	1(2)	1(2)	1(2)	1(2)	2(1)	2(1)	1(1)	2(1)	1(2)
LU (PPM)	1.88	1.69	1.69	1.73	1.68	1.61	1.63	1.67	1.59	0.64
SIGMA(%)	3(2)	3(2)	2(2)	2(2)	3(2)	5(1)	5(1)	5(1)	6(1)	6(2)

ERROR LIMITS ARE ONE STANDARD DEVIATION BASED ON COUNTING STATISTICS ALONE
NUMBER IN PARENTHESES IS NUMBER OF INDIVIDUAL RESULTS, BASED ON REPETITIVE COUNTS, AVERAGED TO YIELD EXPRESSED RESULT

improve the determination of Co, Zn, As, Se, Br, Rb, Cs, Ba, Sm, Tb, Hf, Ta, W and Th to supplement the thermal irradiations done at the NBS reactor.[1]

The project has been analyzing a wide variety of geological materials for numerous programs of the Survey. Gold has been determined in sediments and igneous rocks using a fire assay radiochemical method.[2] Ruthenium and iridium were studied in chromites using a fire assay radiochemical method with collection into a platinum bead[3,4] followed by Ge(Li) or coincidence counting.

The NBS reactor facility has been utilized to provide thermal neutron irradiations leading to the determination of 22 to 24 elements in many geologic matrices (Table 2). In some cases the thermal irradiations have been supplemented by epithermal irradiations to instrumentally determine tungsten, cesium, rubidium, barium, uranium and thorium when they occur at low concentrations.

---

1. Rowe, J. J. and Steinnes, E., "Determination of 30 elements in coal and fly ash by thermal and epithermal neutron activation analysis". (submitted to Talanta)

2. Rowe, J. J. and Simon, F. O., "Determination of gold in geologic materials by neutron activation analysis using fire assay for radiochemical separations". U.S.G.S. Circ 599.

3. Greenland, L. P., Rowe, J. J. and Dinnin, J. I., "Application of triple coincidence counting and of fire-assay separation to the neturon-activation determination of iridium". U.S.G.S. Prof Paper 750-B, p. 175-179 (1971).

4. Page, N. J., Rowe, J. J. and Haffty, J., "Platinum metals in the Stillwater Complex, Montana" (submitted to Econ. Geol.).

TRACE ELEMENTS IN THE ENVIRONMENT
AND RADIOACTIVE DECAY STUDIES

W. H. Zoller, G. E. Gordon and W. B. Walters
(University of Maryland, College Park, MD)

Our group has made extensive use of the NBSR for the irradiation of numerous samples for trace-element analysis using instrumental neutron activation analysis (INAA). We have had our computer-based Northern Scientific analyzer system and two Ge(Li) γ-ray detectors at the Reactor for periods of several weeks during the last year to count short-lived radioactive products. Most of the other samples are returned to the university for counting long-lived activities.

In our "local" air pollution studies we have applied INAA to particles collected in the stacks of coal and oil-fired power plants and municipal incinerators. We have also analyzed particles collected with airplanes in the plumes of the Vienna oil-fired plant, and the Chalk Point (Md.), Dickerson (Md.) and Four Corners (New Mexico) coal-fired plants. (The latter is a joint venture with Lawrence Livermore Laboratory and some of the analyses have been done there.) We have also analyzed ambient aerosols collected from several sites in Washington, D. C. during the summer of 1975. Briefly we find that:

(1) We can now account almost quantitatively for the sources of about thirty elements observed in the Washington atmosphere.

(2) Coal combustion does not appear to be the major source of most toxic elements, exceptions being As, Se and vapor-phase Hg.

(3) From previous years' work, motor vehicles are the major sources of atmospheric Pb, Br, Cl and, possibly, Ba.

(4) Oil-fired plants are major sources of V, Ni and possible Se.

(5) Municipal incinerators release little total mass, but the particles are so rich in many trace elements that they are often a major source of urban, ambient Zn, Cd, Sb and, possibly, Ag and Sn. Since Sb and Cd are clearly toxic, this finding raises a serious question about the proposed use of urban refuse as a supplement to coal in power plants.

Recently we have begun studies on additional sources: cement plants and steel mills.

We are also continuing our studies of global atmospheric particulate samples. We have analyzed additonal particulate samples collected from the very clean air of the South Pole. Since there is essentially total snow cover there, the particles have had to be transported long distances. The enrichment factors of many elements are the same as for urban air, so one might be tempted to assume that those particles originate from anthropogenic sources. However, one cannot assume that without investigating particles from natural sources, of which volcanoes are a major example. In order to obtain better information on volcanic emissions, we collected aerosols from the Jan./Feb. 1976 Mt. Augustine eruption in Alaska with the use of an airplane operated by the National Center for Atmospheric Research in Boulder. Preliminary analyses of these samples indicate that a number of moderately volatile elements are highly enriched on the volcanic particles.

In our decay scheme studies we have completed work on the $\gamma\gamma$ angular correlations in Rh-105 following the decay of 4.4-hr Ru-105 and published the results in Physical Review C. The results of earlier studies of the decay of Te-134 to levels of I-134 have also been published. New coincidence data have been taken for the decay of 100-min Nd-149 to levels of Pm-149, 12-min Nd-151 to levels of Pm-151, 5-hr and 20-min Pd-111 isomers to levels of Ag-111, and 3.4-hr and 2.6-hr Cd-117 isomers to levels of In-117.

THE NON-DESTRUCTIVE DETERMINATION OF TRACE ELEMENT CONCENTRATIONS BY NEUTRON-CAPTURE γ-RAY SPECTROMETRY

G. E. Gordon, W. H. Zoller, D. Anderson,
M. Failer, and W. B. Walters
(University of Maryland, College Park, MD)

In cooperation with Dr. Richard Lindstrom of the NBS Activation Analysis Section, efforts are underway to develop a neutron-capture

γ-ray spectrometer for the purpose of non-destructive trace-element concentration measurements. The system is to include a split-annulus Compton-suppressed Ge(Li) pair spectrometer whose pulses are automatically collected and analyzed by an 80K PDP 11/34. Construction of the reactor beam tube is underway (with design help and some machining by the Reactor staff) and the fabrication of external shielding is being planned.

The computer system has been ordered and the development of the software system is advancing.

G. STAFF ROSTER

ORGANIZATION CHART

REACTOR RADIATION DIVISION

314.00
Division Office

R. S. Carter, Chief
T. M. Raby, Deputy Chief

E. Maxwell, Admin. Officer*
E. Simms, Receptionist
L. Sprecher, Sec'y*

314.01
Reactor Operations
T. M. Raby, Chief
J. F. Torrence, Deputy

D. Ahalt, Sec'y

R. Beasley
M. Bell
N. Bickford
H. Brake
J. Browning
D. Cea
A. Chapman
H. Dilks
W. Mueller
D. Nelson
J. Ring
R. Stiber
D. Wilkison
B. Young

314.02
Engineering Services
J. H. Nicklas, Chief

D. Davitt, Sec'y*

P. Beachley
R. Conway
J. Darr
O. Frizzell
E. Guglielmo
R. Hayes
J. Sturrock

Technical Support

H. Berger
R. Casella
M. Dorsey*
D. Garrett
M. Ganoczy
B. Mozer
V. Myers
F. Shorten

314.03
Neutron S-S Physics
J. J. Rush, Chief

B. Crowther, Sec'y

A. Cinquepalma
D. Fravel
C. Glinka
J. Norvell
E. Prince
J. Rhyne
J. Rowe
W. Rymes
A. Santoro
A. Tudgay

*Temporary or part-time
**NRC post doctoral appointee

119

STAFF ROSTER

NON-RRD NBS STAFF LOCATED AT REACTOR

Division 240.01

P. R. Cassidy
H. E. DeSpain
J. J. Shubiak
F. Moore

Division 241.05

R. A. Dallatore
C. Eisenhauer
R. Fleming
D. Gilliam
J. A. Grundl
I. G. Schroder
R. Schwartz
V. Spiegel

Division 310.08

B. S. Carpenter
B. J. Clipper
K. M. Cunningham
B. N. Garrigues
T. E. Gills
R. R. Greenberg
C. A. Grimm
S. H. Harrison
R. M. Lindstrom
G. J. Lutz
L. T. McClendon
N. Sato
H. L. Rook

GUEST WORKERS AND COLLABORATORS

Division 213.04

D. G. Eitzen

Division 232.06

R. D. Deslattes
E. G. Kessler
W. C. Sauder
J. Snyder

Division 241.05

C. Bowman
K. Duvall
H. Heaton
G. Tamaze

Division 242.06

L. L. Lucas
F. J. Shima

Division 311.03

C. Han

Division 311.05

W. Brown
M. Mathew
L. Schroeder

Division 312.02

R. Reno

Division 313.03

D. B. Minor
R. S. Roth

Division 313.04

G. J. Rosasco

Division 313.06

A. B. Mighell

Building Technology

P. Brown

120

STAFF ROSTER

Argonne National Laboratory

H. Flotow
D. L. Price
K. Skold
S. Susman

Battelle, N. W.

L. Brachenbush
G. Endres
W. Nicholson

Federal Bureau of Investigation

D. B. Davies
J. Haverkost
J. W. Kilty
E. Mitchell
J. P. Riley

Food and Drug Administration

M. Friedman
J. T. Tanner

Harry Diamond Laboratory

C. Heimbach
D. McGarry

National Institutes of Health

D. Davies
R. Frank
W. Hagins
W. Robinson

Naval Air Defense Command

M. Stellabotte
W. Williams

Naval Air Rework Facility

R. Chavez

Naval Engineering Center

P. Soltis

Naval Research Laboratory

P. D'Antonio
B. Das
A. Erlick
J. Karle
R. Meussner
J. Milstein

Naval Surface Weapons Center
(Dahlgren Laboratory)

R. Buckingham

(White Oak Laboratory)

H. Alperin
P. Hesse
D. Polansky
R. Williams

Oak Ridge National Laboratory

H. A. Mook
M. Mostoller
H. G. Smith

Picatinny Arsenal

N. Chesser
C. S. Choi
M. K. Farr
H. J. Prask
S. Trevino

Smithsonian Institution

T. Chase
J. Mishara

U. S. Geological Survey

P. Baedecker
J. J. Rowe

U. S. Treasury Department

J. M. Hoffman
W. Kinard
L. Reid

American University

R. Abbundi
R. A. Segnan

Colorado State University

C. E. Patton

Georgetown University

K. Barkigia
C. Quicksall

Howard University

G. A. Ferguson

Reed College

W. Parker

University of California
(Lawrence Livermore Laboratories)

J. Browne
S. Hankins

University of Chicago

E. Anders

University of Maryland

D. Anderson
C. Choquette
W. Cunningham
M. Failey
P. Gallagher
M. Germani
B. Glagola
M. Glascock
D. Glotfelty
G. Kowalczyk
E. Lepel
J. Levkoff

J. Muhlbaier
D. Reamer
E. Schneider
M. Small
P. Solomon
E. Sombrito
K. Steffansson
W. Walters
W. Zoller

U. S. Naval Academy

C. S. Schneider

University of Rhode Island

S. J. Pickart

Allied Chemical Corporation

G. Liebowitz
A. Maeland
R. O'Handy

General Electric Company

F. Lubursky

Idaho National Engineering Laboratories

H. D. Reeder
J. R. Smith

Old Delft Corporation

D. Bracher

COLLABORATIVE PROGRAMS

ALPERIN, H. A., FLOTOW, H., RUSH, J.J., RHYNE, J.J., "Deuterium-Site Occupancy in the α and β Phases of TiDx," (in press).

ALPERIN, H. A., CULLEN, J.R., and CLARK, A.E., "Magnetic Properties of Bulk Amorphous Tb_xFe_{1-x}," *A.I.P. Conf. Proc.*, 29, 186, (1975).

BERGER, H., "Californium-252 As A Source For Thermal Neutron Radiography," *Symposium International Sur L'Utilization Du Californium-252*, (to be published).

BERGER, H., "Nondestructive Evaluation: A Review of Nuclear Methods," *Instrumentation in the Aerospace Industry*, Vol. 22, (1976).

BERGER, H., "Practical Applications of Neutron Radiography and Gaging," *ASTM STP 586, American Society for Testing and Materials*, (1976).

BERGER, H., "Detection Systems for Neutron Radiography," *Proc. Symposium on Practical Applications of Neutron Radiography and Gaging, ASTM STP 586*, (1976).

BERGER, H., PARKER, W. L., LAPINSKI, N. P., REIMANN, K. J., "Three-Dimensional Inspection by Thermal Neutron Laminagraphy," *Transactions American Nuclear Society*, Vol. 23, (1976).

BERGER, H., "Nondestructive Measurements: How Good Are They," *Materials Evaluation*, 34, 18A-24A, 33A-34A (1976).

BERGER, H. and MOTZ, J. W., "A Qualitative Discussion of Quantitative Radiography," in *Prevention of Structural Failure*, No. 5 *Materials/ Metalworking Technology Series* (1975).

CASELLA, R. C., TREVINO, S. F., and ROWE, J. M., "Determining the Number of Independent Real Parameters in the Phonon Dynamical Matrix," *Phys. Rev.* B12, 4573 (1975).

CHESSER, N. J. and PRASK, H. J., "Quasielastic Neutron Scattering Study of Single Crystal Ammonium Perchlorate," *Proceedings Conf. on Neutron Scattering*, Gatlinburg, TN (in press).

CHOI, C. S., PRASK, H. J., and PRINCE, E., "Ammonium Perchlorate: Re-investigation of the Crystal Structure at 298°K," *Acta. Cryst.* (in press).

CHOI, C. S., "Crystal Structures of the Inorganic Azides," Chapter 73 in *Physics and Chemistry of the Inorganic Azides*, Vol. 1, (R. Walker and H. Fair, Editors), Plenum Press (in press).

CHOI, C. S., SANTORO, A., and MARKINKAS, P. L., "1,3,5-Triacetye-2,4,6-heradhydro-S-triazine (TRAT)," *Acta. Cryst.*, B31, 2934 (1975).

CHOI, C. S., SANTORO, A., and ABEL, J. E., "The Crystal Structure of 3, 7-diacetyl 1,3,5,7 tetraza-bicyclo [3,3,1] nonane (DAPT)," *Acta. Cryst.*, B32, 354 (1976).

CHOI, C. S., and PRINCE, E., "A Neutron Diffraction Study of Structure and Thermal Motion in Several Monovalent Metal Azides," *J. Chem. Phys.*, 64, 4510 (1976).

FARR, M. K. and TREVINO, S. F., "Mode Gruneisen Parameters of KBr Determined by Inelastic Neutron Scattering," *Proceedings of the Conference on Neutron Scattering*, Gatlinburg, TN. (in press).

FARR, M. K., GIGUERE, P. A., and ARNAU, J. L., "The Lattice Dynamics of Deuterium Peroxide," *Proceedings of the Conference on Neutron Scattering*, Gatlinburg, TN. (in press).

GLINKA, C. J., ROWE, J. M., and RUSH, J. J., "Inelastic Neutron Scattering Lineshapes in PdD_{63}," *Proc. Conf. on Neutron Scattering*, Gatlinburg, TN. (in press).

GLINKA, C. J., MINKIEWICZ, V. J., and PASSELL, L., "Absolute Measurement of the Critical Scattering Cross Section in Cobalt," *AIP Conf. Proc.*, 29, 499 (1976).

IQBAL, Z., PRASK, H. J. and TREVINO, S. F., "Molecular Vibrations and Lattice Dynamics of Inorganic Azides," *Physics and Chemistry of the Inorganic Azides*, (R. Wlaker and H. Fair, editors) Plenum Press (in press).

IQBAL, Z., CHOI, C. S., CHRISTOE, C. W., FORSYTH, A. C., PRASK, H. J. and TREVINO, S. F., "Advances in Techniques for Structural and Dynamical Studies of Stability in Energetic Materials, and Applications to Diverse End-Item Problems," *Proceedings of 1976 Army Science Conf.*, DA Publication (in press).

PRINCE, E., TREVINO, S. F., CHOI, C. J., and FARR, M. K., "A Refinement of the Structure of Deuterium Peroxide," *J. Chem. Phys.*, 63, 2620 (1975).

PUBLICATIONS

PRINCE, E., "Dimethyl Sulfone Diimine, A Neutron Study," *Acta Cryst.*
 B31, 2536, (1975).

PRINCE, E., MIGHELL, A., SANTORO, A., and REIMANN, C., "Neutron Diffraction
 Structure Determination of Dichlorotetrapyrazole Copper (II)," *Acta.*
 Cryst., *B31*, 2479 (1975).

RHYNE, J. J., KOON, N. C., MILSTEIN, J., and ALPERIN, H. A., "Spin Waves
 in Ferrimagnetic $ErFe_2$," *Proceedings of Conference on Neutron*
 Scattering, Gatlinburg, TN (in press).

RHYNE, J. J., ABBUNDI, R., SEGNAN, R., and SWEGER, D., "Hyperfine Fields
 in the Absence of Order in DySc Alloys," *AIP Conf. Proc.,* 29, 352
 (1976).

RHYNE, J. J., "Curie Temperatures of Amorphous RFe_2 Alloys," *AIP Conf.*
 Proc., 29, 182 (1976).

ROWE, J. M., "Neutron Scattering Studies of the Diffusion of Hydrogen
 in Metals," *Proceedings of the Conference on Neutron Scattering,*
 Gatlinburg, TN (in press).

ROWE, J. M., RUSH, J. J., PRINCE, E., and CHESSER, N. J., "Neutron
 Scattering Studies of Crystal Dynamics and Order-Disorder Phase
 Transitions in Alkali Cyanides," *Ferroelectrics*, (in press).

ROWE, J. M., VAGELATOS, N., RUSH, J. J., and FLOTOW, H., "The Acoustic
 Modes of the Phonon Dispersion Relation of NbD_x Alloys," *Phys. Rev.,*
 12, 2959 (1975).

RUSH, J. J., ROWE, J. M., GLINKA, C. J., VAGELATOS, N., and FLOTOW, H.,
 "Coherent Neutron Scattering Study of the Vibrations of Interstitial
 Deuterium in α $VD_{0.7}$," *Proceedings of the Conference on Neutron*
 Scattering, Gatlinburg, TN (in press).

RUSH, J. J., ROWE, M. J., VAGELATOS, N., "Crystals Dynamics of KCN and
 NaCN in the Disoriented Cubic Phase," *J. Chem. Phys.,* 62, 4551,
 (1975).

SANTORO, A., PRINCE, E., "The Use of Position-Sensitive Detector in
 Single Crystal Diffractometers," *J. Appl. Cryst.,* (in press).

SANTORO, A., "Powder Neutron Diffraction Analyses of the Crystal Struc-
 tures of $LiNb_3O_8$ & $H-LiTa_3O_8$," *Collected Abstracts Third European*
 Crystallographic Meeting, P105, Zurich, Switzerland, (1976).

PUBLICATIONS

SANTORO, A., NIEGHELL, A., PRINCE, E., and REIMANN, C., "Neutron Diffraction Structure Determination of Dichlorotitra-pyrazolcopper (II), *Acta. Cryst.*, B 31, 2479, (1975).

SANTORO, A., CHOI, C.S., and ABEL, J. E., "1,5-Diacetyl-3,7-Dinitro-1,3, 5,7 Tetraazacyclooctane (DADN)," *Acta. Cryst.* B31, 2126, (1975).

SCHNEIDER, C.S., "Coherent Nuclear Scattering Amplitudes of Germanium, Copper and Oxygen for Thermal Neutrons," *Acta Cryst.*, A32, 375 (1976).

SCHNEIDER, C., "A Precise Refractometer for Thermal Neutrons," *Rev. Sci. Instr.*, 44, 1594, (1975).

SHEN, T. Y., MITRAS, S. S., TREVINO, S. F. and PRASK, H., "Order-Disorder Phenomenon in Sodium Nitrate Studied by Low Frequency Raman Scattering," *Phys. Rev.*, B12, 4530-4533 (1975).

SHORTEN, F. J., "Nuclear Science Education Day," *NBS Technical Note*, 888, (1975).

VAGELATOS, N., ROWE, J. M., and RUSH, J. J., "Lattice Dynamics of Nd$_4$I in the NaCl phase (I) at 2960° K," *Phys. Rev.* B, 12/10, 4522 (1975).

PUBLICATIONS

INDEPENDENT PROGRAMS

CARPENTER, B. S., MYKLEBUST, R. L., "Comparative Boron Analysis by Ion Microproble Mass Analyzer and the Nuclear Track Technique," *Analytica Chemica Acta,* (in press).

DESLATTES, R. D., KESSLER, E. G., SAUDER, W. C., and HENINS, A., *Atomic Masses and Fundamental Constants 5,* Plenum Press, New York, p. 48 (1976).

FARBER, T. M., RITTER, D. L., WEINBERGER, M. A., BIERBOWER, G., TANNER, J. T., FRIEDMAN, M. H., CARTER, C. J., EARL, F. L., and VANLOON, E. J., "The Toxicity of Brominated Sesame Oil and Brominated Soybean Oil in Miniature Swine," *Toxicology,* 5, 319-336 (1976).

FRIEDMAN, M. H., and TANNER, J. T., "Trace Elements in Food by Neutron Activation Analysis," *Trans. of the American Nuclear Society,* 21, 97 (1975).

GLADNEY, E. S. and ROOK, H. L., "Simultaneous Determination of Tellurium and Uranium by Neutron Activation Analysis," *Analytical Chemistry,* 47, 1554-1556 (1975).

GROS, J., TAKAHASHI, H., HERTOGEN, J., MORGAN J. W., and ANDERS, E., "Composition of the Projectile That Bombarded the Lunar Highlands," *Proc. 7th Lunar Sci. Conf.,* Geochim. Cosmochim. Acta, Suppl. 7, (in press).

GRUNDL, J. A., SPIEGEL, V., EISENHAUER, C. M., HEATON, H. T., GILLIAM, D. M., and BIGELOW, J., "A Californium-252 Fission Spectrum Irradiation Facility for Neutron Reaction Rate Measurements," *Nuclear Technology,* (in press).

GRUNDL, J. A., and EISENHAUER, C., "Fission Rate Measurements for Materials Neutron Dosimetry in Reactor Environments," *Proceedings of ASTM-EURATOM Symposium on Reactor Dosimetry,* Petten, The Netherlands.

HARRISON, S. H., LaFLUER, P. D. and ZOLLER, W. H., "Sampling and Sample Handling for Activation Analysis of River Water," Accuracy in Trace Analysis: Sampling, Sample Handling, Analysis, *Vol. 1 NBS Special Publication* 422 (1976).

HARRISON, S. H., LaFLUER, P. D. and ZOLLER, W. H., "An Evaluation of Lyophilization for the Preconcentration of Natural Water Samples Prior to Neutron Activation Analysis," *Analytical Chemistry,* 47, 1685-1688 (1975).

PUBLICATIONS

HARRISON, S. H., "Neutron Activation Analysis: A Useful Tool for Evaluating Water Sampling and Analysis Techniques," *Transactions of the American Nuclear Society,* 21, 110-111 (1975).

HIGUCHI, H. and MORGAN, J. W., "Ancient Meteoritic Component in Apollo 17 Boulders," *Proc. 6th Lunar Sci. Conf., Geochim. Cosmochim. Acta, Suppl.* 6, 1625-1651 (1975).

JAMES, O. B., BRECHER, A., BLANCHARD, D. P., JACOBS, J. W., BRANNON, J. C., KOROTEV, R. L., HASKIN, L. A., HIGUCHI, H., MORGAN, J. W., ANDERS, E., SILVER, L. T., MARTI, K., BRADDY D., HUTCHEON, I. D., KIRSTEN, T., KERRIDGE, J. F., KAPLAN, I. R., PILLINGER, C. T., and GARDINER, L. R., "Consortium Studies of Matrix of Light Gray Breccia 73215," *Proc. 6th Lunar Sci. Conf., Geochim. Cosmochim. Acta, Suppli.* 6, 547-577 (1975).

McGARRY, E. D., ROZI, A. H., DAVID, G. S., GILLIAM, D. M., "Absolute Neutron-Flux Measurement at Fast Pulse Reactor with Calibration Against Californium-252," *IEEE Conf. on Nuclear and Space Radiation,* San Diego (1976).

MORGAN, J. W., GROS, J., TAKHAHSHI, H., and HERTOGEN, J., "Lunar Breccia 73215: Siderophile and Volatile Elements," *Proc. 7th Lunar Sci. Conf., Geochim. Cosmochim. Acta, Suppl.* 7, (in press).

MORGAN, J. W., "Chemical Fractionation in the Solar System," *Proc. 1976 Int. Conf.: Modern Trends in Activation Analysis, J. Radioanal. Chem.,* (in press).

MORGAN, J. W., GANAPATHY, R., HIGUCHI, H., KRÄHENBÜHL, U., "Volatile and Siderophile Trace Elements in Anorthositic Rocks from Fiskenaesset, West Greenland: Comparison with Lunar and Meteoritic Analogues," *Geochim. Cosmochim. Acta* 40, 861-887 (1976).

MORGAN, J. W., HIGUCHI, H., and ANDERS, E., "Meteoritic Material in a Boulder from the Apollo 17 Site: Implications for its Origin," *The Moon* 14, 505-517 (1975).

REIMER, G. M., and CARPENTER, B. S., "Fission-Track Determination of Uranium in Solutions," Abstract, *EOS Transactions, American Geophysical Union,* 56, No. 6, (1975).

ROOK, H. L., SUDDUETH, J. E. and BECKER, D. A., "Determination of Iodine-129 at Natural Levels Using Neutron Activation and Isotopic Separation," *Analytical Chemistry,* 47, No. 9, 1557-1562 (1975).

PUBLICATIONS

ROWE, J. J. and STEINNES, E., "Determination of 30 Elements in Coal and Fly Ash by Thermal and Epithermal Neutron Activation Analysis," *Talanta* (in press).

ROWE, J. J. and SIMON, F. O., "Determination of Gold in Geologic Materials by Neutron Activation Analysis Using Fire Assay for Radiochemical Separations," *U.S.G.S. Circ* 599.

TANNER, J. T., and FRIEDMAN, M. H., "Trace Elements in Food," Modern Trends in Activation Analysis, (to be published) *J. Radioanal Chem.*

TANNER, J. T., "Instrumentation in Applied Nuclear Chemistry," Krugers (Editor), *Journal of the Association of Official Anlaytical Chemists* 58, 626 (1975).

TANNER, J. T. and FORBES, W. S., "Determination of Mercury in Total Diet Samples by Neutron Activation," *Analytica Chimica Acta* , 74, 17-21 (1975).

WAGNER, G. A., REIMER, G. M., CARPENTER, B. S., FAUL, H., VAN der LINDEN, R. and GIJBELS, R., "The Spontaneous Fission-Track Rate of U-238 and Fission-Track Dating," *Geochimica et Coschimica Acta,* 39, 1279-1286, Pergamon Press (1975).

U.S. DEPT. OF COMM. BIBLIOGRAPHIC DATA SHEET	1. PUBLICATION OR REPORT NO. NBS Technical Note 939	2. Gov't Accession No.	3. Recipient's Accession No.
4. TITLE AND SUBTITLE NBS REACTOR: Summary of Activities July 1975 to June 1976			5. Publication Date May 1977 6. Performing Organization Code
7. AUTHOR(S) Frederick J. Shorten			8. Performing Organ. Report No.
9. PERFORMING ORGANIZATION NAME AND ADDRESS NATIONAL BUREAU OF STANDARDS DEPARTMENT OF COMMERCE WASHINGTON, D.C. 20234			10. Project/Task/Work Unit No. 11. Contract/Grant No.
12. Sponsoring Organization Name and Complete Address *(Street, City, State, ZIP)*			13. Type of Report & Period Covered 7/1/75 to 6/30/76 14. Sponsoring Agency Code

15. SUPPLEMENTARY NOTES

16. ABSTRACT *(A 200-word or less factual summary of most significant information. If document includes a significant bibliography or literature survey, mention it here.)*

This report summarizes all those programs which depend on the NBS reactor. It covers the period from July 1975 through June 1976. The programs range from the use of neutron beams to study the structure and dynamics of materials through nuclear physics and neutron standards to sample irradiations for activation analysis, isotope production and radiation effects studies.

17. KEY WORDS *(six to twelve entries; alphabetical order; capitalize only the first letter of the first key word unless a proper name; separated by semicolons)*

Activation analysis; crystal structure; diffraction; isotopes; molecular dynamics; neutron; nuclear reactor; radiation

18. AVAILABILITY [X] Unlimited	19. SECURITY CLASS (THIS REPORT)	21. NO. OF PAGES
[ ] For Official Distribution. Do Not Release to NTIS	UNCLASSIFIED	140
[X] Order From Sup. of Doc., U.S. Government Printing Office Washington, D.C. 20402, <u>SD Cat. No. C13.46:939</u>	20. SECURITY CLASS (THIS PAGE)	22. Price $2.75
[ ] Order From National Technical Information Service (NTIS) Springfield, Virginia 22151	UNCLASSIFIED	

NBS TECHNICAL PUBLICATIONS

PERIODICALS

JOURNAL OF RESEARCH reports National Bureau of Standards research and development in physics, mathematics, and chemistry. It is published in two sections, available separately:

• Physics and Chemistry (Section A)

Papers of interest primarily to scientists working in these fields. This section covers a broad range of physical and chemical research, with major emphasis on standards of physical measurement, fundamental constants, and properties of matter. Issued six times a year. Annual subscription: Domestic, $17.00; Foreign, $21.25.

• Mathematical Sciences (Section B)

Studies and compilations designed mainly for the mathematician and theoretical physicist. Topics in mathematical statistics, theory of experiment design, numerical analysis, theoretical physics and chemistry, logical design and programming of computers and computer systems. Short numerical tables. Issued quarterly. Annual subscription: Domestic, $9.00; Foreign, $11.25.

DIMENSIONS/NBS (formerly Technical News Bulletin)—This monthly magazine is published to inform scientists, engineers, businessmen, industry, teachers, students, and consumers of the latest advances in science and technology, with primary emphasis on the work at NBS. The magazine highlights and reviews such issues as energy research, fire protection, building technology, metric conversion, pollution abatement, health and safety, and consumer product performance. In addition, it reports the results of Bureau programs in measurement standards and techniques, properties of matter and materials, engineering standards and services, instrumentation, and automatic data processing.

Annual subscription: Domestic, $12.50; Foreign, $15.65.

NONPERIODICALS

Monographs—Major contributions to the technical literature on various subjects related to the Bureau's scientific and technical activities.

Handbooks—Recommended codes of engineering and industrial practice (including safety codes) developed in cooperation with interested industries, professional organizations, and regulatory bodies.

Special Publications—Include proceedings of conferences sponsored by NBS, NBS annual reports, and other special publications appropriate to this grouping such as wall charts, pocket cards, and bibliographies.

Applied Mathematics Series—Mathematical tables, manuals, and studies of special interest to physicists, engineers, chemists, biologists, mathematicians, computer programmers, and others engaged in scientific and technical work.

National Standard Reference Data Series—Provides quantitative data on the physical and chemical properties of materials, compiled from the world's literature and critically evaluated. Developed under a world-wide program coordinated by NBS. Program under authority of National Standard Data Act (Public Law 90-396).

NOTE: At present the principal publication outlet for these data is the Journal of Physical and Chemical Reference Data (JPCRD) published quarterly for NBS by the American Chemical Society (ACS) and the American Institute of Physics (AIP). Subscriptions, reprints, and supplements available from ACS, 1155 Sixteenth St. N.W., Wash. D. C. 20056.

Building Science Series—Disseminates technical information developed at the Bureau on building materials, components, systems, and whole structures. The series presents research results, test methods, and performance criteria related to the structural and environmental functions and the durability and safety characteristics of building elements and systems.

Technical Notes—Studies or reports which are complete in themselves but restrictive in their treatment of a subject. Analogous to monographs but not so comprehensive in scope or definitive in treatment of the subject area. Often serve as a vehicle for final reports of work performed at NBS under the sponsorship of other government agencies.

Voluntary Product Standards—Developed under procedures published by the Department of Commerce in Part 10, Title 15, of the Code of Federal Regulations. The purpose of the standards is to establish nationally recognized requirements for products, and to provide all concerned interests with a basis for common understanding of the characteristics of the products. NBS administers this program as a supplement to the activities of the private sector standardizing organizations.

Consumer Information Series—Practical information, based on NBS research and experience, covering areas of interest to the consumer. Easily understandable language and illustrations provide useful background knowledge for shopping in today's technological marketplace.

Order above NBS publications from: Superintendent of Documents, Government Printing Office, Washington, D.C. 20402.

Order following NBS publications—NBSIR's and FIPS from the National Technical Information Services, Springfield, Va. 22161.

Federal Information Processing Standards Publications (FIPS PUBS)—Publications in this series collectively constitute the Federal Information Processing Standards Register. Register serves as the official source of information in the Federal Government regarding standards issued by NBS pursuant to the Federal Property and Administrative Services Act of 1949 as amended, Public Law 89-306 (79 Stat. 1127), and as implemented by Executive Order 11717 (38 FR 12315, dated May 11, 1973) and Part 6 of Title 15 CFR (Code of Federal Regulations).

NBS Interagency Reports (NBSIR)—A special series of interim or final reports on work performed by NBS for outside sponsors (both government and non-government). In general, initial distribution is handled by the sponsor; public distribution is by the National Technical Information Services (Springfield, Va. 22161) in paper copy or microfiche form.

BIBLIOGRAPHIC SUBSCRIPTION SERVICES

The following current-awareness and literature-survey bibliographies are issued periodically by the Bureau:

Cryogenic Data Center Current Awareness Service. A literature survey issued biweekly. Annual subscription: Domestic, $20.00; Foreign, $25.00.

Liquified Natural Gas. A literature survey issued quarterly. Annual subscription: $20.00.

Superconducting Devices and Materials. A literature survey issued quarterly. Annual subscription: $20.00. Send subscription orders and remittances for the preceding bibliographic services to National Bureau of Standards, Cryogenic Data Center (275.02) Boulder, Colorado 80302.